University of Genoa

School of Mathematical, Physical and Natural Sciences

Doctorate in Sciences and Technologies of Chemistry and Materials

Curriculum: Sciences and Technologies of Chemistry

Assessment of the impact of atmospheric pollutants on bacteria viability by an atmospheric simulation chamber

THESIS

FOR THE ATTAINMENT OF THE PHILOSOPHIÆ DOCTOR DEGREE

BY

Silvia Giulia DANELLI

Supervisors:

Dr. Camilla Costa (University of Genoa)

Prof. Paolo Prati (University of Genoa)

Contents

Introduction 4

1. Atmospheric Aerosol and Simulation Chambers 6

1.1 Atmospheric Aerosols 6

1.2 Climate and Health Effects 9

1.3 Bioaerosols 12

1.4 Atmospheric Simulation Chambers 16

1.4.1 ASCs and bioaerosol 18

2. The ChAMBRe facility 19

2.1 ChAMBRe main structure 19

2.2 Basic equipment 21

2.3 Instruments connected to ChAMBRe 21

2.3.1 Gas Analyzers 21

2.3.2 Particle counters 23

2.3.3 Aerosol optical properties measurements 30

2.3.4 Bioaerosol samplers 31

2.4 Aerosol production systems 33

2.4.1 Nebulization systems 33

2.4.2 Soot generator 37

2.5 Characterization of the chamber performances 37

2.5.1 Background levels and blank experiments 37

2.5.2 Mixing 38

2.5.3 Aerosol behaviors 39

2.6 Microbiological laboratory connected to ChAMBRe 40

3. Experimental investigations of bacteria in ChAMBRe 41

3.1 Methodology 41

3.1.1 Bacteria selection 41
3.1.2 Preparation of bacterial suspension 44
3.1.3 Chamber preparation 48
3.1.4 Bacteria injection in ChAMBRe 48
3.1.5 Bacteria collection and extraction methods 48
3.2 Bioaerosol production 49
3.2.1 Determination of nebulization efficiency 50
3.2.2 Reproducibility and application for ASCs experiments 54
3.3 Processing of the WIBS data 60
3.3.1 Coincidence and Dead time losses 64
3.4 Results and Conclusions 67
3.4.1 Baseline experiments 67
3.4.2 Bacteria and pollutants 73
4. Summary and Perspective 84
APPENDIX A 86
APPENDIX B 90
References 102
Acknowledgements 116
Candidate publications 116

Introduction

Aerosols consist in solid or liquid molecular aggregates suspended in a gas. Atmospheric aerosols have diameters in the size range between few nanometers to some tens of micrometers and are an important topic in atmospheric sciences. Aerosol particles are widely dispersed in the Earth's atmosphere and they influence climate, cloud formation, weather, visibility, atmospheric chemistry as well as public health. One of the components of the atmospheric aerosol is the aerosol of biological origin. Primary biological aerosol particles (PBAPs) refers to living and dead microorganisms, dispersal units and fragments of biological materials directly emitted in the atmosphere from the biosphere. Among all the different bioaerosol microorganisms, bacteria play a relevant role. They are ubiquitous in the atmosphere with concentrations typically greater than 1×10^4 m^{-3} over land and, due to their small size, with long atmospheric residence times (Bowers et al., 2011). Therefore, bacteria can be transported over long distances, with important implications at the microbial biogeography level. The presence of bacteria in the atmosphere can influence Earth's climate and cause many adverse health effects (Després et al., 2012). Bacterial viability, including the capability to survive and maintain their pathogenicity, depends on several atmospheric conditions, such as relative humidity, temperature, irradiation, and chemical composition of ambient air (Marthi et al., 1990; Burrows et al., 2009b).

The interaction between bacteria and the other atmospheric constituents has recently attracted interest as part of the broader field of atmospheric sciences (Amato et al., 2015; Brotto et al., 2015; Hussey et al., 2017; Massabó et al., 2018; Noda et al., 2021). The possibility to perform experiments inside confined artificial environments, such as the Atmospheric Simulations Chambers (ASCs), where atmospheric conditions and composition are controlled, can provide valuable information on bio-aerosols viability and on the mechanism of their interaction with other aerosols and atmospheric constituents.

The aim of my PhD project was indeed to make possible systematic studies of the bio-aerosols behavior in different atmospheric conditions, through the use of an atmospheric simulation chamber, ChAMBRe (Chamber for Aerosol Modelling and Bio-aerosol Research), installed at Genoa Division of the National Institute of Nuclear Physics. In particular, I tried to establish the conditions to study the link between pollution levels and bacteria viability.

This thesis work describes the ChAMBRe facility, the experimental procedures developed to perform experiments on bioaerosol inside the chamber as well as the first results on the relationship between air quality and bacteria viability.

In Chapter 1, the main characteristics of atmospheric aerosols are described, with details on the bioaerosol fraction and bacteria. An overview on atmospheric simulation chambers is also given; as well as a detailed description of ChAMBRe and its equipment. The procedures developed to study and analyze airborne bacteria inside ChAMBRe are described in Chapter 3, with details on the reproducibility and sensitivity of the experimental procedure, together with the results of the first studies on the effects of two common pollutants (soot particles and nitrogen oxides) on bacterial viability. Finally, in Chapter 4 a brief summary of the work and the perspectives on the potential chamber studies on bioaerosol are pointed out.

1. Atmospheric Aerosol and Simulation Chambers

1.1 Atmospheric Aerosols

Atmospheric aerosols are defined as colloidal systems of liquid or solid particles suspended in the air, with highly variable chemical composition and size distribution (Finlayson-Pitts and Pitts, 2000; Putaud et al., 2004; Raes et al., 2000; Seinfeld and Pandis, 1998). Thus, in principle, the term "aerosol" comprises both the aerosol particles and the gas phase, in which the particles are suspended. In atmospheric research, however, the term "aerosol" usually refers to the particles.

Particle diameters are typically in the range of ~1 nm to around ~100 μm, where the lower limit is given by the size of small molecular clusters and the upper limit by the rapid sedimentation (high settling velocities comparable to the magnitude of atmospheric updraft velocities, ~1 m s^{-1}), (Seinfeld and Pandis, 1998).

Aerosol particles are either emitted directly to the atmosphere (primary aerosols) or produced in the atmosphere from precursor gases (secondary aerosols) and have a wide variety of natural and anthropogenic sources (Fuzzi et al., 2006; Pöschl, 2005). Primary aerosols consist of both inorganic and organic components. Inorganic primary aerosols are relatively large (often larger than 1 μm) and originate from sea spray, volcanic eruptions, and wind-driven or traffic-related suspension of road, soil, and mineral dust. These coarse aerosols have short atmospheric lifetimes, typically only a few days. Combustion processes of fossil fuels, biomass burning, and plants are sources of primary carbonaceous aerosols, such as the organic carbon (OC) and elemental carbon (EC). When EC is determined by optical methods, it is usually called black carbon (BC), which is the main anthropogenic light-absorbing component of atmospheric aerosols. The two quantities, EC and BC, even if both related to the refractory components of carbonaceous aerosols, do not exactly define the same PM component (Bond and Bergstrom, 2006). Primary BC and OC containing aerosols are generally smaller than 1 μm (Pöschl, 2005). Secondary aerosol particles are produced in the atmosphere by gas-to-particle conversions, such as condensation of gaseous precursor on pre-existing particles or by nucleation of new particles. Secondary aerosols range in size from a few nanometers up to 1 μm and have lifetimes of days to weeks. Secondary aerosols consist of mixtures of compounds, which the main components are sulphate, nitrate, and OC. The main precursor gases are emitted from

fossil fuel combustion, but fires and biogenic emissions of volatile organic compounds (VOCs) are also important (Pöschl, 2005).

As illustrated in Figure 1.1, particles in the atmosphere undergo various physical and chemical interactions and transformations (atmospheric aging), i.e., changes of particle size, structure, and composition such as coagulation, gas uptake or/and chemical reaction.

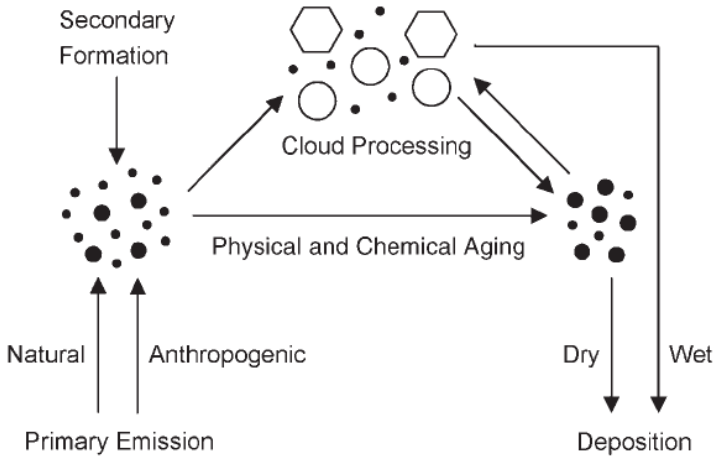

Figure 1. 1 Atmospheric cycling of Aerosols, (Pöschl, 2005).

The aerodynamic properties of the particles govern their transport and removal from the air, as well as the deposition within the human respiratory system. For this reason, particles are classified on the basis of their *aerodynamic diameter* (d_{ae}), defined as the size of a unit-density sphere with the same aerodynamic characteristics (Marple and Willeke, 1976). This parameter is used to determine the residence time of the particles in the air and the regions of the human respiratory system within they can settle. Particles, or *particulate matter*, are thus classified into PM_1, $PM_{2.5}$ and PM_{10}, which refer to particles with aerodynamic diameters less than 1 μm, 2.5 μm or to 10 μm, respectively. The size distribution (in mass or in number) of particles in the atmosphere is determined by the competition between sources and removal mechanisms. In the troposphere, for dry conditions, aerosols tend to form a characteristic bimodal distribution, where most of the mass is confined in two separate modes, or fractions, the *fine* and the *coarse* modes (Johansson et al., 1995), as shown in Figure 1.2. Particles with diameter less than 0.1 μm are generally formed by nucleation, i.e., collisional aggregation of atoms and molecules to form clusters and further on nanoparticles. Particles in this nucleation mode grow rapidly by coagulation (i.e. the combination of two or more particles to form a larger particle) or by condensation (i.e. condensation of gas or vapor molecules on the surface of existing particles). The efficiency of both coagulation and condensation decreases as particle size increases, which effectively produces an upper limit such that particles do not grow by these processes beyond approximately 2-3 μm. All particles smaller then 2-3 μm are generally referred as *fine particles*. The

smallest ones, less than 0.1 μm, are efficiently removed by diffusion. However, neither settling nor diffusion is efficient between 0.1 and 1 μm, thus particles tend to "*accumulate*" in this range, the so-called accumulation range (Figure 1.2). Particles of this size can survive up to 10 days in the lower troposphere and thus travel long distances. However, in wet conditions, such particles are easily incorporated into clouds, and such wet removal processes are very rapid and efficient. Acidic aerosols incorporated into clouds can enhance or cause acidic clouds/fog and acid rain (Johansson et al., 1995). The *coarse fraction* particles are mechanically produced by the break-up of larger solid particles and can include: wind-blown dust (from agricultural processes, uncovered soil, unpaved roads or mining operations), road dust re-suspended by traffic, sea spray particles, and most of the particles of biological origin, such as spores, pollen and plant and insect debris. The amount of energy required to break these particles into smaller sizes increases as the size decreases, which effectively establishes a lower limit for the production of these coarse particles of approximately 1-2 μm. Coarse particles removal is generally by settling and, since the process is quite efficient, the residence time in the atmosphere is short, typically of the order of hours.

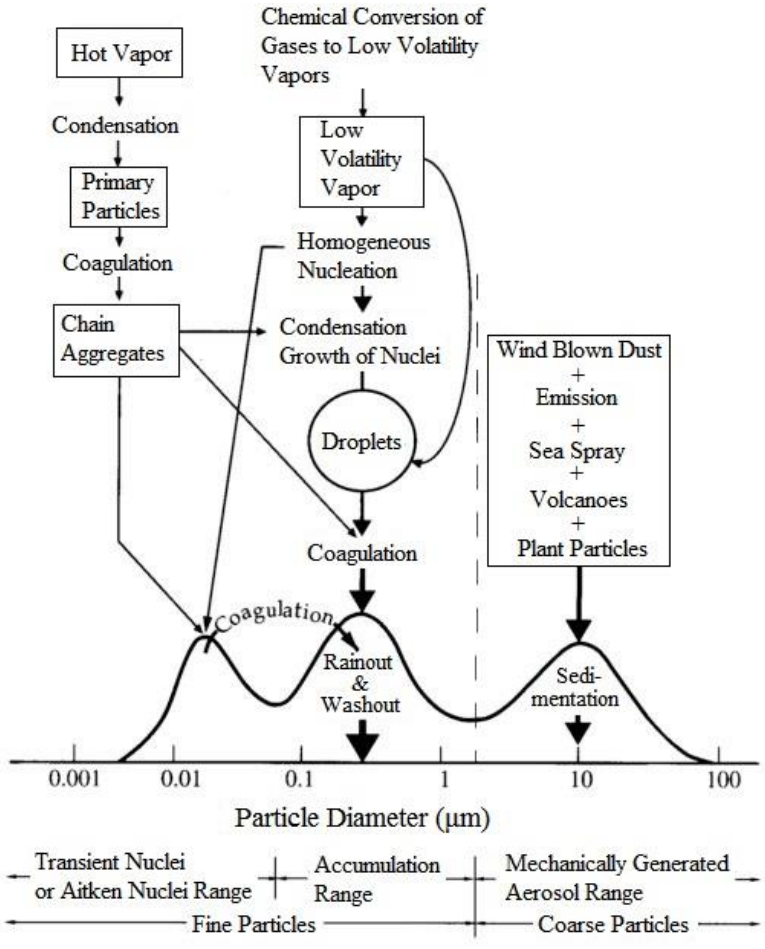

Figure 1.2 Diagram showing the main modes, sources and mechanisms of aerosol formation and deposition, (Whitby and Cantrell, 1976).

1.2 Climate and Health Effects

Aerosol particles are widely dispersed in the Earth's atmosphere and they influence climate, cloud formation, weather, visibility, atmospheric chemistry as well as human health. The effects of aerosols on the atmosphere, climate, and public health are among the central topics in current environmental research.

Both natural and anthropogenic aerosols have a strong impact on climate and human health. However, anthropogenic emissions are major sources of atmospheric aerosols. In particular, the emissions of particles and precursor gases from biomass burning and fossil-fuel combustion have massively increased since preindustrial times and account for a major fraction of fine air particulate matter in polluted urban environments as well as in the global atmosphere (Pöschl, 2005).

Particles in the atmosphere scatter and absorb solar as well as terrestrial radiation. They are involved in the formation of clouds and precipitation as cloud condensation and ice nuclei (CCN and IN), and affect the abundance and distribution of atmospheric trace gases by heterogeneous chemical reactions and other multiphase processes (Finlayson-Pitts and Pitts, 2000; Lohmann and Feichter, 2005; Seinfeld and Pandis, 1998). Besides their impact on climate, airborne particles play an important role in the spreading of biological organisms, reproductive materials, and pathogens (pollen, bacteria, spores, viruses, etc.), and they can cause or enhance respiratory, cardiovascular, infectious, and allergic diseases (Bernstein et al., 2004; Finlayson-Pitts and Pitts, 2000, 1997; Hinds, 1999).

Aerosol effects on climate are generally classified as direct or indirect with respect to radiative forcing (RF) of the climate system. RF is defined as a change in the Earth's radiation balance (energy fluxes of solar radiation and terrestrial radiation) due to a perturbation of anthropogenic or natural origin.

Scattering and reflection of solar radiation by aerosols and clouds are negative forcings, and have a cooling effect on the Earth's surface, whereas the absorption of terrestrial radiation by greenhouse gases and clouds are indicate as positive forcing, and tend to warm it (*greenhouse effect*) (Houghton et al., 2001). In the atmosphere, there is a mixture of scattering and absorbing aerosols, therefore they influence the global radiation budget directly (RF from aerosol–radiation interactions, RFari). Besides their direct effect on the radiation budget, aerosols play an important role in cloud formation because a large fraction of them acts as cloud condensation nuclei (CCN) and ice nuclei (IN). When clouds form in the atmosphere, water condenses on the available cloud condensation nuclei. A changing number concentration of CCN modifies the number concentration and the size of the cloud droplets: an increased amount of aerosols may increase the CCN number concentration and lead to more, but smaller, cloud droplets for fixed liquid water content. This increases the albedo of the cloud, resulting in enhanced reflection and a cooling effect, named the cloud albedo effect. Therefore, the

optical properties and the lifetime of atmospheric clouds change. This influence of particles on the global radiation budget and climate is termed the indirect aerosol effect or RF from aerosol–cloud interactions (RFaci). In addition, absorbing aerosols deposited on snow or ice surfaces may reduce the surface albedo, leading to reduced reflectance of solar radiation, and hence a heating effect. Therefore, the net effect of aerosols on climate is difficult to quantify, as shown in Figure 1.3, extracted from the Intergovernmental Panel on Climate Change *IPCC2013* (Boucher et al., 2013), which reports the components of radiative forcing over the Industrial Era from 1750 to 2011.

In the last decades, as reported in the most recent Intergovernmental Panel on Climate Change (*IPCC, 2021: Climate Change 2021: The Physical Science Basis. Contribution of Working Group I to the Sixth Assessment Report of the Intergovernmental Panel on Climate Change*, 2021) there has been a reduction in the uncertainty of the total aerosol Effective Radiative Forcing (ERF). Separate lines of evidence support the assessment that the total aerosol ERF is negative and it is also assessed to be –1.1 [–1.7 to –0.4] W m^{-2}.

The impact on human health is clearly connected with the composition of particles and their capacity to penetrate into the breathing apparatus, with smaller ones reaching more easily the deeper parts of the lungs and being therefore more dangerous. Particles with d_{ae} greater than 10 μm are stopped in the first part of the respiratory system and then easily expelled. Particles with d_{ae} between about 10 and 3.5 μm tend to be inhaled and stopped in the nose, throat, and upper bronchial tract. Particles smaller than about 3.5 μm enter the deep lung and are retained in the alveoli, while ultrafine particles (d_{ae} < 100 nm) are suspected to be particularly hazardous because they are sufficiently small to penetrate the membranes of the respiratory tract and enter the blood circulation (Nemmar et al., 2002; Oberdörster et al., 2005).

Numerous epidemiological studies show that fine air particulate matter and traffic-related air pollution are correlated with severe health effects, including enhanced mortality, cardiovascular, respiratory, and allergic diseases (Bernstein et al., 2004; Gauderman et al., 2004; Pope et al., 2004; Samet et al., 2005). Many factors influence these health effects, the size of the particles as mentioned, but also their surface and morphology, their solubility and the toxicity of the chemical substances contained in the particles. Exposure to high concentration of aerosol particles including soot, sulphate, organics and dust can lead to inflammation and damage to cellular proteins and DNA (Shiraiwa et al., 2012). Moreover, inhalation of transition metals such as copper and iron, or organic compounds such as soot and polycyclic aromatic compounds (PACs) can trigger the formation of free radicals and reacting reactive oxygen species (ROS) *in vivo,* which can cause oxidative stress, cell death, biological aging and diseases (Li et al., 2003). Bioaerosols can have infectious, allergenic, or toxic

effects on living organisms as well, impacting health and agriculture on local, regional, and global scales (Fröhlich-Nowoisky et al., 2016). However, biochemical mechanisms and molecular processes that cause the toxicological effects have not yet been resolved, as well as the effects of air pollution on the occurrence of allergic diseases. Their understanding, however, is required for the development of efficient air-quality control strategies as well as for the medical treatment of related diseases.

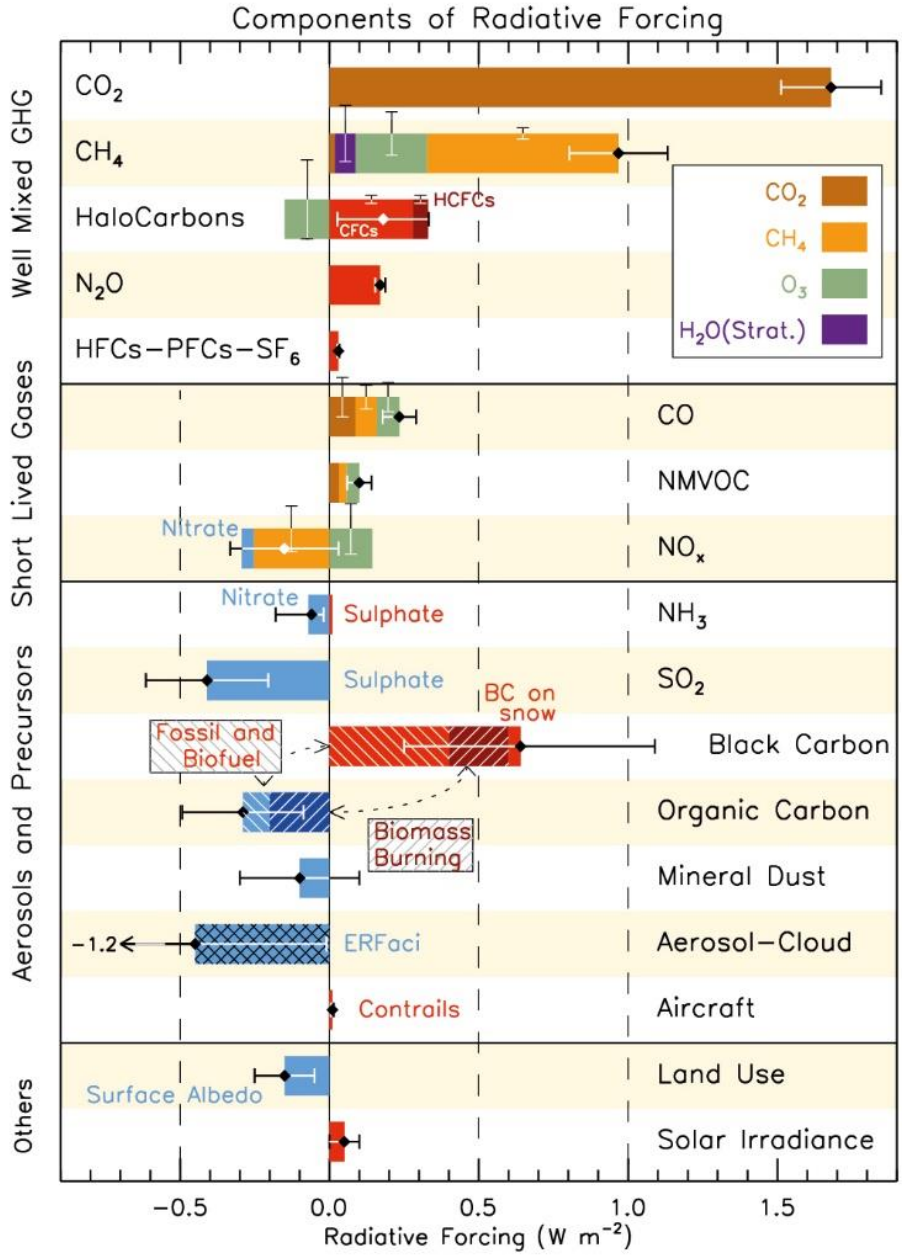

Figure 1.3 Radiative forcing (RF) segregated for relevant components in the period 1750-2011. The horizontal bars indicate the overall uncertainty. From "*Anthropogenic and Natural Radiative Forcing. In: IPCC2013*", (Myhre et al., 2013).

1.3 Bioaerosols

The term *bioaerosol* refers to aerosol of biological origin. The major types of bioaerosols are primary and secondary biological aerosols and biogenic aerosols. Primary biological aerosols (PBA) include living and dead microorganisms (e.g., archaea, algae, bacterial aggregates and single cells), dispersal units (e.g., fungal and bacterial spores, plant pollen), various fragments or excretions (e.g., plant debris, microbial fragments) and virus particles, which are directly released from the biosphere into the atmosphere (Ariya and Amyot, 2004; Després et al., 2012; Fröhlich-Nowoisky et al., 2016). Secondary biological aerosols result from physical or chemical processes (condensation, oxidation, coating, etc.) that modify primary biological aerosols. They are distinct from biogenic secondary organic aerosols, which are formed by atmospheric oxidation and gas-to-particle conversion of volatile organic compounds released from biological organisms (Morris et al., 2014).

As illustrated in Figure 1.4, the size of PBA can range from several nanometers (e.g. viruses, cell fragments) to a few hundred micrometers in aerodynamic diameter (e.g. pollen, plant debris), (Pöschl, 2005). Larger particles of biological material can also be lifted into the air, but due to high settling velocities they are rapidly deposited rather than being suspended over long times. Thus, they are usually not considered to be atmospheric aerosol particles.

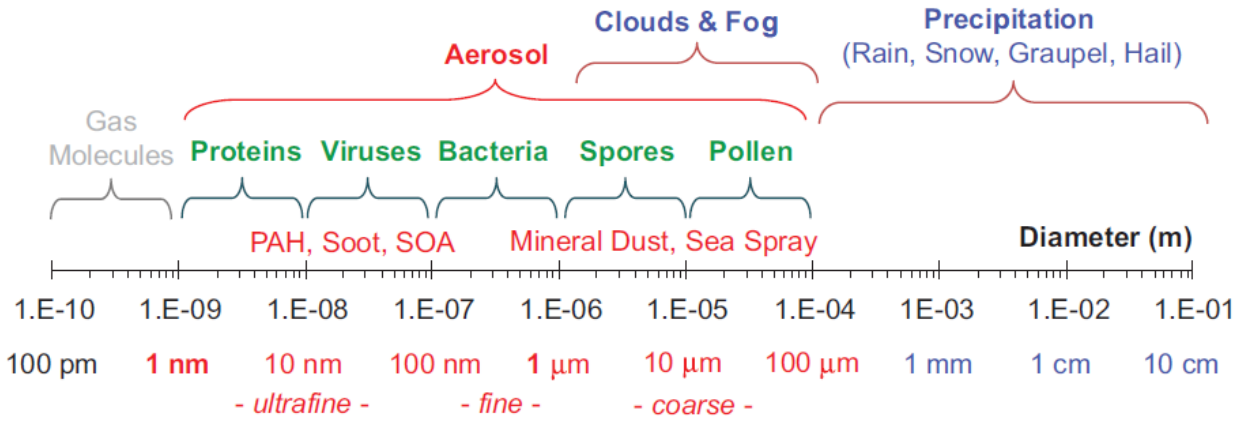

Figure 1.4 Size range of atmospheric aerosols and hydrometeors, (Shiraiwa et al., 2012).

Aerosols of biological origin play an important role in the Earth system, particularly in the interactions between atmosphere, biosphere, climate, and public health. Airborne bacteria, fungal spores, pollen, and other bio-particles are essential for the reproduction and spread of organisms across various ecosystems and they can cause or enhance human, animal, and plant diseases. Moreover, they can serve as nuclei for cloud droplets, ice crystals, and precipitation, thus influencing the hydrological cycle and climate (Després et al., 2012; Fröhlich-Nowoisky et al., 2016). Especially in pristine air over vegetated regions or in marine environment, bioaerosols may contribute

substantially to the abundance of ice nuclei (Burrows et al., 2009a; Huffman et al., 2013; Möhler et al., 2007; Wilson et al., 2015).

In the atmosphere, PBA undergo further chemical and physical transformation, stress, and biological aging upon interaction with UV radiation, photo-oxidants, and various air pollutants like acids, nitrogen oxides, aromatic compounds, and soot particles (Santarpia et al., 2012; Shiraiwa et al., 2012), (Figure 1.5).

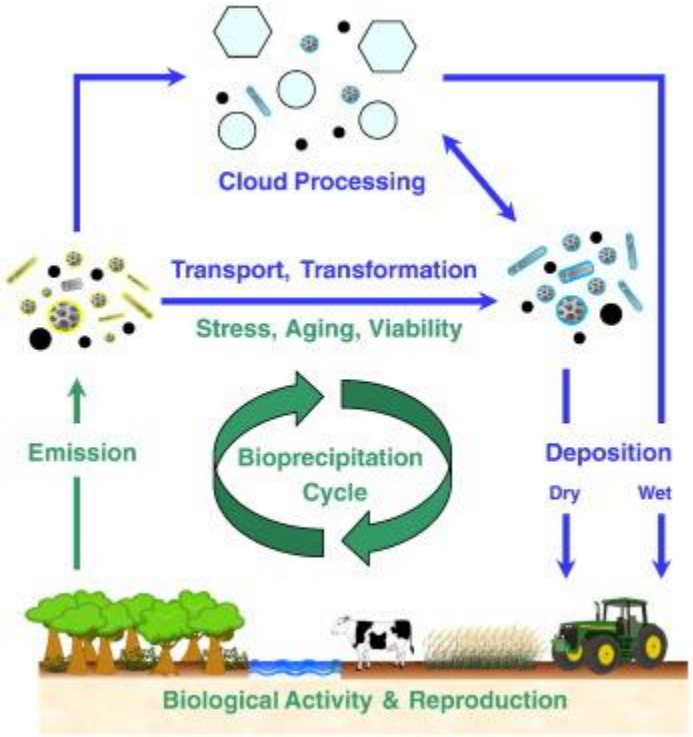

Figure 1.5 Bioaerosol cycling in the Earth system, (Fröhlich-Nowoisky et al., 2016).

After returning to the ground, viable bio-particles can continue biological reproduction and metabolic activity that may generate further emission of PBA particles and secondary organic aerosol (SOA) precursors, thus closing a biogeochemical cycle of biologically-derived aerosols in the Earth system (Deguillaume et al., 2008; Pöhlker et al., 2012; Pöschl, 2005; Pöschl et al., 2010; Suni et al., 2015).

In most terrestrial environments, bioaerosols constitute a substantial fraction of the atmospheric aerosol load. With regard to number and mass concentration in the coarse particle size range with diameters larger than ~1 μm, bioaerosols typically account for around 30% in urban and rural air (Després et al., 2012; Huffman et al., 2013). The number and mass concentrations of PBA particles over vegetated regions are typically in the order of $\sim 10^4$ m^{-3} and ~1 μg m^{-3}, respectively (Bauer et al., 2002a, 2002b; Després et al., 2012; Huffman et al., 2013, 2012). In areas of human activity, such as cities or agricultural managed areas, the numbers and composition of microorganisms such as bacteria or fungi are often increased and altered with respect to rural areas. Oceans are full of living

and decaying organisms, such as bacteria, archaea, fungi and algae, which are ejected from the ocean surface by bubble-bursting mechanisms, similar to the way other particles (e.g. sea salt) are emitted from such surfaces (O'Dowd et al., 2004). In summary, the Earth's biosphere provides many diverse and important sources of PBA.

Among all the different bioaerosol microorganisms, bacteria are supposed to play a relevant role (Bowers et al., 2011). They are ubiquitous in the atmosphere, with concentrations greater than 10^4 cells m^{-3} over land (Bauer et al., 2002a), while concentrations over the sea may be lower by a factor of ~100 - 1000 (Griffin et al., 2006; Prospero et al., 2005). Due to their small size, bacteria have a relatively long atmospheric residence time (on the order of several days or more) compared to larger particles and can be transported over long distances (up to thousands of km) (Després et al., 2012). Airborne bacteria may be suspended as individual cells or attached to other particles, such as soil or leaf fragments, or found as agglomerates of many bacterial cells (Lighthart, 2006). For this reason, whereas individual bacteria are typically on the order of ~1 μm or less in size, the median aerodynamic diameter of particles containing culturable bacteria at several continental sites is reported to be ~ 2 - 4 μm (Shaffer and Lighthart, 1997; Tong and Lighthart, 1999; Wang et al., 2007).

Even if up to now several works have contributed to the identification of bacterial diversity in the atmosphere (Amato et al., 2007; Burrows et al., 2009a; Després et al., 2012), it remains difficult to establish a clear picture of the actual abundance and composition of bacteria in the air. Concentration and composition of bacteria undergo daily, weekly and seasonal changes and strongly dependent on many factors such as meteorological factors, anthropogenic influence, variability of bacterial sources and many other complex variables (Després et al., 2012).

Numerous studies suggest that the presence of bacteria in the atmosphere may impact cloud development, atmospheric chemistry, and microbial biogeography. Airborne bacteria impact cloud formation by acting as ice nuclei and cloud condensation nuclei, with implications for the global distribution of clouds and precipitation, and for climate (Bauer et al., 2003; Möhler et al., 2007; Morris et al., 2014, 2004; Sun and Ariya, 2006). Since bacteria are able to metabolize within cloud droplets, some authors have proposed an impact on the chemistry of cloud droplets and air (Amato et al., 2007, 2006, 2005; Ariya et al., 2002; Ariya and Amyot, 2004; Deguillaume et al., 2008). Finally, the transport of bacteria through the air is relevant to the field of microbial biogeography, the study of the geographic distribution of microbial taxa (Martiny et al., 2006). The dispersal through the air is a pathway for rapid long-distance dispersal of microbes, allowing some species to overcome geographic barriers.

Bacteria enter the atmosphere as aerosol particles from basically all surfaces, including soil, water, and plant surfaces (Burrows et al., 2009a) . Once in the air, bacteria are carried upwards by air currents and may remain in the atmosphere for many days before being removed by precipitation or direct deposition onto surfaces. Nevertheless, mechanisms controlling transport, survival and bacterial activity in the atmosphere need to be further investigated, mainly because of the complicated interactions between bacteria and their living environment.

As mentioned before, in the atmosphere PBA can undergo further chemical and physical transformation. In fact, the atmosphere not only acts as a passive transport medium, but also modifies the microphysical and chemical properties of living and dead biological matter. Bioaerosol particles can undergo fragmentation in the atmosphere, alterations surface and bulk composition or hygroscopicity, thus influencing their atmospheric transport and processing (Fröhlich-Nowoisky et al., 2016; Morris et al., 2004). Heterogeneous and multiphase chemical reactions can lead to oxidation, nitration or degradation of proteins and other primary biological substances, modifying the molecular composition and biological activity of bio-particles. For example, reactions with air pollutants (e.g., O_3 and NO_2) can enhance the allergenic potential of airborne allergens, such as pollens and spores (Lang-Yona et al., 2016; Zhao et al., 2016). In addition, the stresses induced in the airborne microorganisms such as bacteria, fungi, and viruses, influence their activity and vitality and thus their capability to colonize new habitats and to survive. This include, for those microorganisms that are pathogenic, the capability to survive in aerosol and maintain their pathogenic potential. The vitality of these organisms is dependent on their adaptation or ability to react actively to changing environmental conditions. How airborne transport affects different microorganisms and their ability to settle and then proliferate again is currently not well understood. Knowledge on how bioaerosol pathogens maintain viability/pathogenicity in such atmospheric ambient conditions is still limited.

Atmospheric stress can be considered an evolutionary force exposing airborne bioaerosols to selection pressure, thereby affecting the dispersal and evolution of microorganisms. Among the most significant stress factors are temperature, humidity, oxidative stress, starvation, radiation, and osmotic stress (Amato et al., 2015; Tong and Lighthart, 1998). Furthermore, recent studies show the significance of other atmospheric components on airborne bacteria. Atmospheric pollutants like NO_x and soot particles or dust events are hypothesized to enhance bacteria viability, by preventing bacteria from degradation processes (e.g., during UV irradiation) or inducing structural changes in their survival strategies (Bowers et al., 2011; Brotto et al., 2015; Hussey et al., 2017; Noda et al., 2021, 2019). Dust particles carrying biological materials, including bacteria with pathogenic, allergenic, and adjuvant activity, can cause and aggravate respiratory disorders (He et al., 2012; Reinmuth-Selzle et al., 2017). Laboratory experiments have demonstrated that the ice nucleation ability of dust

particles is enhanced by biological components, including bacteria in the particles (Boose et al., 2019; Conen et al., 2011; Tobo et al., 2019).

Up to now, different sampling methods and analysis techniques are adopted for study bioaerosol (Georgakopoulos et al., 2009; Lindsley et al., 1984), and infield campaigns performed around the world provide information on both the physical and biological properties of PBAP (examples: Brodie et al., 2007; Gandolfi et al., 2015). Researches on atmospheric bacteria in outdoor environments pointed out that the distribution of the bacterial populations in air masses depends on the sample provenance, furthermore they are often focused on potential correlations between the aerosol main chemical characteristics and the airborne bacterial communities (Federici et al., 2018; Petroselli et al., 2021). Nevertheless, the mechanisms of interaction between bioaerosols and other aerosols or other atmospheric constituents and the behavior of airborne microorganisms in different atmospheric conditions are still poorly known and require deeper investigation.

In this framework, my PhD work want to pave the way for systematic investigations on this topic by using a scientific intermediate approach between *in vitro* and *in vivo* analysis: aerosols with realistic composition, including living microorganisms, can be accurately studied through the use of atmospheric simulation chambers, artificial environments with controlled physical and chemical parameters. The aspiration is indeed to make available to the scientific community a new experimental platform that could bridge the knowledge gap still existing in the field of bioaerosols and air quality.

1.4 Atmospheric Simulation Chambers

Atmospheric simulation chambers (ASCs in the following) are research tools for investigating chemical and physical processes that occur in the atmosphere. Usually, the study of the relevant processes taking place in the atmosphere is pursued through a wide range of field observations where complicated and interconnected effects are often difficult to disentangle. The possibility to provide a controlled environment to study the formation and evolution of atmospheric pollutants, by isolating specific compounds of interest and environmental conditions, has triggered the conception and development of the atmospheric simulation chambers. ASCs are therefore small to large-scale facilities (with volumes ranging between a few to hundreds cubic meters) where atmospheric conditions can be maintained and monitored in real time for periods long enough to mimic the realistic environments and to study interactions among the atmospheric constituents (Finlayson-Pitts and Pitts, 2000).

The first large volume photoreactors (often referred to as smog chambers) were originally developed in the 1960s and have been used to investigate and understand many different aspects of atmospheric

chemistry related to air pollution problems, such as atmospheric oxidation mechanisms in the gas phase and the formation of photochemical smog (Becker, 2006).

Nowadays ASCs are used in many applications, ranging from air quality and climate change to cloud microphysics, cultural heritage and human health. Chamber observations are used to study chemical and photochemical processes that occur in the atmosphere, such as secondary organic aerosols (SOA) formation (Carter et al., 2005; Dodge, 2000; Finlayson-Pitts and Pitts, 2000), cloud chemistry (Wagner et al., 2006) or aerosol–cloud interaction (Benz et al., 2005). Chambers are also essential tools for validation of atmospheric chemical models, studies of atmospheric chemistry reaction mechanisms and gas phase reaction kinetics, but they can also be perfect platform for testing new analytical and technical developments such as environmental monitors.

Different design of chambers have been developed over the year (e.g., outdoor versus indoor chambers), with different associated measurement technologies and analytical facilities. As pointed out by Finlayson-Pitts and Pitts Jr., 2000, although the general aims of all chamber studies are similar, i.e., to simulate reactions in ambient air under controlled conditions, the number of combinations in design criteria and properties makes these reactors to be more complementary than redundant and means that chambers are being adapted to a growing number of applications.

Simulation chambers are not without limitations or possible artifacts. There are some critical aspects to keep in mind when designing an atmospheric simulation chamber or approaching experiments inside this kind of facility. For example, chamber walls are crucial elements where reactions can occur and affect the realism of the simulation. As a result, background levels, off-gassing materials or memory effects can complicate the outcomes of the experiments (Dodge, 2000; Wang et al., 2011). Size and material are therefore important parameters. For comparable shapes, the larger the reactor, the smaller the surface-to-volume ratio (S / V), and therefore the less important the unwanted surface reactions. Large volume is also desirable for the use of several analytical instruments developed for field measurements, which commonly have sampling rates in the range of liters per minute. Usually, for technical and economic reasons, size and material are often strongly correlated: most of the bigger chambers (more than few tens cubic-meters) are made of Teflon® film (Cocker et al., 2001; Ren et al., 2017; Zádor et al., 2006) and are often installed outdoors with natural solar light. On the contrary, smaller chambers are typically indoor and they can be made with various materials, such as Teflon® film (Carter et al., 2005), Pyrex® (Doussin et al., 1997), quartz (Barnes et al., 1994) or stainless steel (Wang et al., 2011). These indoor chambers are generally equipped with irradiation systems such as black fluorescent lamps (Becker, 2006; Cocker et al., 2001) or xenon arc lamps (Carter et al., 2005; Wang et al., 2011), with the irradiation and transmitted spectrum inside the chamber more or less comparable with the solar spectrum.

A full list and review of the approach and of the main facilities around the world can be found in Becker (2006), Seakins (2010) or Finlayson-Pitts and Pitts Jr. (2000).

In Europe, there are several ASCs, so far organized through the network EUROCHAMP-2020 (https://www.eurochamp.org) and presently included in the larger ACTRIS infrastructure (Aerosols Clouds and Trace gases Research Infrastructure, https://www.actris.eu) and in the on-going ATMO-ACCESS project (https://www.atmo-access.eu). The EUROCHAMP project promoted the integration of the most advanced European atmospheric simulation chambers into a world-class infrastructure for research and innovation, now moved into the ACTRIS project. More details as well as an updated list of the most recent ASCs works are available at the link https://www.eurochamp.org.

1.4.1 ASCs and bioaerosol

ASCs have been widely used to study chemical and photochemical atmospheric processes, but the high versatility of these facilities allows for a wider application covering all fields of atmospheric aerosol science. For example, a consistent improvement in characterizing bioaerosols, in understanding the mechanisms affecting their behavior in the atmosphere and finally in elucidating their impacts can be provided by the use of atmospheric chamber facilities, where transdisciplinary studies gathering atmospheric physics, chemistry, and biology issues are possible.

In the last decades, the use of atmospheric simulation chambers has been much more focused on the potential interest of bioaerosol as ice nuclei and cloud condensation activity (Möhler et al., 2008b; Bundke et al., 2010; Chou, 2011). Recently, considering the public health issue related with bio-aero-contamination, the number of unknowns about the survival and the transformation of bioaerosols in the atmospheric environment, innovative chamber works have been started to address these questions (Amato et al, 2015, Brotto et al, 2015). These works have led to the development of a new dedicated indoor simulation chamber, ChAMBRe (Chamber for Aerosol Modelling and Bio-aerosol Research). The chamber, installed at the National Institute of Nuclear Physics in Genoa (INFN-Genova, www.ge.infn.it) in collaboration with the Environmental Physics Laboratory at the Physics Department of Genoa University (www.labfisa.ge.infn.it), is a node of the EUROCHAMP2020 network and partner of the ACTRIS initiative. The main scientific target related to ChAMBRe is the description of biological micro-organisms behavior in the atmosphere and the development of analysis and forecasting tools for socio-economic and healthcare applications. The main result expected is a deeper understanding of the still unclear mechanisms that control the evolution of bioaerosols (bacteria in particular) in the atmosphere. The long-term goal is the parameterization of survival and activity of bioaerosols, in order to develop a specific software to be implemented in chemical transport models, which are presently limited to the dispersion of not-biological pollutants.

2. The ChAMBRe facility

2.1 ChAMBRe main structure

CHAMBRe is a stainless steel chamber with cylindrical shape with maximum height and diameter of 2.9 and 1 m, respectively, and with a total volume of around 2.2 m^3 (Figure 2.1). The main body is divided into two domed cylinders (see Figure 2.1) connected by a central ring at a 60 cm height. The lower dome has a bottom aperture with a pass through for the shaft of a fan and two lateral ISO-K250 flanges. The central ring allocates different flanges, two with a diameter of 40 cm and four with a diameter of 10 cm. The top cylinder is equipped with two symmetrical ISO-K100 flanges plus another flanged aperture (ISO-K250) on the dome. One of these two flanges is connected through a pneumatic valve to a smaller horizontal cylinder (length 1 m), which hosts a movable shelf designed to move specific samples inside the chamber, as described in the following paragraph 2.3.4. The second ISO-K250 flange of the lower cylinder is connected to a composite pumping system (a rotary pump model TRIVAC® D65B, Leybold Vacuum, followed by a root pump model RUVAC WAU 251, Leybold Vacuum, and a Leybold Turbovac 1000), which can evacuate the internal volume to a vacuum level of about 10^{-5} mbar. A safety valve (Leycon Secuvac DN 63, Oerlikon Leybold Vacuum), mounted between the pumping system and ChAMBRE, guarantees, in the event of a power failure, to automatically isolate the chamber in less than 1 ms, thus preventing possible oil backwashes of the pumps inside the chamber. To return to atmospheric pressure, ambient air can enter the chamber throughout a five-stage filtering/purifying/drying inlet system (including a HEPA filter, model: PFIHE842; 99.97% efficient at 0.3 μm), which reduces the ambient relative humidity to about 15 % (possibly lowered down to 0% by filling the chamber directly with synthetic air from a cylinder). This filtering system ensures an excellent purification of the air entering the chamber. After venting, particle and gas concentrations inside the chamber are lower than the typical environmental values and close to the particle counters and gas monitors sensitivity (for a more detailed description of the chamber cleaning procedure and the background levels, see paragraph 2.5.1).

Acquisition and control of devices connected to ChAMBRe are handled by a National Instruments based system made up of a main controller (NI9057 cRIO) and several modules (C Series modules), which allow communication with the peripheral devices via analog, serial, and ethernet data exchange. A custom NI Labview SCADA (supervisory control and data acquisition) application

allows the user to interact with the system using a user-friendly graphical interface. A full description of the facility is reported in Massabò et al., 2018.

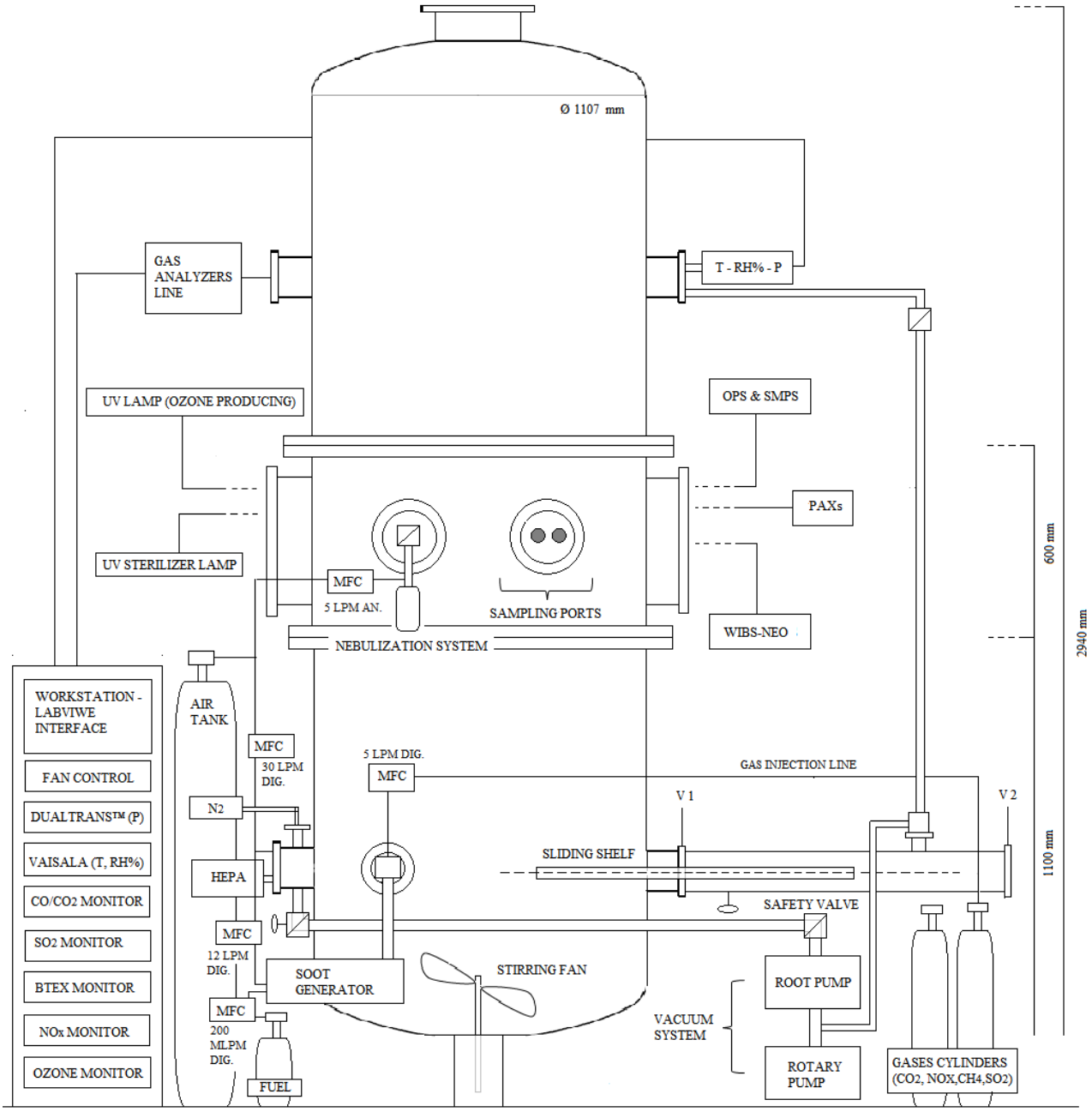

Figure 2.1 ChAMBRe layout.

2.2 Basic equipment

To favor the mixing of the gas and aerosol species in the reactor a fan is installed in the bottom part of the chamber (Figure 2.1). The fan speed can be regulated by an external controller and varied between 0.0 and 50 Hz in steps of 0.1 Hz (0 to 3000 rpm, in steps of 6 rpm).

An MKS Instruments 910 Dual- Trans™ transducer is installed inside the chamber (measuring range: from 5×10^{-4} to 2×10^{3} hPa; accuracy of ±0.75% of the reading in the range of 15–1000 hPa). A Vaisala BAROCAP® Barometer PTB110 is installed in the laboratory outside the chamber with a measuring range from 5×10^{2} to 1.1×10^{3} hPa and accuracy of ± 0.3 hPa at 20 °C.

Water vapor can be directly injected into ChAMBRe, thus adjusting the relative humidity inside the chamber from about 15% to about 99 %. Temperature and relative humidity (RH %) inside the chamber are monitored using a HMT334 Vaisala® Humicap® transmitter. In the operative range (from 15 to 25 °C), the RH accuracy is ± 1% RH (0% to 90% RH) and ± 1.7% RH (90% to 100% RH); the temperature accuracy is ± 0.2 °C at 20 °C.

ChAMBRe is also equipped with a sterilization system: a 58 cm long UV lamp (UV-STYLO-F-60H, Light Progress Srl) can be insert through a lateral flange without perturbing the internal conditions. The lamp produces 60W UV radiation at $\lambda = 253{,}7$ nm, which is used to sterilize the chamber volume without producing ozone before or after any experiment with bioaerosols.

Two different mercury lamps (length = 5 cm, power = 6W and length = 20 cm, power = 10W; both of BHK Incorporated, Analamp models), producing UV radiation at $\lambda < 240$ nm, can be inserted through one of the ISOK100 flanges of the central ring to generate ozone.

2.3 Instruments connected to ChAMBRe

The large number of free flanges and ports in the main structure gives the possibility of connecting several external instruments to ChAMBRe.

2.3.1 Gas Analyzers

Ambient gas monitors from Envea, model O342e, AC32e, CO12e, AF22e, and VOC72M, continuously measure the concentration of ozone, nitrogen oxides, carbon monoxide and dioxide, sulfur dioxide, and BTEX (benzene, toluene, ethylbenzene and the three xylene isomers), inside the chamber volume.

2.3.1.1 O342e

The O342e uses a system based on the Lambert–Beer law for measuring ozone in ambient air. A 254 nm UV light signal is passed through the sample cell where it is absorbed in proportion to the amount

of the ozone present (maximum range of ozone absorption 250-270 nm). Periodically, a switching valve alternates measurement between the sample stream and a sample that has been scrubbed of ozone. The instrument has a sampling rate of approximately 1 L min^{-1}, a response time of 20 s and a detection limit of 0.2 ppb.

2.3.1.2 AC32e

The AC32e utilizes the principle of chemiluminescence, which is the standard method for the measurement of NO and NO_2 concentration (EN 1421), for automatically analyzing the NO-NO_x and NO_2 concentration within a gaseous sample. The analyzer measures the photons emitted after the reaction between NO and O_3 (eq. 1 and 2). The analyzer initially measures the NO concentration in the sample, through NO ozone oxidation. Subsequently, the sample passes through the heated molybdenum converter, which reduces NO_2 to NO (eq. 3) and is then mixed with ozone in the reaction chamber and the resulting NO concentration is determined. In this way, the signal is proportional to the sum of the molecule NO and NO_2 (reduced to NO in the converter) in the sample.
The chemilunescence reaction and the reduction processes can be summarized as follow:

$$NO + O_3 \rightarrow NO_2^* + O_2 \quad (1)$$

$$NO_2^* \rightarrow NO_2 + hv \quad (2)$$

$$Mo + 3NO_2 \rightarrow MoO_3 + 3NO \quad (3)$$

With a sampling rate of 0.66 L min^{-1} this instrument reaches a detection limit of 0.2 ppb with a response time of 40 s.

2.3.1.3 CO12e

The CO12e is a continuous carbon monoxide analyzer. Its measurement principle is based on carbon monoxide detection by absorption of infrared light. The concentration of CO in the sample is determined by measuring the quantity of infrared light, at the specific wavelength of 4.67 μm, absorbed by the sample gas as it flows through a multi-reflection chamber. The model available at ChAMBRe provides also for a built-in module for CO_2 monitoring (range: 0-2000 ppm by NDIR). The instrument has a sampling rate of approximately 1 L min^{-1}, a response time of 20 s and a detection limit of 0.05 ppm.

2.3.1.4 AF22e

The AF22e is based on the ultraviolet fluorescence, which is the standard method for the measurement of SO_2 concentrations in ambient air (EN 14212). A hydrocarbons scrubber guarantees the elimination of hydrocarbon interferences. The hydrocarbons free sample is sent to a reaction chamber to be irradiated by an UV radiation centered at 214 nm, which is the SO_2 molecule absorption

wavelength. The fluorescence is optically filtered between 300 and 400 nm to eliminate some interfering gases. With a sampling rate of 0.4 L min^{-1} this instrument reaches a detection limit of 0.4 ppb with a response time of 20 s.

2.3.1.5 VOC72M

The VOC72e's metrology, in accordance with EN 14662-3 standard for benzene measurement, is based on gas chromatography (GC) coupled with a photo-ionization detector (PID). The VOC72e performs three main functions: the sampling, the GC analysis and the data processing. The sampling is achieved with a single trap filled with a specific sorbent. Its flow through the trap is about 12 ml min^{-1} which gives a sampled volume of 165 ml with the standard 15 minute cycle (sampling time >90% of cycle time). At the end of the sampling cycle, the trap is connected to the GC column and quickly heated from 35 to 380°C within 2 seconds. The compounds are thermally desorbed and flushed with hydrogen into the GC column. Then the trap is cooled with a fan for a new sampling cycle. Inside the GC column, the compounds are moved forward by the hydrogen flow (the mobile phase) and retained by the internal coating (the stationary phase) causing a selective retardation of the compounds. In order to achieve an optimal separation within a minimal time, the GC column follows a multi slope thermal cycle from a cold step (25°C) for the injection to a hot step (160°C) for flushing all the heavy compounds (i.e. compounds with a high boiling point). At the end of the hot step, the GC column is cooled to the cold step for the next cycle. The GC column output is connected to a photo ionization detector where the compound concentration is converted into a small electric signal. The PID detector includes a 10.6 eV UV lamp that is able to ionize all the compounds which ionization potential (IP) is less than 10.6 e V. The 240 volt electric field between the polarization electrode (-240 volt) and the signal electrode (0 volt) moves the ionized particles (positive ions and negative electrons) towards the electrodes creating a small electrical conduction. The resulting electric signal is amplified and digitalized in the electrometer board. Its recording gives the chromatogram which exhibits a peak for each detected compound. The standard measured compounds are Benzene, Toluene, Ethylbenzene, m+p-Xylene, o-Xylene, 1-3 Butadiene. Sample flow is around 50 mL min^{-1}, with a low detection limit of ≤ 0.05 µg m^{-3} (benzene).

2.3.2 Particle counters

Particles concentration inside ChAMBRe can be monitored by three different instruments: a Scanning Mobility Particle Sizer (SMPS, Model 3938 TSI, Inc.), an Optical Particle Sizer Spectrometer (OPS, Model 3330, TSI, Inc.) and a Wideband Integrated Bioaerosol Sensor (WIBS-NEO, Droplet Measurement Technologies).

2.3.2.1 OPS

The Model 3330 OPS is an optical particle sizer spectrometer that provides measurement of particle number concentration and particle size distribution based on single-particle counting technology. The OPS has an inlet flow rate of 1.0 L min^{-1} ± 5% and measures particles from 0.3 µm to 10 µm in 16 user-adjustable size channels (particles above 10 µm are counted but not sized). The OPS 3330 works on the principle of optical scattering from single particles. The OPS uses a laser beam (λ = 660 nm) and a detector to detect particles passing through a sensing volume illuminated by the laser. As shown in Figure 2.2, particles pass through the beam and light scattered by the particles is picked up by an elliptical mirror and focused onto the photodetector. Particle pulses are counted individually and binned in to the 16 channels based on their pulse heights. The OPS measures particle concentration by counting individual pulses from the photodetector while pulse heights are proportional to the optical particle size. The OPS is factory calibrated using different monodispersed Polystyrene Latex particles (PSL) for size classification; size resolution is 5% at 0.5 µm per ISO 21501-1. Particles exiting the chamber are trapped by a gravimetric filter for eventually chemical analysis after the sampling.

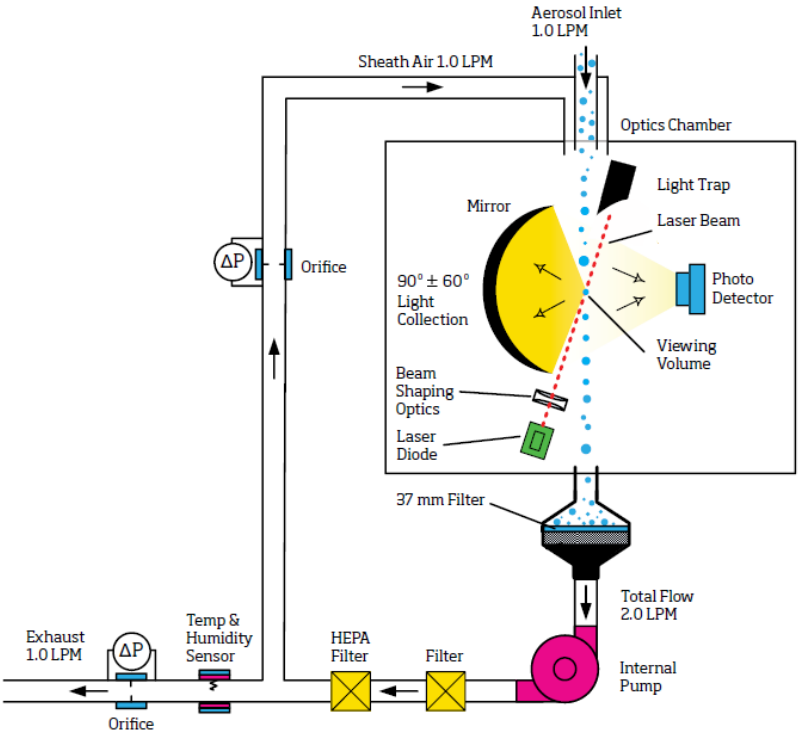

Figure 2.2 Sample Flow Path in the OPS Model 3330, adapted from OPS manual.

2.3.2.2 SMPS

The SMPS is formed by three components: a neutralizer (i.e. a bipolar diffusion charger), a differential mobility analyzer (DMA, series 3080) and a condensation particle counter (W-CPC,

model 3789), from TSI Inc. A schematic representation of an SMPS is reported in Figure 2.3. The model 3088 Neutralizer uses a low-energy (<9.5keV) soft X-ray source to generate high concentrations of both positive and negative ions to bring the aerosol to a defined, steady-state charge distribution. The DMA is available with two different columns: model 3081 Long DMA, which provides the widest size range of 10-1000 nm, and the model 3085 Nano DMA, which covers the range of particle diameter from 2 and 150 nm. In a DMA, an electric field is created and the airborne particles drift in the DMA according to their electrical mobility (Figure 2.4). Particle size is then calculated from the mobility distribution. In the CPC, downstream of the DMA, the particle size is increased by water condensation on their surface and then the particles are optically counted (Figure 2.4). The maximum measurable concentration can reach 2×10^5 particles cm^{-3}. Both the CPC and the SMPS are operated at an airflow of 0.3 L min^{-1}.

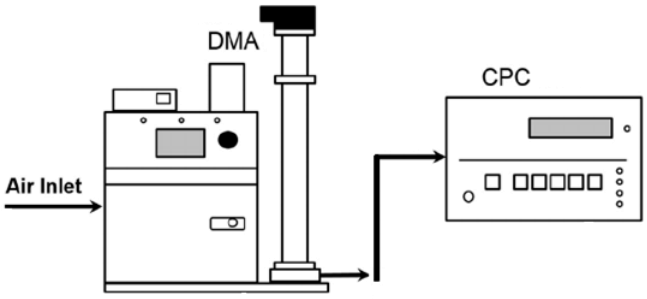

Figure 2.3 Schematic representation of an SMPS.

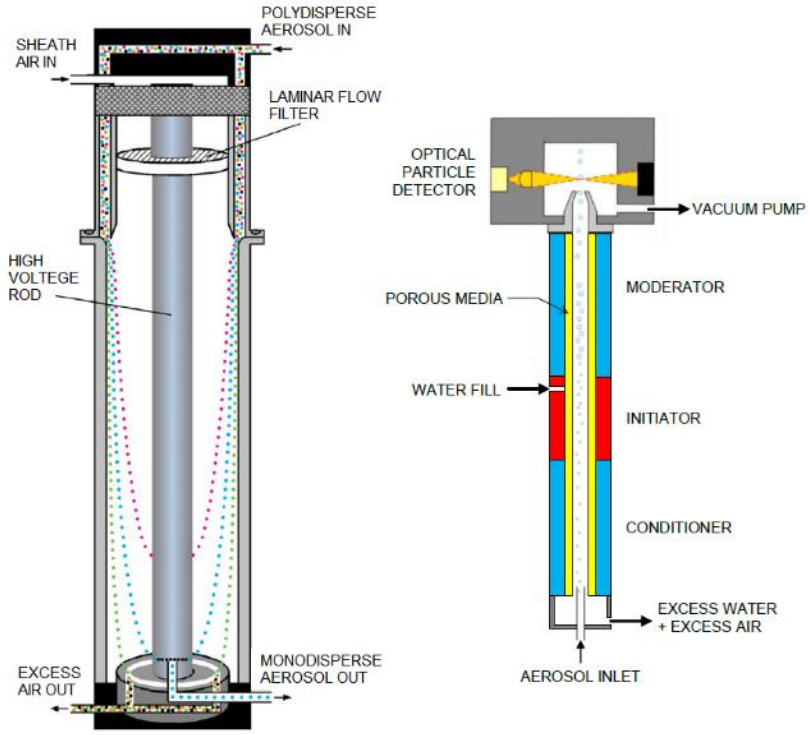

Figure 2.4 DMA 3081 and W-CPC flow schematic representation.

2.3.2.3 WIBS-NEO

The Wideband Integrated Bioaerosol Sensor-New Electronics Option (WIBS-NEO) is designed to provide the size-segregated, real-time monitoring of bio-aerosol particles. The original WIBS detector was developed by the University of Hertfordshire and is licensed to and manufactured by Droplet Measurement Technologies, Longmont, CO, USA. WIBS analysis and detection of bioaerosols is based on ultraviolet light-induced fluorescence (UV-LIF).

As shown in Figure 2.5, this single-particle fluorescence sensor employs a central optical chamber around which are arranged the following components:

1. A continuous-wave, 635 nm diode laser used as a light scattering source for particle sizing and shape detection.
2. A quadrant photomultiplier tube (PMT) used to determine particle shape from forward scattered light.
3. Two pulsed Xenon sources emitting at different UV wavelengths (Xe1 at λ_1 = 280 nm, Xe2 at λ_2 = 370 nm).
4. Two fluorescence detector channels: FL1 (310-400 nm), which detects particle fluorescence emission and FL2 (420-650 nm), which detects particle fluorescence emission, particle count, and particle size.

The two excitation wavelengths and two emission bands were selected to optimize detection of common components of bioaerosols, i.e., the amino acid tryptophan and the coenzyme NADH.

WIBS provides the number and size distribution (between 0.5 and 30 µm) of all the aerosol particles by the analysis of the scattering of the light of the laser beam at 635 nm. The side-scattered light is collected by two mirrors and detected by the FL2 detector. The light is converted to an electrical pulse, which is used to size the particle and trigger the UV flash lamps to fire in succession. Particles pass through the two excitation wavelengths (λ_1 = 280 nm and λ_2 = 370 nm) and the possible fluorescent emission is monitored in two emission bands: FL1, filtered to detect fluorescence emission only in the 310 to 400 nm range, and FL2, filtered to detect fluorescence emission only in the 420-650 nm range. For each particle, from the laser light scattered in the forward direction, a semi-quantitative asphericity factor is finally measured as the root mean square variation across a quadrant photomultiplier.

The measurement cycle of particles flowing inside the WIBS is represented in Figure 2.6.

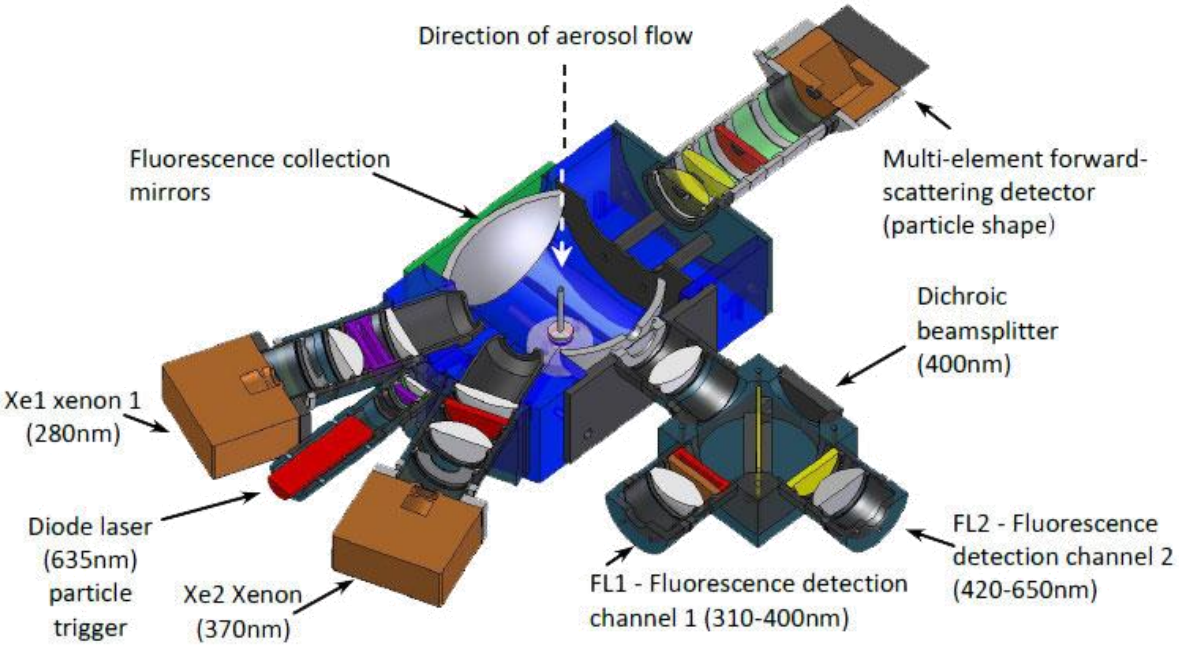

Figure 2.5 WIBS-NEO design and optical configuration.

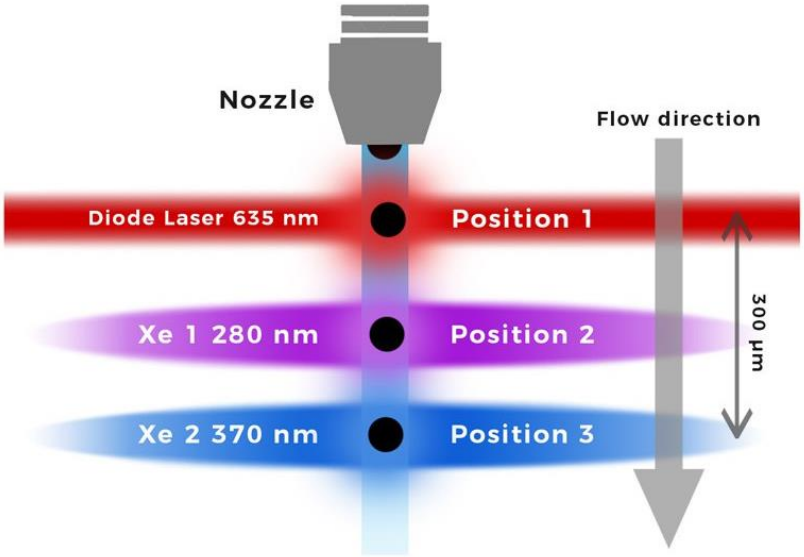

Figure 2.6 WIBS measurement cycle.

For each particle, the WIBS provides five essential pieces of information:

- Equivalent optical diameter (EOD)
- Fluorescence peak from excitation by the 280 nm and response at 310-400 nm (FL1)
- Fluorescence peak from excitation by the 280 nm and response at 420-650 nm (FL2)
- Fluorescence peak from excitation by the 370 nm and response at 420-650 nm (FL3)
- Shape factor (asphericity)

The instrument classifies particles into 13 categories, as reported in Table 2.1, based on their fluorescence characteristics.

Table 2.1 Classification of particles

All	All particles
Excited	Particles excited by the flash lamp
Fluorescent	Fluorescent particle detected in any channel
FL1	Fluorescent particles detected in channel FL1
FL2	Fluorescent particles detected in channel FL2
FL3	Fluorescent particles detected in channel FL3
A	fluorescent particle detected in channel FL1 only
B	fluorescent particle detected in channel FL2 only
C	fluorescent particle detected in channel FL3 only
AB	fluorescent particles detected in channels FL1 and FL2 only
AC	fluorescent particles detected in channels FL1 and FL3 only
BC	fluorescent particles detected in channels FL2 and FL3 only
ABC	fluorescent particles detected channels FL1, FL2, and FL3

In Table 3.5, *All particles* refer to the total number of the particles not rejected by any criteria counted by the 635 nm laser beam. This number is used by the instrument to calculate the total particle concentration (count cm^{-3}). *Excited particles* refer to the total number of particles not rejected by any criteria and that have been excited, i.e., lighted by the UV flashlamps. This number is used for the particles excited concentration calculations (count cm^{-3}). *Fluorescent particles* indicate particles that give a fluorescence emission, in any one of the three fluorescence channels, with an intensity

exceeding the baseline threshold, defined as the average + 3 standard deviation of the Force Trigger, FT (Gabey et al., 2010). FT data are the background data recorded without particles flow. *FL1*, *FL2* and *FL3* indicate particles that give a fluorescent emission in each specific fluorescence channel. For example, a particle that shows fluorescence peaks above the FT threshold in both the detector (FL1 and FL2) caused by the Xe1 flashlamp excitation, is categorized as a *FL1* and *FL2* particle. A particle that shows fluorescence peak in the first detector following the excitation from the Xe1 lamp and a further fluorescence peak in the second detector, caused by the Xe2 lamp excitation, is categorized as a *FL1* and *FL3* particle (use Figure 2.5 for references). Depending on how the particle fluorescence signals are measured, in single channels only or in multiple combinations, particles can be further categorized into seven fluorescent particle types: A, B, C, AB, AC, BC, or ABC. Figure 2.7 clearly outlines the WIBS fluorescent particle type classification. In the figure, each circle represents one fluorescence channel (FL1, FL2 and FL3) and the colored zones represent particle types that exhibit fluorescence in one, two, or three channels.

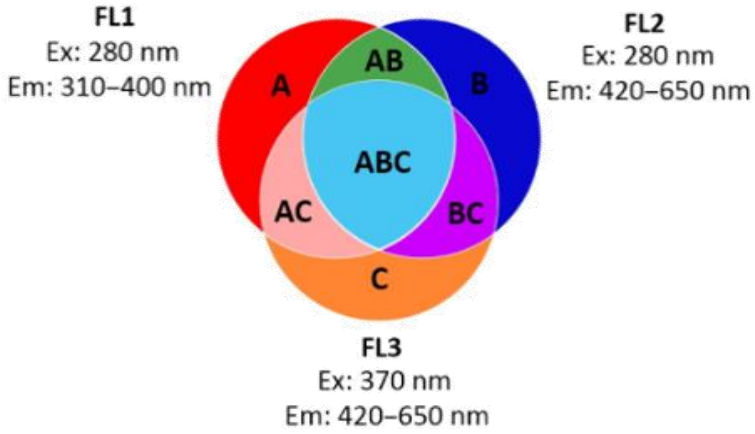

Figure 2.7 WIBS fluorescent particle type classification (Savage et al., 2017).

From the fluorescence information and the size distribution of the particles measured with the WIBS, users can be able to categorize biological particles, e.g. pollen vs. fungi vs. bacteria. Laboratory characterization of biological particles samples shows that fluorescence and size characteristics are similar within a bioaerosol particle type (e.g. pollen, bacteria, fungi) (Hernandez et al., 2016). WIBS-NEO is factory calibrated with standard monodisperse polystyrene latex microspheres. The maximum nominal concentration for particle counting is ~ 2×10^4 particles L^{-1} (full measurement at 10% coincidence). A recent work shows that in the range of bacteria size (0.9 – 2 μm) WIBS NEO shows its best counting efficiency (close to 90%) and provides precise sizing for particle within this size range (Lieberherr et al., 2021). The sample flow rate is 0.3 L min^{-1} with a 2.1 L min^{-1} as sheath flow in a recirculation mode, filtered before being re-introduced.

2.3.3 Aerosol optical properties measurements

Three Photoacoustic Extinctiometers (PAXs, Droplet Measurement Technologies, Boulder, CO, USA) are deployed at ChAMBRe to measure aerosol optical properties at λ = 405 nm, 532 nm and 870 nm. The PAX directly measures in-situ light absorption and scattering of aerosol particles, from which it derives extinction, single scattering albedo and black carbon mass concentration. PAX uses a modulated diode laser to simultaneously measure light scattering and absorption. The standard infrared, 870 nm wavelength option, is highly specific to black carbon particles, since there is relatively little absorption from gases and non-BC aerosol species at this wavelength. A nominal 1 L min^{-1} aerosol sample flow is drawn into the PAX using an internal vacuum pump controlled by two critical orifices. The flow is split between the two distinct measurement regions: a nephelometer, for the light scattering measurement and a photoacoustic resonator for the absorption measurement. Absorbing particles heat up and quickly transfer heat to the surrounding air. A sensitive microphone detects the pressure waves produced by the heating, which intensities are interpreted to infer the particle absorption coefficient (Moosmüller et al., 2009). In the nephelometer, a photodiode set at 90° respect to the beam detects the radiation reflected by the sampled particles. The scattering measurement responds to all particle types regardless of chemical makeup, mixing state, or morphology. The operative scheme of the PAX instrument is shown in Figure 2.8.

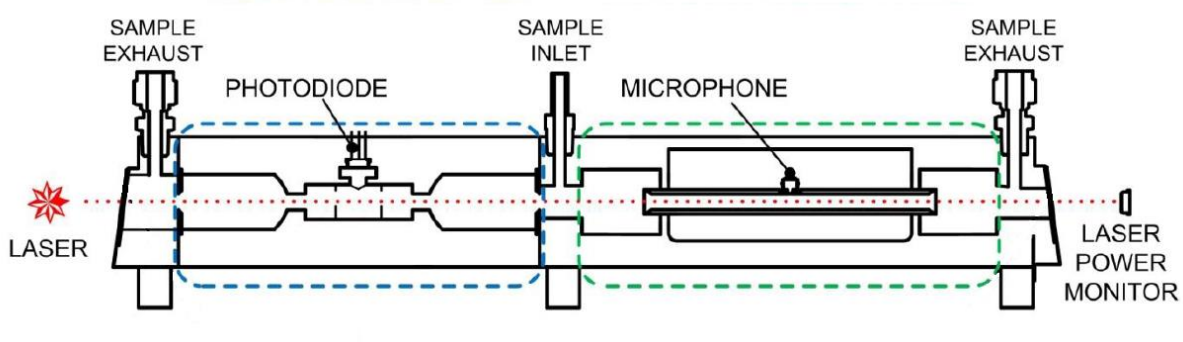

Figure 2.8 Diagram showing the scattering region (blue dashed box, nephelometer) and absorption region (green dashed box, photoacoustic cell) in the photoacoustic extinctiometer. (Figure adapted from PAX manual).

2.3.4 Bioaerosol samplers

The main body of ChAMBRe is connected through an ISOKF250 pneumatic valve (V1) to a cylindrical horizontal volume, which is accessible from a second ISO-KF250 gate valve (V2) (see Figures 2.1 and 2.9). The two gate valves completely separate the cylinder, which can be connected to the main chamber or alternatively opened without perturbing the ChAMBRe atmosphere. This tool has been specifically developed to ensure the insertion and extraction of different object, in order to minimize the risk of contamination. Inside the cylinder, there is a sliding tray that can be inserted in ChAMBRe by an external manual control (Figure 2.9). The tray can host up to six Petri dishes (diameter 10 cm, each) to collect bacteria (or in general BPA) directly by deposition onto a proper culture medium. The gravitational settling method has been adopted to collect and count viable bioaerosol sample, in order to minimize microbial damage. The procedure to insert the Petri dishes in ChAMBRe is reported in Ch. 3, par. 3.1.5.

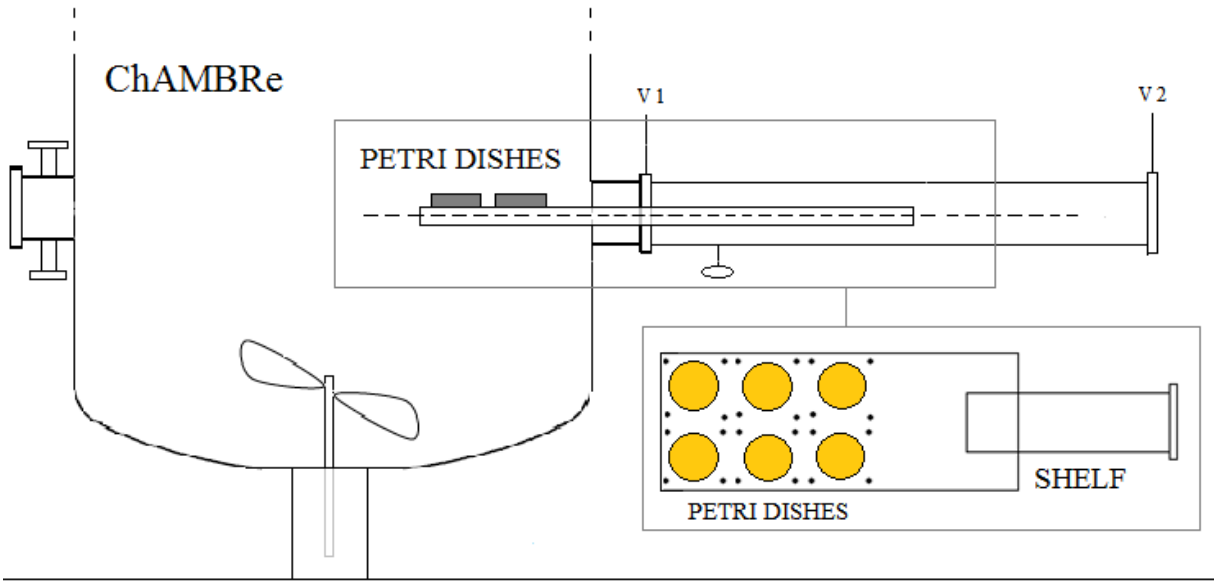

Figure 2.9 A schematic view of the cylindrical volume that hosts the sliding tray used to introduce up to six Petri dishes (or other objects) inside the main ChAMBRe body.

Moreover, bioaerosol can be collected thought liquid impinger, (Flow Impinger, Aquaria srl), filled with 20 mL of sterile liquid solution, allowing subsequent offline laboratory analysis. Such device can be easily connected to the chamber volume through the ISO-K flanges. Impinger operates at a constant airflow of 12.5 L min^{-1} (e.g. by a low capacity pump: Model LCP5, Copley Scientific).

Table 2.2 ChAMBRe instrumentation summary.

Media	Instruments/Reference	Measured quantity	Sampling (method/time)	LDL/Accuracy
Gas	NO_x monitor Envea AC32e	NO_x (NO_2)	Continuous 40 s	0.2 ppb
Gas	O_3 monitor Envea O342e	O_3	Continuous 20 s	0.2 ppb
Gas	SO_2 monitor Envea AF22e	SO_2	Continuous 20 s	0.4 ppb
Gas	VOCs monitor Envea VOC72M	BTEX	Cartridges 15 min	0.02 ppb
Gas	CO/CO_2 monitor Envea CO12e	CO/CO_2	Continuous 20 s	0.05 ppm
Gas	HMT334 Vaisala® Humicap® transmitter	Relative Humidity	In situ 60 s	1%
Aerosol phase	SMPS System TSI DMA model 3080 TSI W-CPC model 3789	Aerosol size distribution and concentration	Continuous	10 to 1000 nm Max. input conc. 10^8 particles cm^{-3} at 10 nm
Aerosol phase	Optical particle sizer TSI OPS model 3330	Aerosol size distribution and concentration	Continuous	0.3 to 10 µm Max. input conc. 10^4 particles cm^{-1}
Aerosol phase	UV-LIF bio-aerosol sensor DMT WIBS-NEO	Aerosol size distribution and concentration	Continuous	0.5 to 30 µm Max. input conc. 2×10^4 particle L^{-1} (full measurement)
Aerosol phase	Photoacoustic Extinctiometers DMT PAXs (405, 532, 870 nm)	optical properties	Continuous < 10 s	< 1 Mm^{-1} - 100000 Mm^{-1} (870 nm)
Physical parameter	HMT334 Vaisala® Humicap® transmitter	Temperature	In situ 60 s	± 0.2 °C
Physical parameter	Pressure Gauges MKS 910 Dual-Trans™ Vaisala BAROCAP® PTB110	Pressure	In situ	±0.75% ± 0.3 hPa

2.4 Aerosol production systems

2.4.1 Nebulization systems

At ChAMBRe three nebulizers, designed for bioaerosol applications, are available: the Collison nebulizer, the Blaustein Atomizing Modules (BLAM), and the Sparging Liquid Aerosol Generator (SLAG), all manufactured and distributed by CH TECHNOLOGIES Inc.

2.4.1.1 Collison nebulizer

The Collison instrument is a pneumatic nebulizer with widespread applications. This device generates droplets by physical shearing and impaction onto a vessel wall. The solution to be sprayed is positioned directly in the glass jar. A flow of compressed air is used to aspirate the liquid from the reservoir into a sonic velocity air jet, wherein the liquid is sheared into droplets. The resulting liquid jet impacts against the wall of the jar, removing the larger fraction (in size) of the droplets. The resulting smaller droplets are carried out by the airflow while the larger particles return to the liquid reservoir are then re-aerosolized (May, 1973).

At ChAMBre the one-nozzle version of the Collison nebulizer is available. The upstream pressure can span in the 1–6 bar range, which corresponds to an airflow rate from 2 to 7 L min $^{-1}$ for the one-jet model. A schematic of the Collison device is reported in Figure 2.10.

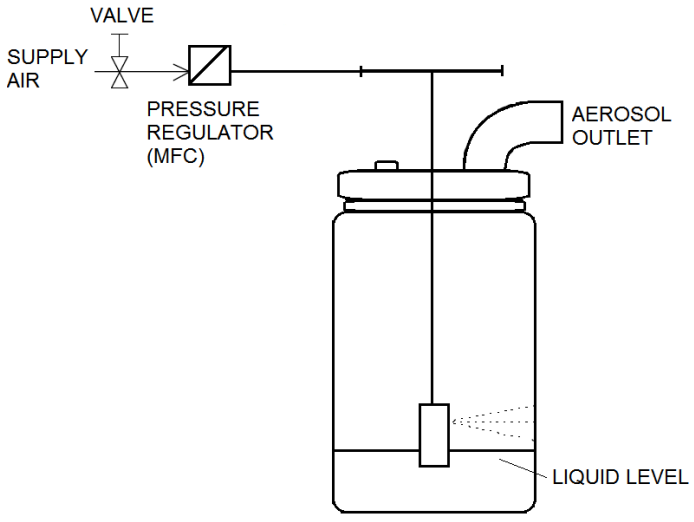

Figure 2.10 Schematic diagram of Collison nebulizer. Extracted and modified from the Collison user manual.

The main disadvantage of this device is the recirculation of the liquid; the repetitive exposure to shear forces during atomization and impaction against the vessel wall can progressively cause damage and loss of viability to biological entities (Zhen et al., 2014).

Several literature studies on the Collison nebulizer performance report high particle concentrations but with resulting cell damage, especially during prolonged nebulization and with those microbes with a cell membrane, such as bacteria (Mainelis et al., 2005; Reponen et al., 1997; Thomas et al., 2011; Zhen et al., 2014).

2.4.1.2 Blaustein Atomizing Modules

The single-jet BLAM nebulizer is an improvement of the pneumatic nebulization without liquid recirculation, aiming to reduce the damage to bacterial culturability and structural integrity. The BLAM module is a single-pass atomizer where the liquid medium is subjected to the sonic air jet only one time. The atomizing head is composed of two main parts: nozzle body and expansion plate (Figure 2.11). The atomizer features a modular design, composed of five interchangeable plates (Table 2.3) with different cavity depth and cone diameter to accommodate liquids with different properties (mainly viscosity).

Table 2.3 Characteristics of BLAM expansion plates.

Plate ID	Cavity Depth (inch)	Cone Diameter (inch)
1-20	0.001	0.020
1-30	0.001	0.030
4-30	0.004	0.030
4-40	0.004	0.040
10-40	0.10	0.040

The atomization process is generated using a vacuum effect produced in the cavity between the body of the nozzle and the expansion plate when pressurized air passes at sonic velocity through a precisely laser cut ruby crystal (fixed size of 0.025 cm in diameter) located in the nozzle body (Figure 2.11). This effect pushes the liquid hosted in the cavity into the air jet, which breaks up the liquid into droplets. Only the droplets smaller than a certain critical size can follow the airflow to the outlet tube located on top of the BLAM unit; this critical size is determined by the speed of the airflow through the nebulizer. The jar should be filled with 20 mL of test solution, which serves only as a soft impact surface for the larger droplets; it is not used for atomization. The liquid is delivered to the nozzle body with a desired flow rate (range of liquid feed rate: 0.1 – 6 mL min^{-1}) using a precision pump (NE-300 Just Infusion™ Syringe Pump, New Era Pump Systems, Inc.). The upstream air pressure

determines the resulting airflow rate in the range of 1 to 4 L min^{-1}, which is kept constant using a mass flow controller. The properties of the aerosol generated by the single-jet BLAM nebulizer are, nominally, a function of the jet hole size, depth of the liquid cavity, expansion cone size, and liquid viscosity (see APPENDIX A). A schematic of the Single-Jet BLAM setup is reported in Figure 2.12.

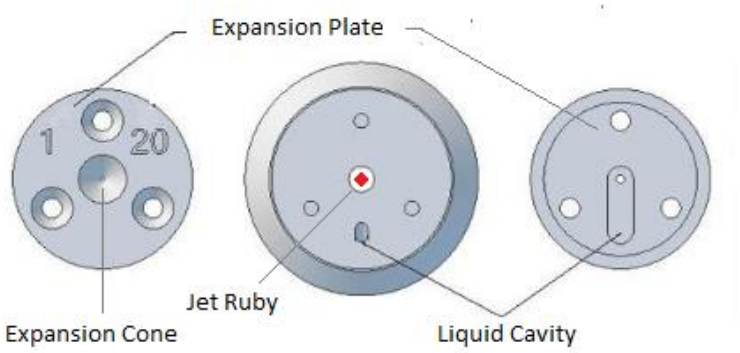

Figure 2.11 Components of the BLAM nozzle body. Extracted and modified from the BLAM user manual.

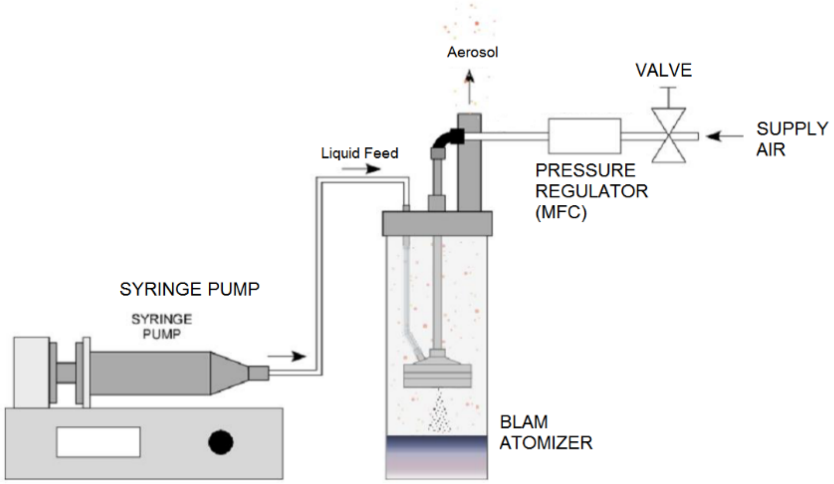

Figure 2.12 Schematic Single-Jet BLAM-setup. Extracted and modified from the BLAM user manual.

2.4.1.3 Sparging Liquid Aerosol Generator

The SLAG model is a single-pass bubbling generator where a suspension of particles or microorganisms is pumped at a certain flow rate to the top surface of a porous stainless-steel disc where it forms a liquid film (Mainelis et al., 2005). The airflow is delivered through the porous disc creating fine bubbles in the liquid film that subsequently burst, releasing particles into the air. Particles are carried out of the device by the same air stream. The SLAG nebulizer available at ChAMBRe is equipped with a 1.9 cm-diameter porous disc with nominal pore size of 2 μm. The recommended airflow ranges between 2 and 6 L min^{-1} and it is set using a mass flow controller. This principle of gentle bubbling aerosolization is expected to reduce stress and damage to microorganisms compared to pneumatic nebulization (Simon et al., 2011). A schematic of the SLAG device is reported in Figure 2.13.

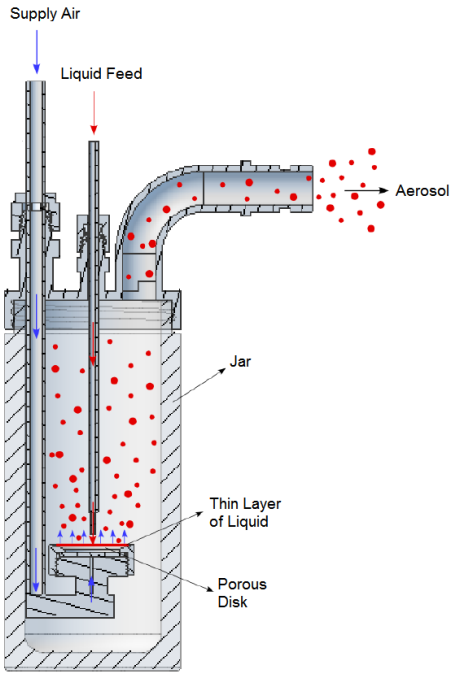

Figure 2.13 Schematic SLAG method. Extracted and modified from the SLAG user manual.

2.4.2 Soot generator

A Miniature Inverted Soot Generator (MISG, Argonaut Scientific) gives the possibility to generate soot particles. MISG, represented in Figure 2.14, is a miniaturized version of a traditional flame burner with the feature of using a downward-flowing diffusion flame to generate soot particles. This characteristic improves the burner flame stability (Bischof et al., 2020). Concentration and size of soot can be changed by varying fuel or airflow rates. The generator consists of two co-annular tubes that provide the fuel and co-flow air and can be feed with different fuels as ethylene, propane, ethane or fuel blends with methane and nitrogen. MISG has been characterized with different fuel (Bischof et al., 2020; Moallemi et al., 2019) and a recent study of the performance of a MISG coupled with ChAMBRe is reported in Vernocchi et al., 2021. For the experiments discussed in this work, MSIG has been fueled with propane which is known to have a good propensity of sooting.

Figure 2.14 Representation of the MSIG.

2.5 Characterization of the chamber performances

The first assessment of the ChAMBRe features is reported in Massabò et al., 2018. I focus here on background levels and sterility assurance, the measurements of the mixing time and the aerosol particle lifetime inside ChAMBRe.

2.5.1 Background levels and blank experiments

The background level of particles inside the chamber can be measured by SMPS and OPS. The coupling of the two counters provides a comprehensive picture from few nm up to 10 μm. After each experiment, the chamber is cleaned by a multistep procedure: the UV lamp is first switched on for 10 min, the chamber is then evacuated down to 2×10^{-3} mbar, maintained at such vacuum level for at least 20 min and then vented back to atmospheric pressure through the HEPA filter and gases traps. Periodically, a high ozone concentration (> 500 ppb) is produced to be sure to sterilize any part of the

set-up possibly not reached by the UV rays; after this step, the chamber is evacuated and vented again. Background level measurements performed subsequently to chamber cleaning always turned out to be lower than the instruments sensitivity (i.e. about 2 and 0.5 particle cm^{-3}, respectively, in the SMPS-LDMA and OPS range). Background concentrations of O_3, SO_2, NOx and BTEX turned out to be smaller than 1–2 ppb, i.e. close to the analyzers sensitivity. CO_2 level after re-venting of the chamber remained around 200 ppm, lower than the typical atmospheric concentration.

The chamber sterility is periodically checked through a blank experiment performed immediately after a cleaning procedure. Chamber sterility is tested by injecting sterile physiological solution only, to observe possible bio-aero contamination on four Petri dishes filled with non-selective culture media positioned inside the chamber. The exposure time of Petri dishes is the same of standard experiments: 5 hours. Usually, no bacterial contamination (i.e. bacterial colonies) can be observed on the petri dishes after the overnight incubation at 37 °C.

2.5.2 Mixing

The gas phase mixing time inside ChAMBRe was measured using a sufficiently inert gas (nitric oxide, NO) as a tracer. The good stability exhibit by the NO can be easily explained by the metallic nature of the chamber body and the non-oxidative property of the walls. NO from a cylinder was injected into the chamber at atmospheric pressure with a mass flow controller and monitored by the AC32e nitrogen oxides monitor. Three different fan rotation speed were tested: 0.8, 1.0 and 2.5 Hz (corresponding to the nominal values of 3, 5 and 10 Hz).

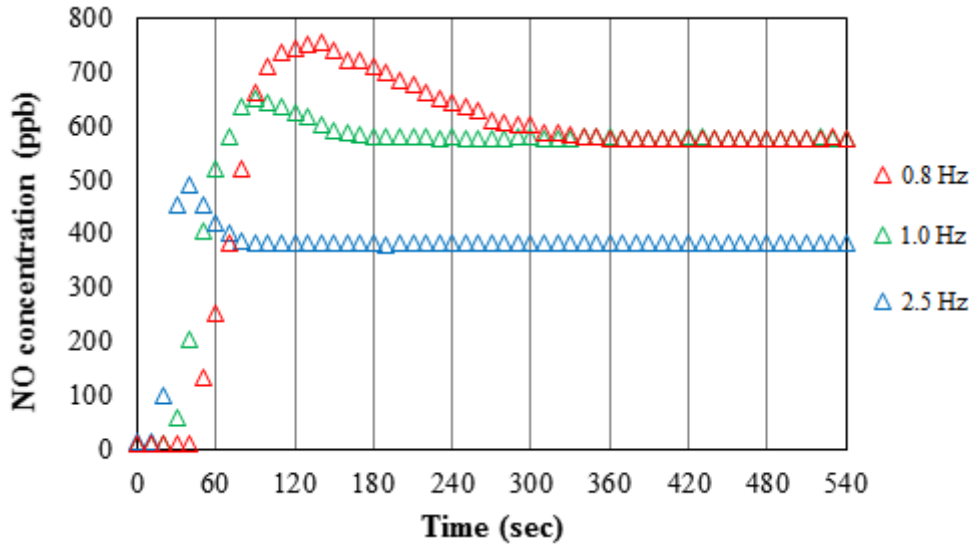

Figure 2.15 Concentration-time evolution of NO inside ChAMBRe.

Figure 2.15 shows that the tracer injected in the chamber can be considered as well-mixed in less than 180 s by using the 1 Hz fan speed (the typical fan speed adopted during the chamber experiments). This mixing time is relatively short comparing to experiment durations, which may last for several hours.

2.5.3 Aerosol behaviors

Depending on kinetics, processes in the atmosphere have typical times ranging from a few seconds up to several days, furthermore the presence of walls obviously influences the chemical and physical dynamics of the experiments carried out inside simulation chambers. For this reason, the evaluation of aerosol particle lifetime is of primary importance since it determines the range of realistic experiments: it depends on many factors e.g., wall losses caused by adsorption or deposition, mixing regime, gravitational settling, all of them depending of course on particle properties (i.e., density, dimensions, shape).

For the characterization of particle lifetime in ChAMBRe a polydispersed aerosol of NaCl is generated using the BLAM nebulizer, the mixing fan is kept on at a constant rotation speed of 1 Hz and the number size-distribution of the particles is measured as a function of time (by SMPS or OPC accordingly to particle size). Particle lifetime is determined by fitting in each size-bin the decay with a first order law:

$$y = y_0 e^{-k_d t} e^{-\beta t}$$

Where y_0 and k_d are fixed values, y_0 is the particle concentration at time t_0, k_d is the dilution factor corresponding to the air flow through the two counters and β is particle loss-rate coefficient, which correspond to the opposite of the lifetime.

Results, firstly reported in Massabò et al, 2018, and here recalculated, are comparable to the values for similar structure reported in the literature (Cocker et al., 2001; Lai and Nazaroff, 2000; Wang et al., 2011). In particular, experimental data are reproduced (with a mean discrepancy between measured and calculated values around 50 %) by the wall deposition model described in Lai and Nazaroff (2000) treating ChAMBRe as a rectangular cavity with a friction velocity of ca 6 cm s^{-1} (Figure 2.16). Particle lifetime in ChAMBRe varies from a few hours to about 1 day depending on particle size. The uncertainty on particle lifetime plotted in Figure 2.16 is evaluated on a pure statistical basis. Actually, in the size region between 300 and 600 nm, both the SMPS and OPC data could be particularly sensitive to other effects (e.g. background fluctuation for the SMPS, systematic artifacts in the first OPC bins) which are not fully investigated in this work. Regarding this thesis work, it is important to underline that the lifetime of particles having dimensions comparable to those of airborne bacteria (1-2 μm) is approximated to be around 5 h.

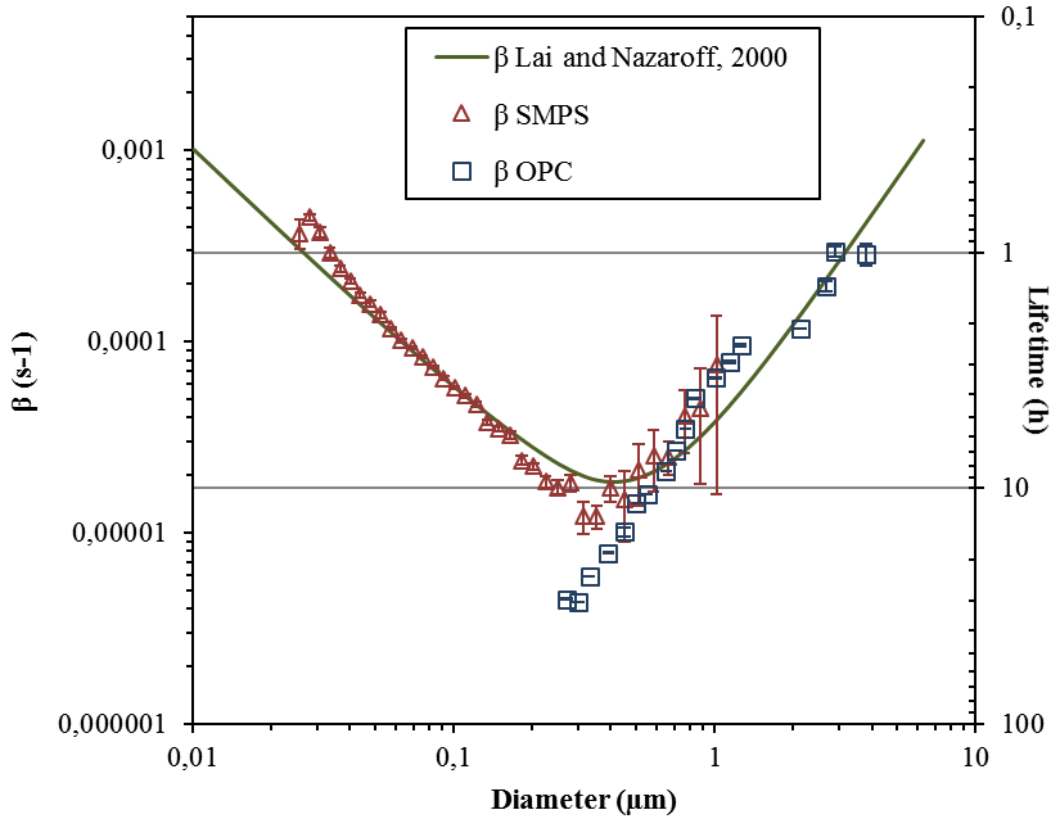

Figure 2.16 Particle loss coefficient (β) and lifetime (secondary vertical axis), vs. aerosol size measured in ChAMBRe measured for NaCl particles. The curve resulting from the Lai and Nazaroff (2000) model is also shown for reference.

2.6 Microbiological laboratory connected to ChAMBRe

Experiments at ChAMBRe benefit of several techniques for bacteria and bio-aerosol characterization. In the same building that hosts the atmospheric simulation chamber there is a basic microbiology laboratory allowing for culture analysis in vitro (isolation, identification, growth) and basic biochemical tests. The lab is equipped with autoclave (Asal mod.760), vortex, centrifuge and microcentrifuge (Eppendorf centrifuge 5417R), water purification system Milli-Q (Millipore-Elix), incubator for temperature control Ecocell and FriocellMMM Group, Steril-VBH Compact "microbiological safety" cabinet, Thermo electron corporation steri-cycle HEPA Class 100 incubator. An optical microscope (Nikon Eclipse TE300) is available for bacterial detection and live–dead discrimination by epifluorescence with specific dyes and for immunoassay fluorescence to label the antigenic bacterial target, fluorescent molecule or enzyme.

The transfer of biological sample from the laboratory to the simulation chamber takes only a few minutes, ensuring a quickly execution of the chamber experiments, once the biological sample reach the desired growth phase, and then a quick treatment of the samples collected after the experiments in the chamber.

3. Experimental investigations of bacteria in ChAMBRe

The effectiveness of ASCs for studying bacteria, and other biological particles dispersed in air, depends on the experimental protocols, which are essential to understand how the microorganisms survive and if they are able to grow and reproduce in the atmospheric conditions of the simulation chamber. Storage conditions (e.g., media, temperature, and time), culture conditions (e.g. preparation methods and growth phase) may all influence the quality of the material to be aerosolized and introduce variability in the results (Alsved et al., 2020). Moreover, the survival of aerosolized bacteria depends on a large number of factors, including the relative humidity and temperature of the air, the nature of the microorganisms, the nature of the gaseous environment and the composition of the liquid medium in which they are suspended (Benbough, 1967; Cox, 1966; Dunklin and Puck, 1948). All these aspects must be considered as important variables for the reproducibility of the results.

I dedicated an intense effort to develop a procedure to handle and prepare the microorganisms to be aerosolized and to run the chamber experiments. In this chapter, the methodology developed for the bio-aerosol (bacteria in particular) experiments is described. A typical experiment consists of several phases: *in vitro* microorganism's growth, injection in ChAMBRe, exposure to desired conditions, samples collection and laboratory analysis. The survival rate of the airborne bacteria is firstly evaluated in a set of "*baseline experiments*", i.e. exposing bacteria to clean air, without contaminants or pollutants. Baseline conditions fix the reference for the experiments in which bacteria are exposed to various levels and types of pollutants (paragraph 3.4).

3.1 Methodology

3.1.1 Bacteria selection

Experimental procedures involved two bacterial strains consisting of *Bacillus subtilis* (ATCC® 6633™) and *Escherichia coli* (ATCC® 25922™). These microorganisms are extensively used as model organisms in microbiology and molecular biology fundamental and applied studies (Lee et al., 2002; Lee and Kim, 2003; Lee and Lee, 2006; Silhavy et al., 2010; Stone and Johnson, 2002; Thomas et al., 2011).

Historically, bacteria are divided into Gram-positive and Gram-negative bacteria depending on their behavior when their cell walls are treated by Gram staining. In 1884, Hans Christian Gram developed a staining procedure that allowed to classify nearly all bacteria into two large groups: one group retains Gram's stain, Gram-positive, while the other does not, Gram-negative. The basis for the Gram stain lies in fundamental structural differences in the cell envelope of these two groups of bacteria. The bacteria cell envelope is a complex multilayered structure that serves to protect these organisms from the environment. As illustrated in Figure 3.1, the Gram-negative cell envelope is formed by three principal layers: the outer membrane, the peptidoglycan-cell wall, the cytoplasmic or inner membrane and an aqueous cellular compartment, named periplasm, delimited by the two concentric membrane layers. Indeed, in the Gram-positive cell envelope the outer-membrane is absent and the layers of peptidoglycan are many times thicker than is found in Gram-negative, to withstand the turgor pressure exerted on the plasma membrane (Silhavy et al., 2010). Ultimately, the outer membrane plays a major role in protecting Gram-negative organisms from the environment by excluding toxic molecules and providing an additional stabilizing layer around the cell; e.g. it is generally true that Gram-negative bacteria are more resistant to antibiotics than their Gram-positive cousins (Breijyeh et al., 2020).

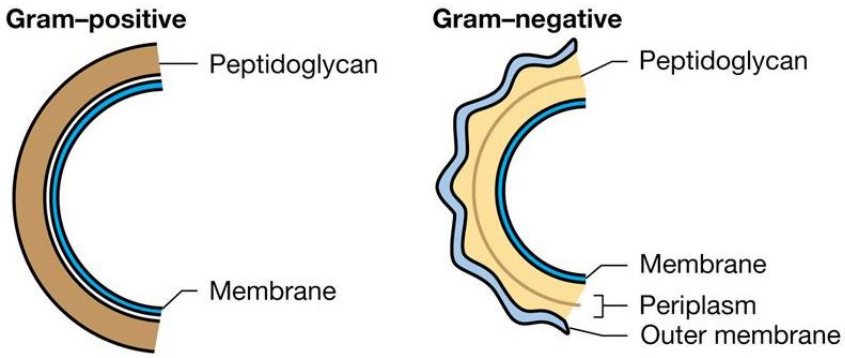

Figure 3.1 Representation of Gram-positive and Gram-negative cell envelopes.

In my PhD work, one non-pathogenic model for each macro-group of bacteria was chosen as investigation subject.

Bacillus subtilis is a Gram-positive, rod-shaped bacterium with a length ranging between 2.5 and 6.5 μm. It is commonly found in soils but has been also observed in other environmental matrices such as water and air (Earl et al., 2008). It has a wide commercial use, as it is nonpathogenic. *B. subtilis* serves as a model organism and is considered a reference for cell differentiation and adaptation. This model status makes it one of the most extensively studied organisms in nature given its ability to survive and even thrive in a wide range of harsh environments (Earl et al., 2008).

Escherichia coli is a Gram-negative, rod-shaped, Enterobacter, is about 1–2 μm long and about 0.25 μm in diameter. It is a common inhabitant of the gastrointestinal tract of warm-blooded animals, including humans, but recent studies have reported that some specific strains of *E. coli* can also survive for long periods of time, and potentially reproduce, in extra-intestinal environments (Jang et al., 2017). *E. coli* is among one of the most studied model organisms. Its fast-growth characteristics under optimal conditions make it suitable to be used as host organism for many gene manipulation systems and to study the evolution of microorganisms (Jang et al., 2017).
Details of the two bacteria models are shown in the Figures 3.2 and 3.3.

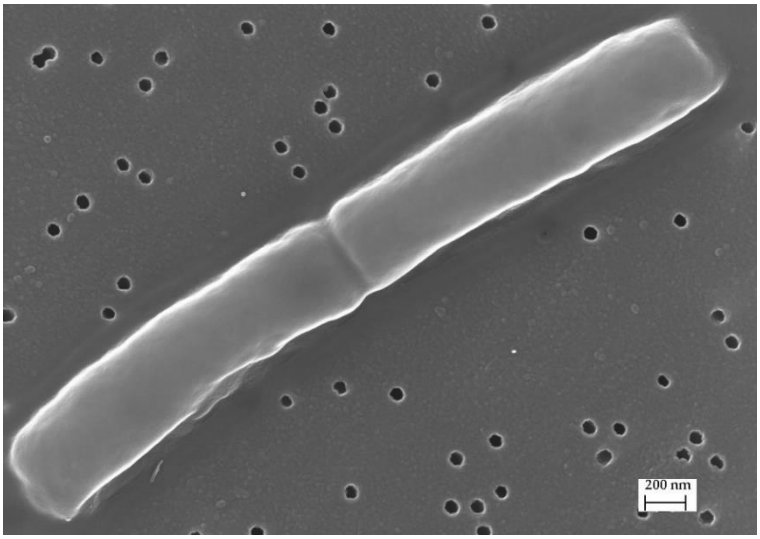

Figure 3.2 Detail of *Bacillus subtilis* in saline solution, magnifications 100 000×, (Massabó et al., 2018).

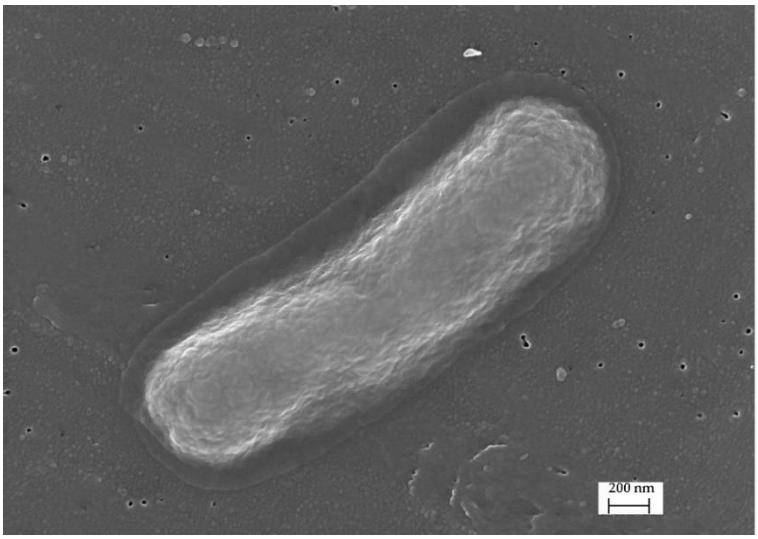

Figure 3.3 Detail of *Escherichia coli* in saline solution, magnifications 100 000×, (Massabó et al., 2018).

3.1.2 Preparation of bacterial suspension

The same culture preparation technique was applied at both the bacterial strains. Firstly, it is important to ensure the maximum bacteria cells viability prior to the experiment. Typically, to understand and define the growth of a particular microbial isolate, cells are placed in a culture medium in which the nutrients and environmental conditions are controlled. If the medium provides all nutrients required for growth and environmental parameters are optimal, a growth curve can be obtained by measuring the increase in bacterial number or mass as a function of time. Different distinct growth phases can be observed within a growth curve: these include the lag phase, the log phase, the stationary phase, and the death phase (Figure 3.4). The lag phase, where growth is absent (i.e. bacteria adapt themselves to growth conditions and synthesize proteins and other molecules necessary for replication) is followed by an acceleration phase during which the growth rate increases until a constant growth rate is achieved during the exponential phase. Eventually, the growth rate begins to decline during the deceleration phase and in the end, during the stationary phase, growth ceases due to resource exhaustion and/or waste accumulation. Stationary phase results from a situation in which growth rate and death rate are equal. The number of new cells created is limited by the growth factor and, as a result, the rate of cell growth matches the rate of cell death. At death phase, bacteria die, as nutrients become less available and waste products increase. Therefore, each of these phases represents a distinct period of growth that is associated with typical physiological changes in the cell culture.

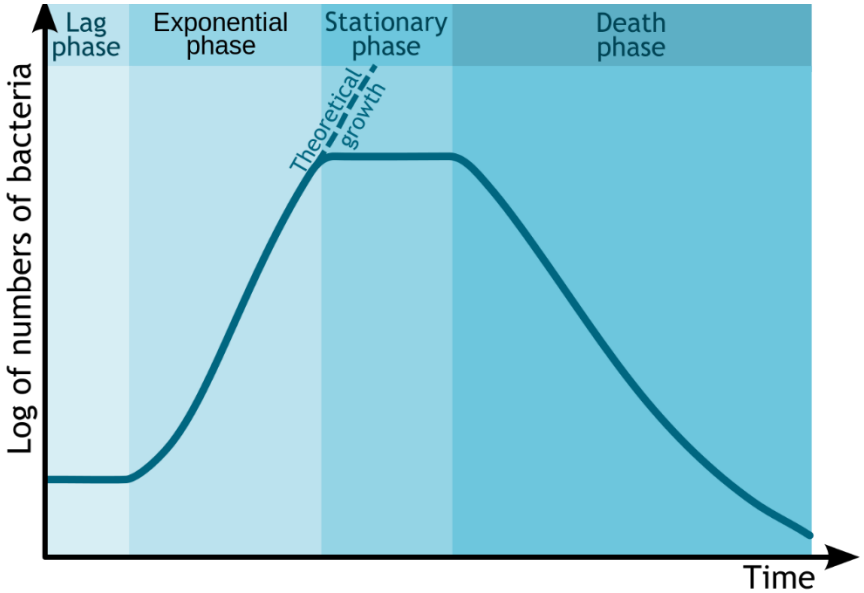

Figure 3.4 Representation of a generic bacteria growth curve.

Hence, the growth curve for both of bacterial strains was obtained quantifying the rate of change in the number of cells in a culture per unit time thus identifying the mid-exponential phase (log phase),

where the maximum viability of the cells is ensured and the number of dead microorganisms is at a minimum (Hall et al., 2014).

Both the bacteria strains were purchased by Thermo Scientific™ Culti-Loops™, which are disposable bacteriological loops containing stabilized viable microorganisms in a gel matrix. To recover the organism, the loops were placed directly on warm agar medium for 10-15 seconds; the agar plate was subsequently incubated overnight at 37 °C. The next day, bacteria cells were scraped off agar medium using sterile plastic loops and suspended in a sterile, non selective culture broth medium: the Tryptic Soy Broth (TSB), also known as soybean-casein digest medium (SCDM).

In general, the agar plate directly inoculated from the Culti-Loops™ is used as reference stock culture and it can be conserved at 4 °C for maximum one month. The day before each experiments, one colony of the bacteria strain is scraped off from the reference culture, refreshed on a new agar plate, incubated and used for the experiment the next day.

The growth curve was followed, once every hour, with a spectrophotometer V-530 UV-vis (Jasco International Co. Ltd, Hachioji, Japan), where the number of cells per mL of culture was estimated from the turbidity of the culture. Turbidity, defined as the amount of light scattering caused by the cells in a liquid culture, is expressed as apparent absorbance or optical density (OD). The OD of the bacterial solution, measured at a wavelength of 600 nm, OD_{600nm}, is a common method for estimating the concentration of bacterial cells in a liquid. The amount of the light scattered by the microorganisms suspension is an indication of the biomass contents (Sutton, 2011). The mid-exponential phase is typically reached when OD_{600nm} is about 0.5 (Hall et al., 2014; Mytilinaios et al., 2012). For Gram-positive strains, the relationship between the OD_{600nm} and the bacteria concentration is:

$$OD = 1 \rightarrow 10^8\ CFU\ ml^{-1} \quad (1)$$

Instead, for Gram-negative strains, the relationship is:

$$OD = 1 \rightarrow 5 \times 10^8\ CFU\ ml^{-1} \quad (2)$$

Actually, the number of cultivable cells in the bacteria suspension was determined as Colony Forming Units (CFU). With this method, viable microorganism can be counted by plating a suspension of bacteria, properly diluted, on solid media. Each live bacterial cell grows to form a colony, which is large enough to be seen. The bacteria solution must possibly be diluted several times to obtain not-overlapping colonies as reported in the follow.

A volume of 20 mL of bacterial solution in TSB was centrifuged at 4000g for 10 minutes. The surnatante was discarded and the bacteria pellet was resuspended in sterile saline solution (NaCl 0.9 %) to prepare a bacterial solution with the same concentration of the starting one (same final volume, 20 mL). The OD_{600nm} was measured again to evaluate the indicative bacteria concentration, using eq.

(1) or (2). With a bacteria concentration of about 10^7 CFU mL^{-1}, the bacteria solution was diluted by a factor ten for five times, plus an intermediate dilution, as reported in Figure 3.5 (for more details on the choice of dilutions see the APPENDIX B).

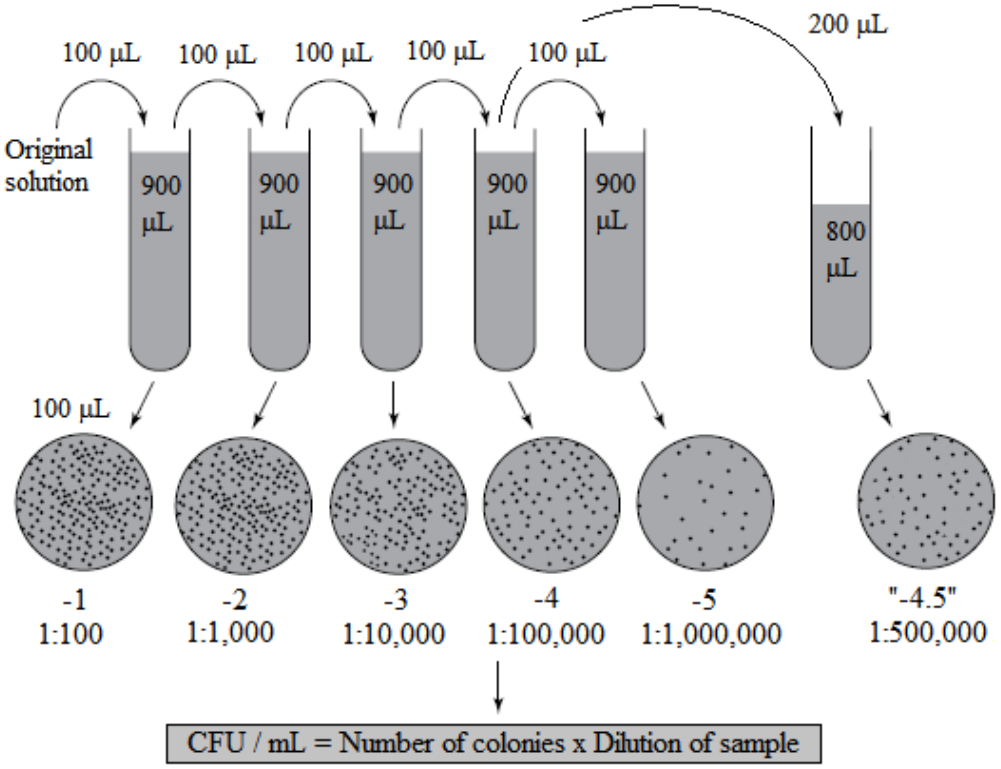

Figure 3.5 Schematic representation of serial dilutions.

Finally, 100 µL of the last three dilutions were spread in duplicate on an agar non-selective culture medium (trypticase soy agar, TSA). The liquid was spread on the culture medium in small droplets, using automatic pipet. Each Petri dish was then gently shaken to spread the liquid onto the entire surface of the petri and then incubated overnight at 37 °C. The concentration of culturable cells was then determined by counting the colonies formed and multiplying by the appropriate dilution factor to determine the colony forming units (CFU) per mL in the original solution. The procedure here described was optimized to obtain a suitable level of reproducibility; a detailed description of the whole procedure is reported in the APPENDIX B. Data, obtained by CFU counting on agar plates, were averaged and used to estimate the uncertainty range of the bacterial concentration in the solution following the Poisson statistics (i.e., the square root of the number of colonies counted in the petri dishes). Examples of the growth curves for the two strains are reported in Figure 3.6 and 3.7.

The cells solutions used in chamber experiments were prepared waiting until to the mid-exponential phase, reached in about 4 h, following the steps described above. Finally, a volume of about 10 mL of the cells suspension in saline solution was taken out and prepared for the nebulization inside the atmospheric simulation chamber (see paragraph 3.1.4).

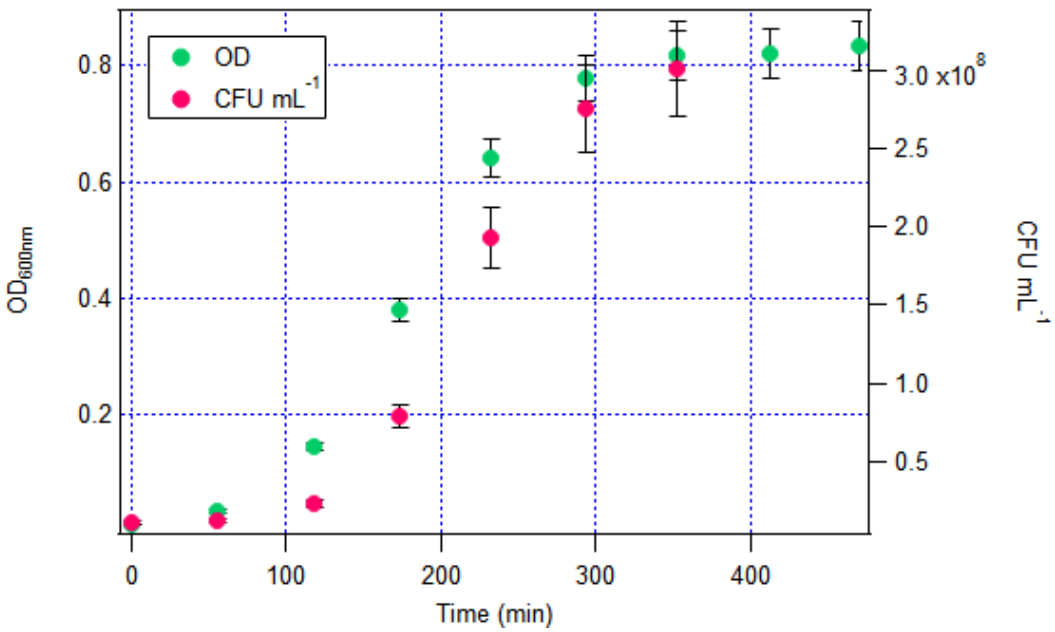

Figure 3.6 Typical grow curve for *Escherichia coli*: optical density ($OD_{600\ nm}$) and the corresponding bacteria concentration (CFU mL^{-1}) plotted vs. time. Data are reported up to the onset of the stationary phase.

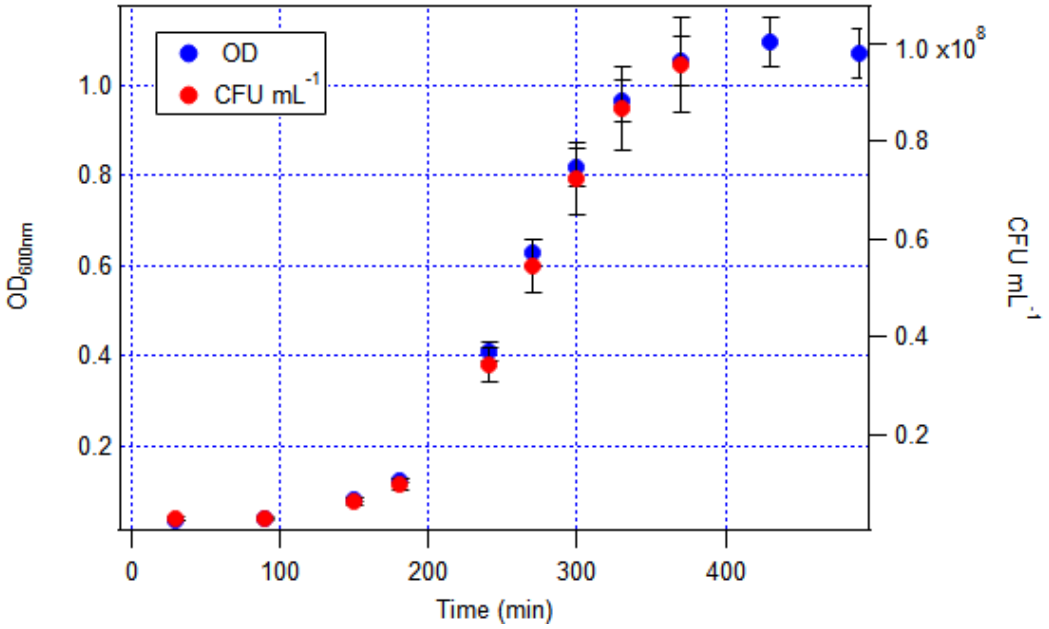

Figure 3.7 Typical grow curve for *Bacillus subtilis*: optical density ($OD_{600\ nm}$) and the corresponding bacteria concentration (CFU mL^{-1}) plotted vs. time. Data of concentration curves are reported up to the onset of the stationary phase.

3.1.3 Chamber preparation

In a standard experiment ("*baseline experiment*"), viability of the airborne bacteria was determined at temperature in the range between 20 °C and 25 °C, atmospheric pressure and relative humidity around 60%-70%. This range of air parameters was chosen to reproduce a suitable environment for bacteria survival, as reported in several works (Benbough, 1967; Cox, 1966; Dunklin and Puck, 1948). Relative humidity was adjusted by injecting directly water vapour inside ChAMBRe trough a humidifier, while the control of the internal temperature of the chamber was carried out indirectly by controlling the temperature of the laboratory by an air conditioning system. CO_2 concentration was kept constant at 450 ppm thanks to a feedback control system. Background level of particles and any harmful gases were negligible (see Chapter 2, paragraph 2.5.1 for the background levels after a chamber cleaning).

3.1.4 Bacteria injection in ChAMBRe

Bacteria injections inside ChAMBRe were carried out alternatively by one of the nebulizers described in Chapter 2, paragraph 2.4.1.

In the chamber experiments, the operation conditions for each nebulizers were:

- BLAM: liquid feed rate 0.4 mL min^{-1}, injection time 5 min, volume of injected solution 2 mL, air flow 2.4 L min^{-1} and expansion plate "1-20" (see Table 2.2).
- SLAG: liquid feed rate 0.4 mL min^{-1}, volume of injected solution 2 mL, injection time 5 min and air flow 3.5 L min^{-1}.
- Collison: liquid feed rate 0.4 mL min^{-1}, injection time 4 min, and air flow 3.0 L min^{-1}. Since the Collison nebulizer works in a recirculation mode, it is not possible to quantify the absolute value of the liquid volume passing through the nozzle.

The operation conditions here mentioned, were selected and optimized through a comprehensive characterization of the three different nebulizers described in paragraph 3.2 and published in Danelli et al., 2021.

3.1.5 Bacteria collection and extraction methods

Bacteria were collected by gravitational deposition on up to six Petri dishes, filled with TSA culture medium, placed in the bottom of the chamber through an automated shelf (see Chapter 2, paragraph 2.3.4) and maintained in that position during the whole experiment (usually, 5 hours). At the end of the experiment, the Petri dishes were extracted and incubated overnight at 37 °C, to determine the bacteria culturable fraction by CFU visual counting. The gravitational settling method was adopted to minimize microbial damage (Aydogdu et al., 2010; Brotto et al., 2015; Xu and Yao, 2011). The

living microorganisms in the aerosol were expected to settle down without suffering any stress apart from those related to the permanence in the chamber atmosphere. In addition, losses due to particle bouncing were expected to be minimal due to low impaction velocity. In this way, the number of CFUs counted on a Petri dish was assumed to be proportional to the concentration of viable bacteria in ChAMBRe.

The maneuvering to insert the Petri dishes in ChAMBRe follows few steps (reference to Figure 2.9 for the valves names):

1. With V1 closed, the V2 valve is opened to allow the positioning of the Petri dishes (pre-filled with a suitable amount of culture medium) on the sliding tray.
2. Valve V2 is closed and V1 is opened.
3. The sliding tray is completely inserted in ChAMBRe.
4. The sterilizing UV lamp (see section 2.2) is switched on for 10 min to guarantee the Petri dishes sterilization.
5. The UV lamp is switched off and ChAMBRe is ready for injection of bacteria.

The fan positioned in the bottom of the chamber was kept on at 1 Hz during the experiments to maintain a homogeneous distribution of particles.

The time window of a typical exposure experiments in ChAMBRe was about 5 hours and it was initially chosen looking at particle lifetime in ChAMBRe. The average aerodynamic diameters of airborne *E. coli* and *B. subtilis* are around 0.6 and 0.7 μm respectively (Hernandez et al., 2016; Lee et al., 2002) and their lifetime (see Figure 2.15) is expected to be around 5 h. Bacteria lifetime was subsequently confirmed by the WIBS-NEO, as reported in the section 3.3 of this chapter.

3.2 Bioaerosol production

The aerosolization of a reproducible number of viable bacteria inside an ASC is the first and non trivial step of the experimental procedure and deserves special attention. Bio-aerosol experiments require nebulization devices that can provide high particle concentrations with minimal damage to microorganisms and their viability. So far, different aerosol generators have been designed to improve the preservation of cultivability and structural integrity of the aerosolized microorganisms (Zhen et al., 2014), but the choice of the best equipment for a given application is often hampered by the lack of information on performance or drawbacks of single instruments. This is particularly evident for those nebulizers that do not have a widespread use, such as the BLAM and SLAG nebulizers. For this reason, the performances of the three bio-aerosol nebulizer available at ChAMBRe were investigated to measure the reproducibility of the nebulization procedures and assess their application in

experiments inside ASCs. The comparison focused on the operation conditions and the concentration of viable bacteria at the nebulizer outlet.

For such characterization the *E. coli* ATCC® 25922™ model strain was selected.

In all the three devices deployed at ChAMBRe, Collison, BLAM and SLAG, the nebulization efficiency depends on the airflow maintained by an external system (i.e. air cylinder and mass flow controller). Bacteria were aerosolized at different air pressures and collected by a liquid impinger to obtain a correlation curve between airflow and nebulized bacteria for each generator (section 3.2.1). Afterwards, (section 3.2.2), bacteria were aerosolized directly into ChAMBRe to measure the reproducibility of the whole procedure by selecting a proper and single working condition for each nebulizer.

3.2.1 Determination of nebulization efficiency

In the first phase, the nebulization efficiency of each device was measured at different airflows. A schematic diagram of the experimental setup is shown in Figure 3.8. The aerosol was sampled directly at the output of the nebulizer through a flanged connection using a liquid impinger filled with 20 mL of sterile saline solution and operated at a constant airflow of 12.5 L min^{-1} (Terzieva et al., 1996; Zheng and Yao, 2017). Impinging systems are widely used instruments for bio-aerosol sampling with a nominal bioaerosol collection efficiency in standard operative conditions (12.5 L min^{-1} sampling flow rate and 20 mL of collection liquid) of about 95% for particles in the range of 1–10 μm (Zheng and Yao, 2017).

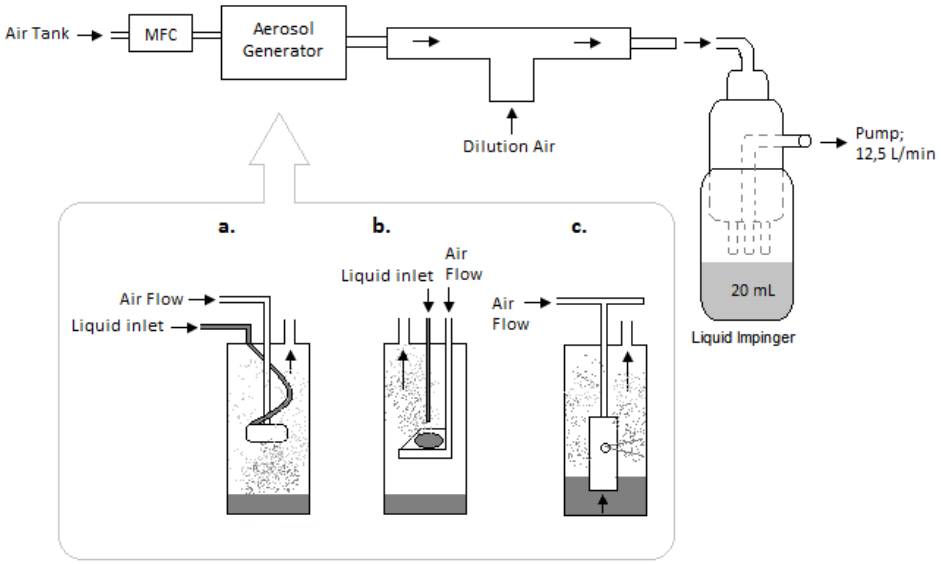

Figure 3.8 Experimental setup for the tests with the impinger. (a) BLAM, (b) SLAG, and (c) Collison (Danelli et al., 2021).

Prior to experiments, bacteria were cultivated as reported in paragraph 3.1.2 and resuspended in sterile saline solution to prepare a solution of approximately 10^8 CFU mL^{-1}, as verified by standard dilution plating. The average of the CFU counting was used to estimate the uncertainty range of the bacterial concentration in the solution. The bacteria suspension was then sprayed and directly collected by the liquid impinger. The number of cultivable cells inside the impinger was then determined in CFU by standard dilution plating: 100 μL of serial dilutions of the solution was spread on TSA agar medium and incubated overnight at 37 ° C before CFU counting. For each nebulizer, different airflows were tested using a mass flow controller (Bronkhorst, model F201C-FA), and the nebulization efficiency was determined in terms of culturable fraction of aerosolized bacteria using the equation below:

$$Nebulization\ Efficiency = \frac{CFU_{IMP}}{CFU_{SOL}} \times 100$$

were CFU_{IMP} is the total CFUs collected in the impinger liquid, i.e. the product between the CFU concentration, CFU mL^{-1}, and the liquid volume contained in the impinger (20 mL); and CFU_{SOL} is the CFU introduced in the liquid solution of the nebulizer. With the BLAM and SLAG nebulizers, CFU_{SOL} corresponds to the product between the concentration (i.e., CFU mL^{-1}) in the bacterial solution and the volume of liquid (2 mL) used in each single test. Since the Collison nebulizer works in a recirculation mode, (i) it is not possible to quantify the absolute value of the liquid volume passing through the nozzle and (ii) an unknown fraction of the liquid passes through the nozzle more than once. Therefore, the volume of the liquid is substituted with the injection time (5 min; the same used with other two nebulizers) in the experiments with the Collison nebulizer. Even if this operative choice does not meet a strict metrological criterion, it makes possible a direct comparison of the three devices in well-defined operative conditions (see Table 3.1).

Table 3.1 Working condition of each nebulizer during the tests with liquid impinger.

Nebulizer	Liquid Feed Rate (mL min^{-1})	Volume of liquid (mL)	Injection time (min)	Air Flow range (L min^{-1})
BLAM	0.4	2	5	1.4 - 3.7
SLAG	0.4	2	5	2 - 5
COLLISON	/	/	5	2 - 5

Aerosolization conditions were selected according to the requirements for experiments in atmospheric simulation chambers: a single, short (i.e. 4-5 min) injection with (possibly) high output concentration of biological particles. The aerosolization airflow varied in the range of 1.4 - 3.5 L min^{-1} for BLAM and 2 - 5 L min^{-1} for SLAG and Collison. The bacteria suspension was supplied to BLAM and SLAG at the same liquid flow rate of 0.4 mL min^{-1} (see Table 3.1).

The nebulization efficiency in these conditions with the BLAM, SLAG, and Collison nebulizers is shown in Figure 3.9, 3.10 and 3.11, respectively. The average of the colonies counted on the Petri dishes was used to evaluate the uncertainty range of the bacterial concentration in the solutions, while the uncertainty on the airflow was taken as the 1% of the flow controller full scale value.

The BLAM nebulizer shows the highest nebulization efficiency, followed by the Collison and SLAG (e.g., at 3.5 L min $^{-1}$ the BLAM nebulization efficiency is about 2 and 4 times higher than the Collison and SLAG figures, respectively).

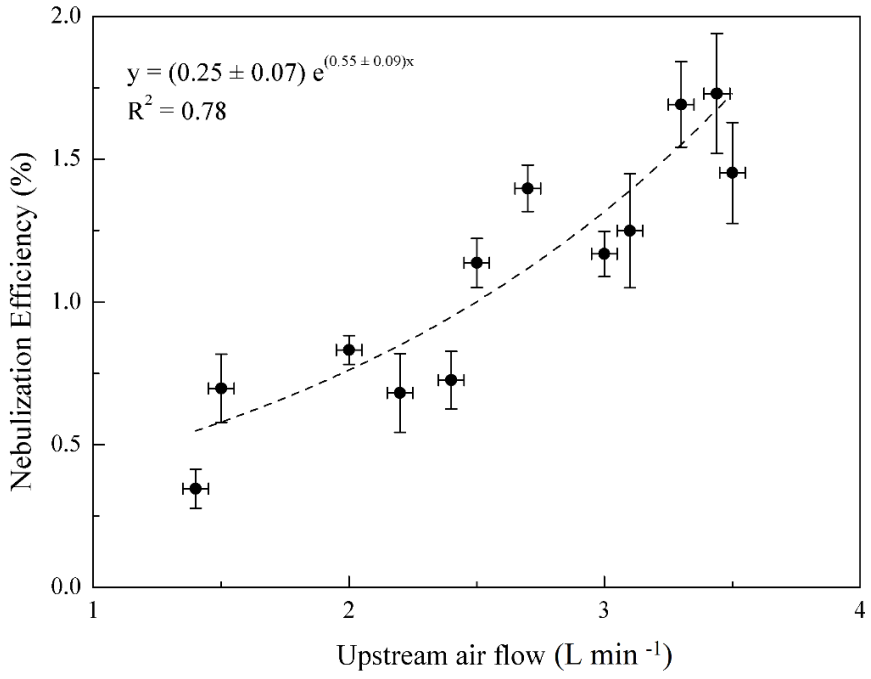

Figure 3.9 BLAM nebulization efficiency (percentage values) vs. upstream airflow. Liquid feed rate 0.4 mL min^{-1}. (Danelli et al., 2021).

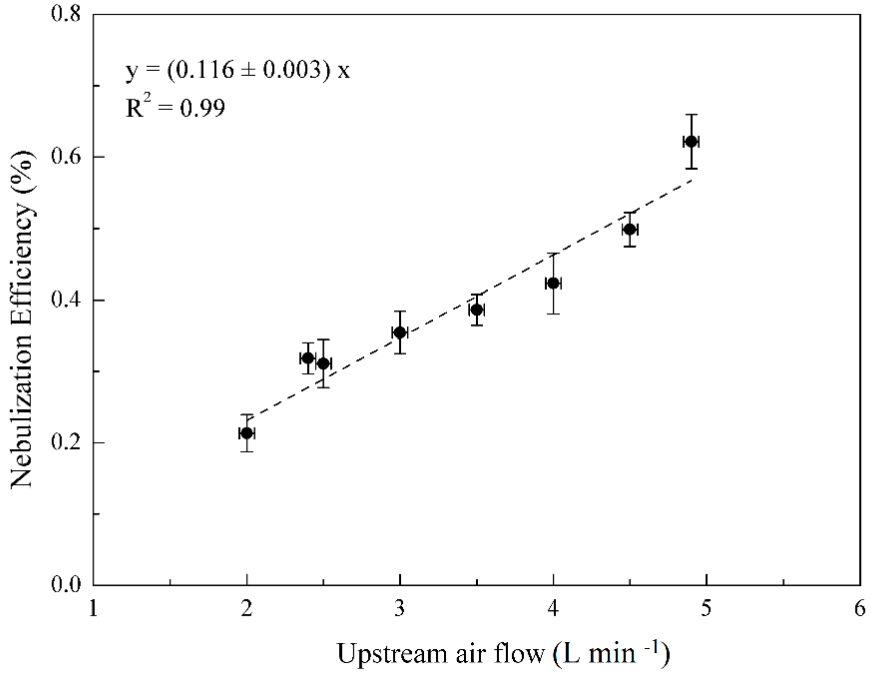

Figure 3.10 SLAG nebulization efficiency (percentage values) vs. upstream airflow. Liquid feed rate 0.4 mL min^{-1}. (Danelli et al., 2021).

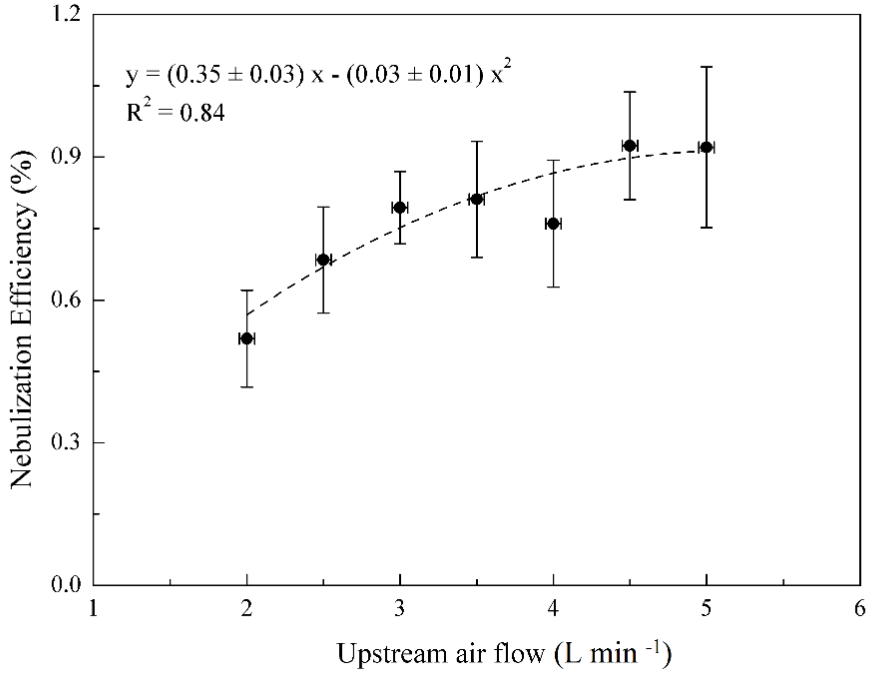

Figure 3.11 Collison nebulization efficiency (percentage values) vs. upstream airflow. (Danelli et al., 2021).

The three nebulizers show significant differences: while BLAM and Collison provide a higher nebulization efficiency, the SLAG requires a lower upstream pressure and this, according to the producer claim, results in a softer injection (and then less bio-damage) of viable bacteria. With its gentle nebulization mechanism, the SLAG nebulizer looks best suited for experiments with the more fragile bacteria. The Collison produces a high particle concentration, but possible cell damage is reported in several studies (Mainelis et al., 2005; Thomas et al., 2011; Zhen et al., 2014). The experimental procedure here applied do not allow a direct control of the damaged bacteria fraction during the nebulization phase, but, in the specific case of the Collison nebulizer (Figure 3.11), the nebulization efficiency of the culturable fraction increases linearly with the airflow until about 3 L min^{-1}; after that the curve bends, probably because the cell damage becomes more relevant. However, with the described injection conditions (5 min; air flow <5 L min^{-1}) the output of viable bacteria turned out to be comparable with the results obtained with the other two nebulizers. The BLAM efficiency seems subjected to a higher variability; such a feature is likely due to the coupling between the nebulizer and the impinger since the experiments with injection directly into the simulation chamber remained much more stable (see Sect. 3.2.2).

3.2.2 Reproducibility and application for ASCs experiments

In the second set of experiments, the focus was on the performance of the three nebulizers when used to inject bacteria directly inside an atmospheric simulation chamber. A series of experiments was performed with each nebulizers (actually, 4 with BLAM and Collison and 5 with SLAG), with different concentration of bacteria in the suspension for each test and therefore variable amount of bacteria injected in the chamber.

Prior to each experiment, bacteria were cultivated as reported in paragraph 3.1.2 and resuspended in sterile saline solution and diluted to prepare a solution of approximately 10^7 CFU mL^{-1} (verified by standard dilution plating). Inside the chamber, bacteria were collected as described in section 3.1.5.

The working conditions for each device were fixed (see Table 3.2) and the stability/reproducibility of the whole procedure was investigated.

Table 3.2 Nebulizers operation conditions during chamber experiments

Nebulizer	Liquid feed rate (mL min^{-1})	Volume of injected solution (mL)	Injection time (min)	Air flow (L min^{-1})
BLAM	0.4	2	5	2.4
SLAG	0.4	2	5	3.5
Collison	/	/	4	3.0

The Collison injection time was here reduced from 5 min to 4 min because that configuration resulted, immediately after the injection, in a PM_{10} concentration inside the chamber of about 200 µg m^{-3}, similar to the value produced by BLAM in the reported conditions (Table 3.4). The initial PM_{10} concentration, as determined by the OPS, was taken as a rough reference for the aerosolization efficiency and quantity of aerosol generated (bacteria plus NaCl particles, deriving from the saline solution aerosolization). Indeed, the particle size distribution determined by the OPS inside the chamber after the bacteria injection is usually dominated by particles smaller than 700-800 nm (NaCl particles from the saline solution), thus making difficult to discriminate the signal of the bacteria, which are larger in size (i.e. about 1 µm). Figure 3.12 shows examples of the number size distribution after *E. coli* injections performed by the three nebulizers. A more detailed investigation of the size distribution of salt particles produced by the BLAM is reported in APPENDIX A.

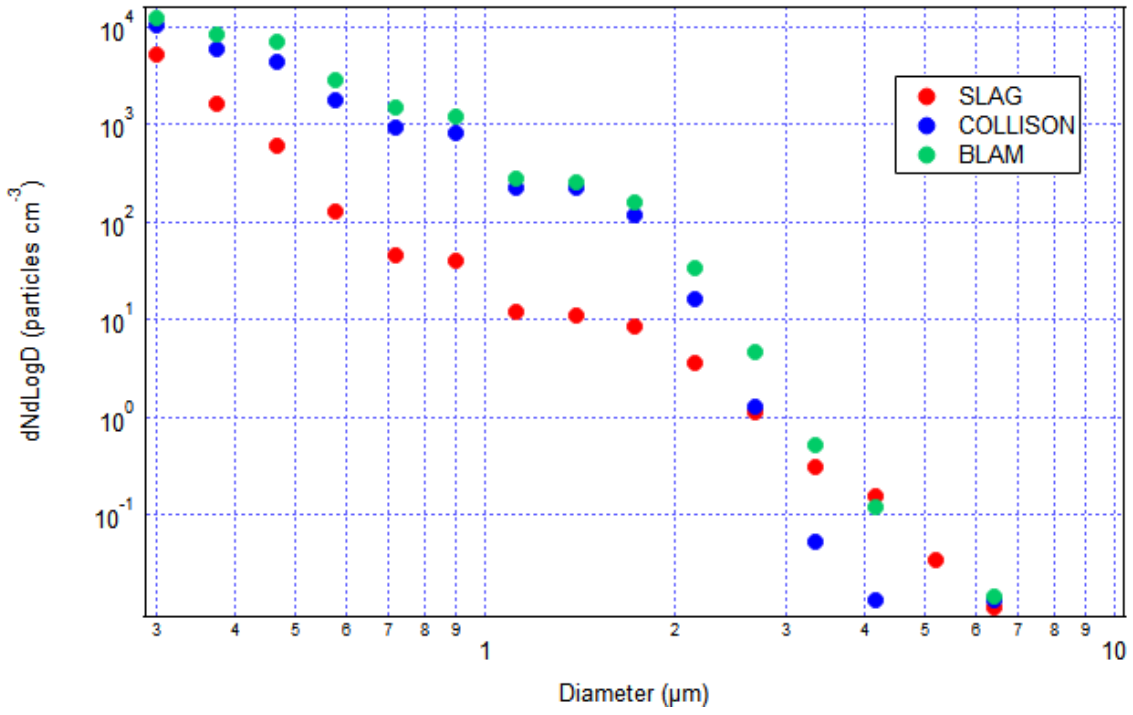

Figure 3. 12 OPS particle size distribution during *E. coli* chamber experiments.

The experimental conditions are reported in Table 3.3.

Table 3.3 Meteorological parameters (P, T, RH) in ChAMBRe during each experiments.

Experiment	External Pressure (mbar)	Internal Pressure (mbar)	Temperature (°C)	Relative Humidity (%)
BLAM.1	1010	1008	23.3	61.1
BLAM.2	1009	1006	23.2	61.9
BLAM.3	1007	1004	25.1	64.3
BLAM.4	1009	1006	22.8	60.8
SLAG.1	1007	1006	20.7	57.8
SLAG.2	1007	1007	22.8	59.4
SLAG.3	1008	1007	23.2	63.0
SLAG.4	998.2	997.7	22.6	60.0
SLAG.5	1008	1008	21.8	58.1
Collison.1	1010	1009	24.3	66.7
Collison.2	1013	1010	24.0	63.5
Collison.3	1016	1014	23.9	63.0
Collison.4	1014	1012	24.1	62.7

The amount of injected bacteria (corresponding to the product between bacteria concentration in the initial solution and the volume or time of injection, as pointed out in the Nebulization Efficiency definition; previous paragraph) and the average number of colonies collected on the Petri dishes inside the chamber are shown in Table 3.4. The uncertainties quoted on both injected and collected bacteria are just those deriving from the Poisson fluctuation and they do not include any other systematic or statistical contributions. In particular, the values of the collected CFU are the average of the CFU counts of the four Petri dishes exposed in each experiment; the four counts of each group turned out to be compatible within one standard deviation.

Table 3.4 Injected bacteria, average number of colonies counted on the Petri dishes placed inside ChAMBRe and value of PM_{10} level measured inside the chamber at the end of each injection.

Experiment	Bacteria Injected (CFU)	Average CFU Collected	PM_{10} ($\mu g\ m^{-3}$)
B.1	$(6.72 \pm 0.47) \times 10^7$	464 ± 21	190 ± 14
B.2	$(4.20 \pm 0.37) \times 10^7$	278 ± 17	170 ± 13
B.3	$(4.60 \pm 0.43) \times 10^7$	257 ± 16	190 ± 14
B.4	$(1.96 \pm 0.13) \times 10^7$	97 ± 10	190 ± 14
S.1	$(0.70 \pm 0.07) \times 10^8$	70 ± 8	60 ± 8
S.2	$(2.31 \pm 0.20) \times 10^8$	267 ± 16	85 ± 9
S.3	$(2.28 \pm 0.20) \times 10^8$	206 ± 14	85 ± 9
S.4	$(1.60 \pm 0.13) \times 10^8$	152 ± 12	110 ± 10
S.5	$(0.95 \pm 0.10) \times 10^8$	107 ± 10	90 ± 9
C.1	$(0.86 \pm 0.08) \times 10^8$	273 ± 17	190 ± 14
C.2	$(0.89 \pm 0.04) \times 10^8$	327 ± 18	230 ± 15
C.3	$(0.27 \pm 0.02) \times 10^8$	98 ± 10	230 ± 15
C.4	$(1.34 \pm 0.12) \times 10^8$	505 ± 23	240 ± 16

Data in Table 3.4 are also plotted in Figures 3.13, 3.14 and 3.15, which refer to BLAM, SLAG, and Collison, respectively. A good correlation (i.e. $R^2 = 0.98$, BLAM and SLAG, $R^2 = 0.99$, Collison) between the number of injected and collected CFU was obtained for each nebulizer (Figures 3.10 - 3.12). In Figures 3.12, 3.13 and 3.14, the slope decreases from the BLAM, to the Collison, and finally to the SLAG (see Figures 3.9, 3.10, 3.11). The concentration of injected bacteria was not corrected by the nebulization efficiency; this way, values on the x-axis are directly and simply determined by the bacteria concentration in the initial solution and the volume or time of injection. The uncertainty on the slope of the correlation curves always turn out to be <5% and the overall standard deviation around the average ratio (collected/injected CFU) is 11 %. This value corresponds to the standard deviation of the results of the entire bunch of experiments around the mean value of the collected to injected CFU ratio (taking into account the results of all three nebulizers). This level of reproducibility appears to be adequate to design experiments within an ASC's facility: it roughly give the sensitivity of the procedure to change in bacteria viability induced by the presence in the chamber of specific pollutants or conditions. The results of such "*baseline experiments*" show again that both the Collison nebulizer and BLAM are able to produce higher viable bacteria concentrations compared to the SLAG

device. In particular, the Collison, despite the known problems related to the cells damage, in the specific conditions here described, appears to be a stable and easier to use system. As previously reported, cells damage could become more evident during prolonged injections and therefore may not have been detected by our tests.

Definitely, the aim of this bunch of experiments was to find a quantitative and reproducible relationship between the number of injected and of collected viable bacteria: this depends on the deposition losses on the chamber walls, on the viability reduction due to the nebulization procedure and finally, on the time spent in the chamber environment.

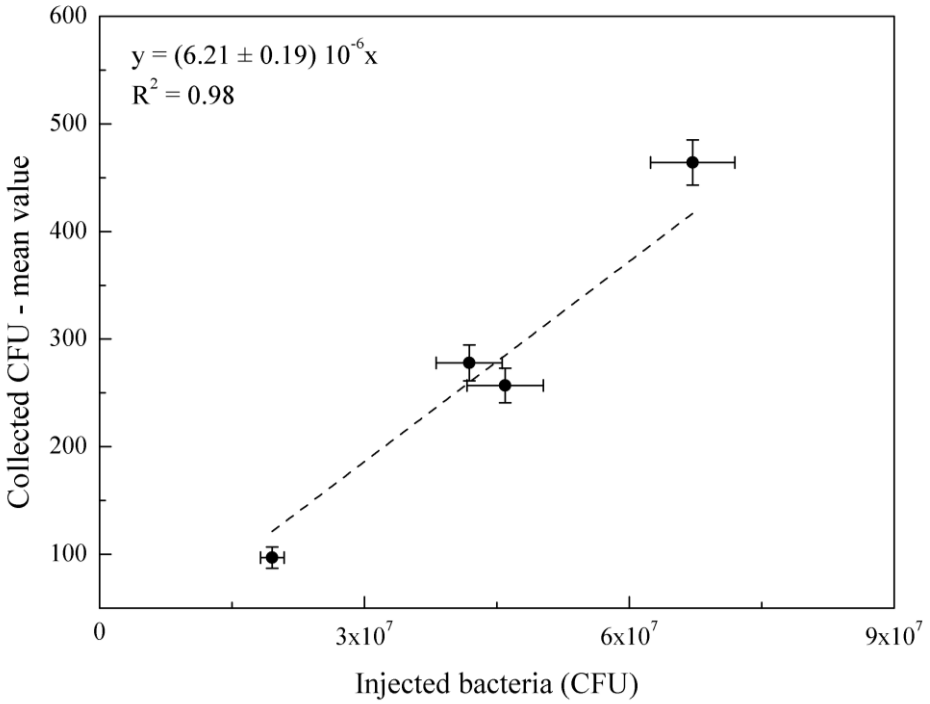

Figure 3.13 Correlation curve of the average count on the four Petri dishes exposed in each experiment with the number of *E. coli* bacteria injected in ChAMBRe by BLAM. (Danelli et al., 2021).

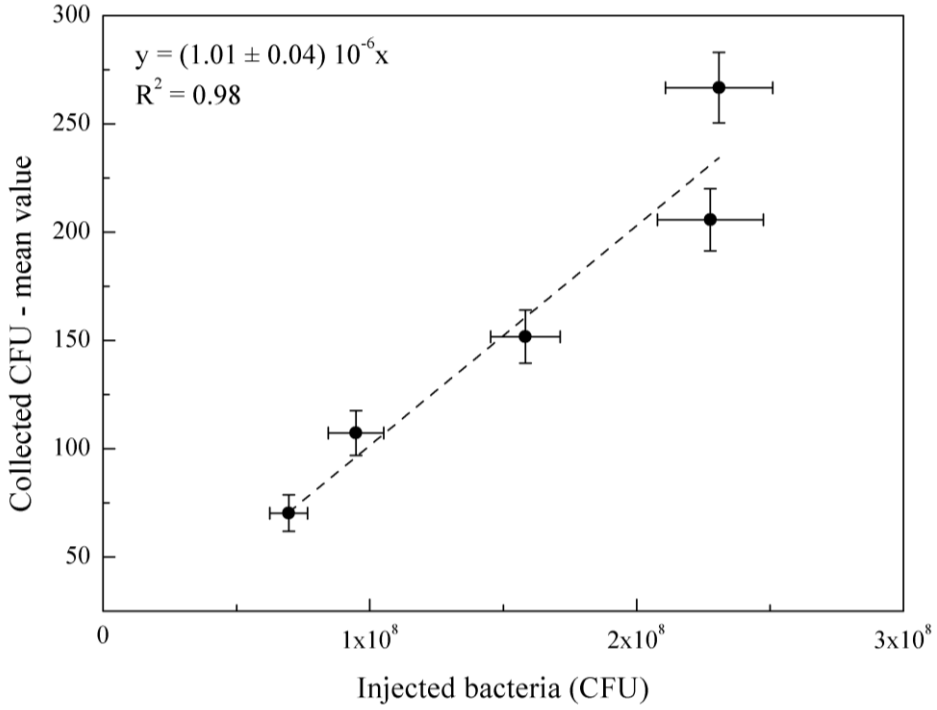

Figure 3.14 Correlation curve of the average count on the four Petri dishes exposed in each experiment with the number of *E. coli* bacteria injected in ChAMBRe by SLAG. (Danelli et al., 2021).

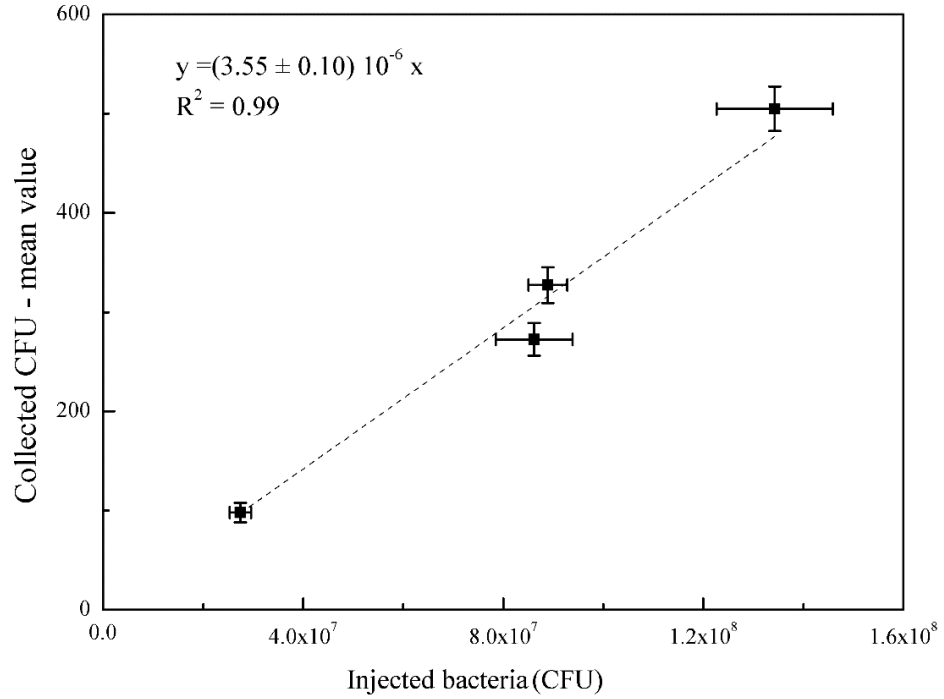

Figure 3.15 Correlation curve of the average count on the four Petri dishes exposed in each experiment with the number of *E. coli* bacteria injected in ChAMBRe by Collison. (Danelli et al., 2021).

The nebulizer characterization above described should be assumed as an indication of each nebulizer performance. However, it is recommended that the effect of aerosol generation be assessed whenever the type of microorganism to be aerosolized is changed.

The absolute value of the nebulization efficiency depends on the pressure at the outlet of the nebulizer, i.e. the pressure inside the atmospheric chamber, (Feng et al., 2021), especially for BLAM and Collison, in which nebulization occurs thanks to an induced negative pressure inside the nebulizers cavity by the high-speed jet of compressed air. The results shown in Figures 3.13, 3.14 and 3.15 were obtained in a particular pressure regime: the ChAMBRe internal pressure was about 2 mbar lower than the ambient pressure, to favor the bacteria confinement inside the chamber. This specific working condition could be used in case of experiments with pathogenic strains. Actually, at ChAMBRe, the inner pressure can be maintained in the range ± 5 mbar with respect to the ambient pressure by a feedback control system based on a PID (proportional-integral-derivative control) algorithm. With ASCs, internal overpressure to prevent contamination from the external environment is a more typical working condition. Actually, most of the results described in the following paragraphs were obtained by operating the chamber in such overpressure regime.

3.3 Processing of the WIBS data

WIBS-NEO, deployed at ChAMBRe in July 2020, provides the real-time monitoring of the concentration of bio-aerosol particles inside the chamber: this piece of information is complementary to the direct measurement of bacteria viability through the CFUs counting and is a fundamental tile of the entire puzzle.

In the instrument, particle data are reported and stored in list mode for each detected particle and this can generate a significant amount of data, especially in the chamber experiments where particle concentration is usually quite high: each run produces quite big files (about 3 GB). This issue required the development of a refined off-line data reduction procedure, since the software interface released with the instrument, the so called WIBS NEO Toolkit, resulted too time (and CPU) consuming (total time necessary for loading, processing, visualization, and inspection of data generated by the WIBS-NEO). Toolkit converts particle-by-particle data into averaged time-resolved particle concentrations and size distributions, and allows the user to plot the data. On the other hand, the software does not allow to carry out immediate and quantitative analysis on the particles divided into each category (fluorescence channels, see Ch. 2, par. 2.3.2.3), it only provides averaged information for each category, such as the average concentration of particles or the average fluorescence intensity of the particles detected in each fluorescence channel.

Actually, WIBS-NEO has been originally designed for outdoor monitoring where typical aerosol and bio-aerosol concentration are much lower than the values obtained at ChAMBRe and semi-quantitative analysis, such as discrimination between different biological particles, are performed only. On the contrary, in the experiments at ChAMBRe, the WIBS has to provide accurate concentration values of a specific bioaerosol category (bacteria, in particular) inside the chamber. Therefore, I developed and implemented a new Igor-based procedure (WaveMatrics, Inc.), which reduces significantly the processing time and the size of the output data block. Moreover, the new procedure implements a refined multi-parametric data reduction to retrieve the airborne bacteria concentration inside the chamber as a function of time.

Once raw and Force Trigger data files have been loaded, the procedure calculates the average Force Trigger background and selects particles with a fluorescence signal greater than the FT threshold. Particles are then grouped into the three channels FL1, FL2 and FL3 and, through a matching loop, into seven more specific channels (A, B, C, AB, AC, BC, ABC) (see Figure 2.7). Fiducial cuts are applied to isolate and count bacteria candidate particles (dead-time corrections are discussed in paragraph 3.3.1). Finally, the whole analysis is cycled over selectable time intervals to retrieve the time-resolved particle concentration during the whole experiment.

To find the best criteria, i.e. combination of fluorescent intensity and size information, to identify bacteria candidates among the detected particles, I performed, separately, several injection in ChAMBRe of pure bacteria cultures of *B. subtilis* and *E. coli*, to measure their optical and fluorescence properties. Data were also compared with the signal obtained by spraying saline solution (in which bacteria are usually suspended) only, to highlight possible interferences. Bacteria are known to be dominated by a single fluorescence type, falling in the channel A (Hernandez et al., 2016). The criteria to select bacteria particle were therefore identified by comparing the fluorescence peak intensity of the particles detected in channel A and the particles size. Examples of the particles size distribution in the channel A compared to the particles fluorescence intensity are given in Figure 3.16 and 3.17, which data correspond to an injection of *E. coli* strain and *B. subtilis* strain respectively. In both figures, on the left side is shown the particle background in the chamber before the bacteria injection and, on the right side, the particles population after the bacteria injection. The observed particle background depends on the chamber humidification procedure performed prior to the bacteria experiments. Considering the average aerodynamic diameters of airborne *E. coli* and *B. subtilis,* 0.6 and 0.7 μm respectively (Hernandez et al., 2016; Lee et al., 2002) and the fluorescence intensity observed during the chamber injection, different fiducial cuts were tested. The best result were obtained by identifying bacteria particles with those particles having a fluorescence in channel FL1

only (channel A), with an intensity between 3.0×10^6 and 1.5×10^7 and size range is between 0.7 and 2 µm.

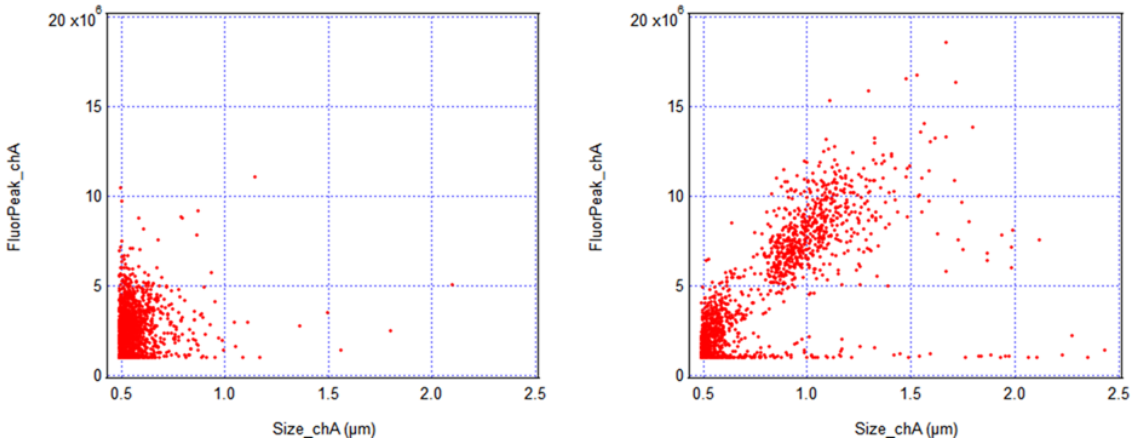

Figure 3.16 Size distribution of particles in channel A. Left side: particles background. Right side: particles population after the *E. coli* injection.

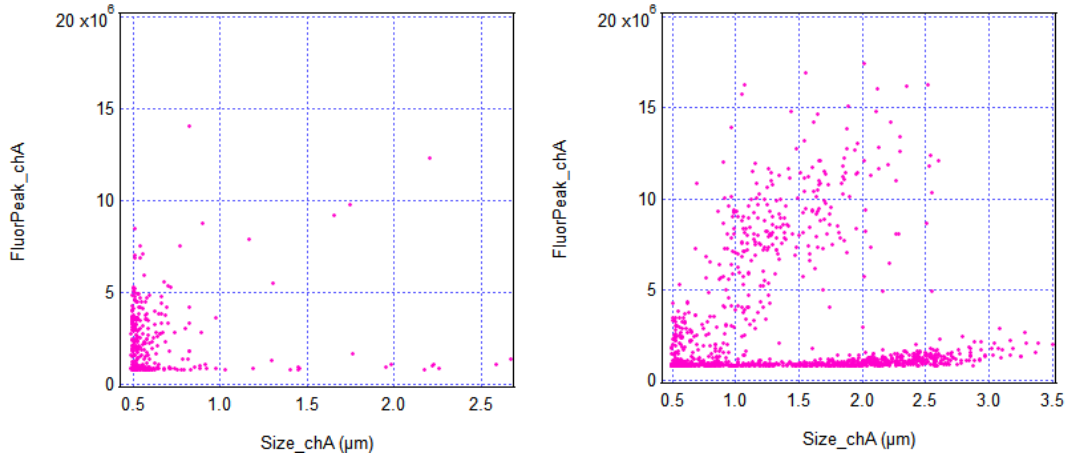

Figure 3.17 Size distribution of particles in channel A. Left side: particles background. Right side: particles population after the *B. subtilis* injection.

The multi-parametric analysis of the WIBS data above described give the possibility to follow, along the experiment, the concentration of bacteria particles inside ChAMBRe. The initial bacteria concentration reached immediately after the injection is the parameter used during the chamber experiments, described in the next section, to be compared with the number of bacteria colonies collected on the petri dishes placed inside ChAMBRe. Examples of the temporal trend of two the bacteria models, *E. coli* and *B. subtilis*, during typical chamber experiments are reported in Figure 3.18 and 3.19, respectively. Each point of the graph represents the bacteria concentration in time intervals of 300 s. In the figures is also shown the curve fit; used to estimate the lifetime of the bacteria particles inside ChAMBRe, applying the same approach described for NaCl particles in Chapter 2,

paragraph 2.5.3. By following the particle concentration as a function of time and fitting the decay curve with the following first order law, particles lifetime is retrieved off:

$$y = y_0 e^{-k_d t} e^{-\beta t}$$

Where y_0 is the particle concentration at time t_0, k_d is the dilution factor corresponding to the air flow exiting the chamber, due to the instruments airflow, during the experiment (here, 1.7×10^{-5} s^{-1}) and β is particle loss-rate coefficients. Hence, I confirmed the lifetime of bacteria particles inside the chamber, previously estimated by the optical particle counter and NaCl particles (Chapter 2, paragraph 2.5.3). Particle loss-rate coefficients for bacteria particle in the range (4-6) $\times 10^{-5}$ s^{-1}, and correspond to a particle lifetime of around 5 h, confirming that way the time slot suitable for the experiments at ChAMBRe.

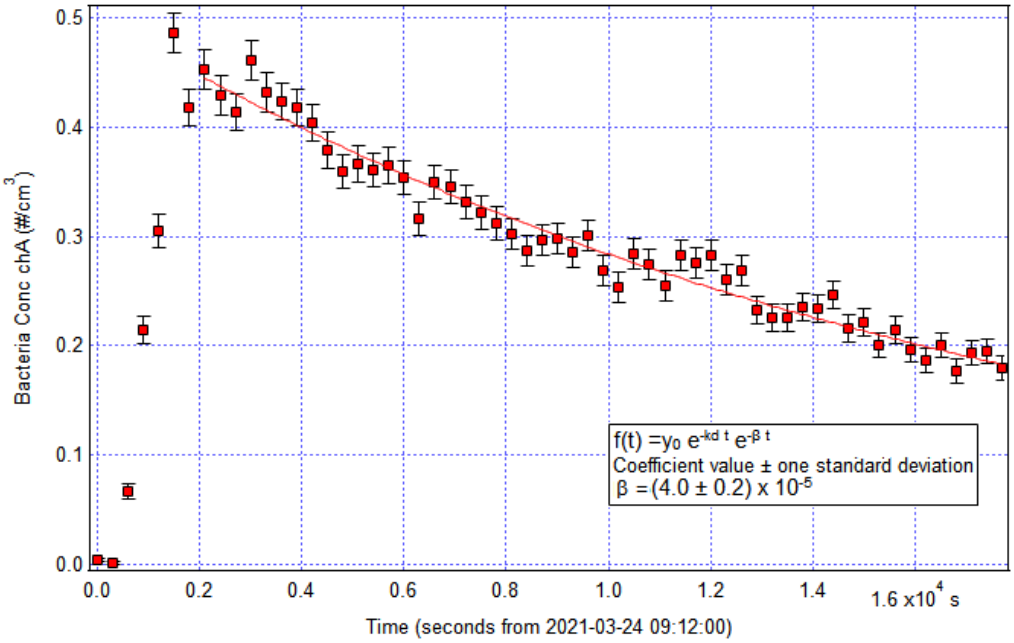

Figure 3.18 Temporal trend of *E. coli* particles inside the chamber. The curve fit is also shown, where β is the particle loss rate coefficient and k_d is the dilution factor (here 1.7 10^{-5} s^{-1}).

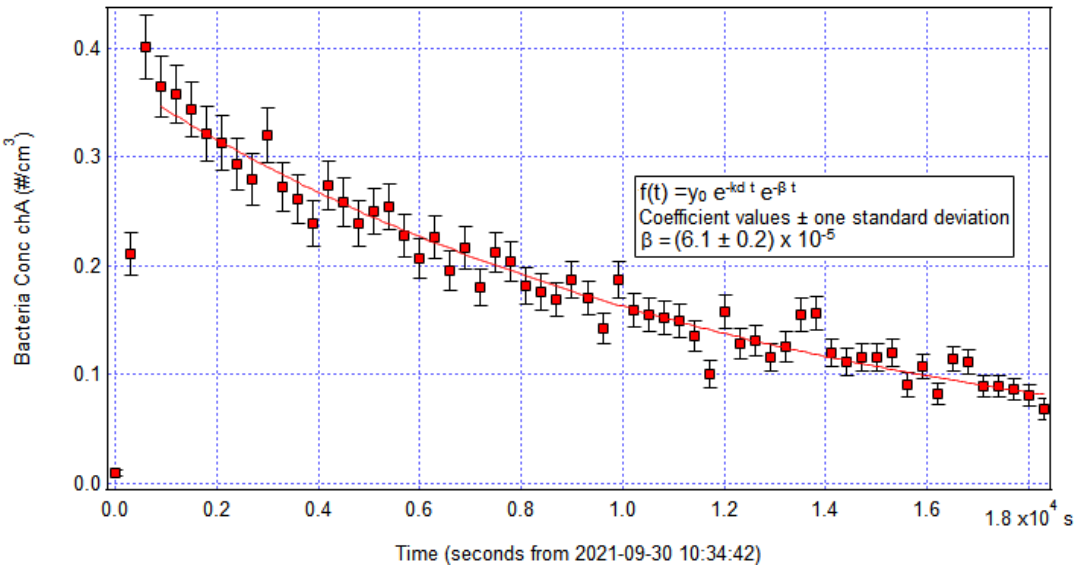

Figure 3.19 Temporal trend of *B. subtilis* particles inside the chamber. The curve fit is also shown, where β is the particle loss rate coefficient and k_d is the dilution factor (here 1.7 10^{-5} s^{-1}).

3.3.1 Coincidence and Dead time losses

To overcome the limitations and uncertainties intrinsic to the WIBS-NEO operation principle, such as particles coincidence and dead time losses, some precaution and corrections are necessary.

Particle coincidence cannot be avoided other than keeping the concentrations that are sampled as low as possible since the probability that two or more particles are close enough to occupy the same scattering volume (laser or xenon lamp volume) increases with the concentration. Under the assumption that the particles arrive to the beam with a randomly spaced distribution, the probability of coincidence particles, i.e., the probability that the spacing between particles is less than or equal to the width of the laser beam, can be estimated using an exponential probability density function (Baumgardner et al., 1985):

$$P\ (0 <\ d \leq BW) = 1 -\ e^{-BW/w}$$

Where d is the spacing between particles, BW is the width of the laser beam in centimeters and w is the average spacing between particles, given by

$$w =\ N^{-1/3}$$

N is the concentration of particles in number per cubic centimeter. The nominal width of the WIBS NEO laser beam is 0.0078 cm. When $N \geq 1000$ cm^{-3}, the probability goes to about 8%. In ChAMBRe experiments, the particles in the size range of the WIBS (0.5 - 30 µm), rarely exceed 1000 cm^{-3}, so corrections for undercounting due to coincidence in the laser are relatively small.

Dead time losses for fluorescence bioaerosol particles (FBAPs) occur when a FBAP is not illuminated by the Xenon lamp since it is recharging after a previous pulse. Figure 3.20 illustrates the

measurement cycle where a particle P_1, detected by the 635 nm laser beam and which triggers the xenon lamp, is followed by another particle, P_2 that also triggers the xenon lamp. If the time interval between P_1 and P_2, ΔT, is longer than the lamp recharge time, T_{charge}, both the particles are excited by the lamps (Figure 3.20a). When ΔT is shorter than the lamp recharge time, P_2 is not excited and is subsequently recorded as having no fluorescence signal. This condition is shown in Figure 3.20b and c, where the difference in the two schemes is the composition of particle P_1: in Figure 3.20b P_1 is a FBAP while in Figure 3.20c P_1 is a non-FBAP. This is an important distinction because both non-FBAPs and FBAPs send trigger signals to the flash lamps and since the concentration of non-FBAPs is typically much higher, the probability that the detection of a non-FBAP lead to a dead-time event is higher than an FBAP doing so.

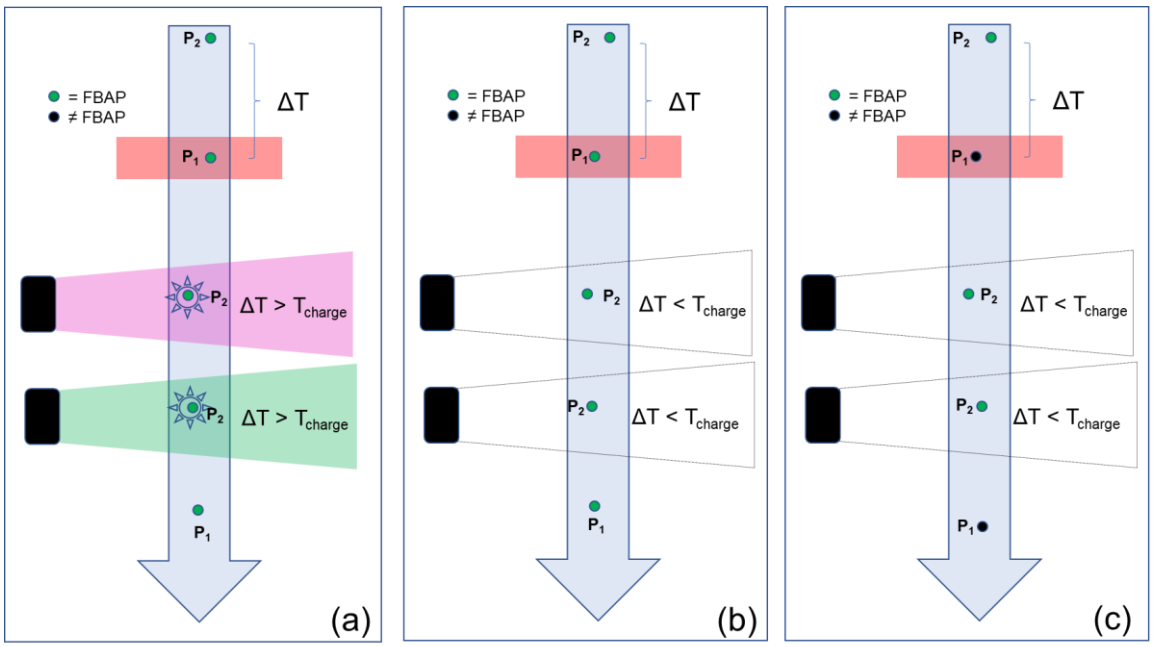

Figure 3.20 Examples of dead time loss (extracted from the WIBS manual).

The recharge time of the flashlamps is approximately 8 ms, which limits a maximum of 125 excitations each second, i.e. 125 particle detections each second. This rarely occurs in the natural environment because nature tends to order particle spacing in a more random distribution. The sample volume flowrate of the instrument is 5 cm^3 s^{-1} so that a flow of 125 particle s^{-1} corresponds to a concentration of 20 particle cm^{-3}. When particle concentration exceed this value, some of them are not identified as FBAP since they pass through the cavity of the xenon lamps during the recharge (dead) time. The WIBS returns the rate of "Valid_Particle_Count, VPC" and "Total_Particle_Count, TPC". VPC is the number of lamp flashes, i.e., the number of times that the trigger sent to the flashlamp circuit produces an excitation (which also identifies the "exited particle counts"). The second parameter is the number of triggers sent to the lamp circuit, regardless of whether the lamps

flashes or not. The plot of VPT vs TPC (Figure 3.21) is fully compatible with a dead time of about 8 ms.

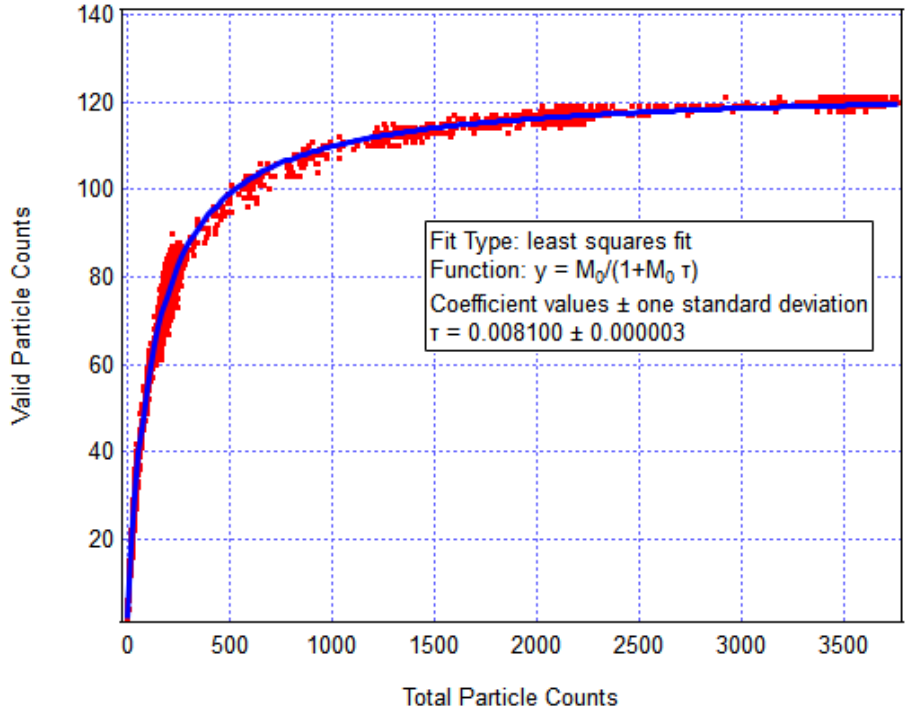

Figure 3.21 Plot of Valid Particle Count (VPC) vs Total Particle Counts (TPC) collected in three different chamber experiments at different particles concentration. The curve follows exactly the prevision for the dead time correction for a detector with τ = 8 ms (par. τ in the fit, being M_0= TPC and y =VPC).

Dead time losses directly affect FBAPs (TPC undercounting due to coincidence in the laser beam is usually lower than 10%). As particle concentration increases, the losses become increasingly significant and must be corrected. Assuming the ratio of measured FBAP counts (M_{FBAP}) to VPC is the same as the ratio of total FBAP counts (T_{FBAP}) to TPC, the correction factor is defined as the ratio between the total particles and the excited particles:

$$T_{FBAP} /TPC = M_{FBAP} /VPC$$

$$T_{FBAP} = M_{FBAP} (TPC/VPC)$$

$$\text{Correction Factor} = TPC/VPC$$

This issue is particularly relevant in chamber experiments, where, as previously pointed out, the aerosol concentration can be much greater than those typically found in ambient air.

3.4 Results and Conclusions

3.4.1 Baseline experiments

The experiments to study the correlation between bacterial viability and atmospheric composition and conditions in ChAMBRe rely on the protocol for injecting and extracting bacteria from the chamber.

A set of experiments were performed with a "clean" atmosphere (i.e., with the background levels given in Chapter 2, paragraph 2.5.1) inside ChAMBRe to measure the reproducibility of the whole procedure. In these experiments the inner pressure inside the chamber was maintained about four mbar above the ambient pressure by a feedback control system. During each experiment, one specific strain was injected into the simulation chamber and exposed to standard setting (T= 22 °C, R.H.= 60 %, CO_2 = 450 ppm) for 5 h. For both the strains, injections were performed by all the three nebulizers (BLAM, SLAG and Collison). The working conditions of each device were the same reported in Table 3.2. Gas species concentration, temperature, pressure, relative humidity and PM_{10} concentration (measured by OPS and WIBS-NEO) were constantly monitored inside the chamber.

The initial PM_{10} concentration (bacteria plus NaCl particles) determined by the OPS, was taken as a rough proxy of aerosolization efficiency while the bacteria concentration inside ChAMBRe was retrieved by the WIBS data.

For each strain, ten different experiments were performed; the results are described in the follow.

Values of the atmospheric parameters in ChAMBRe during each experiment are reported in Table 3.5 and 3.6 for the *E. coli* and *B. subtilis*, respectively. The amount of CFU injected, the airborne bacteria concentrations inside ChAMBRe and the average number of colonies counted on the Petri dishes after the chamber exposure are reported in Table 3.7 and 3.8. The volume of the bacterial suspension injected through the nebulizers was equal to 2 mL, except during the injection performed with the Collison atomizer: in this case, the reference parameter used to calculate the injected CFU was the injection time, set at 4 minutes as described in paragraph 3.2.2.

Table 3.5 Environmental parameters in ChAMBRe during the "*E. coli baseline experiments*". The value of PM_{10} measured inside the chamber after each injection and the average concentration of the CO_2 along the experiments are also reported.

Exp.	Temperature (°C)	Relative Humidity (%)	External Pressure (mbar)	Internal Pressure (mbar)	PM_{10} ($\mu g\ m^{-3}$)	CO_2 (ppm)
1	22	62	1016	1020	38	398
2	22	61	1012	1017	46	401
3	22	63	1019	1023	2	400
4	22	60	1010	1014	45	400
5	20	63	1008	1013	286	397
6	22	59	1013	1018	406	398
7	22	63	1010	1014	336	400
8	22	65	1010	1015	245	395
9	22	60	1007	1011	6	398
10	23	53	1014	1013	35	415

Table 3.6 Environmental parameters in ChAMBRe during the "*B. Subtilis baseline experiments*". The value of PM_{10} measured inside the chamber after each injection and the average concentration of the CO_2 along the experiments are also reported.

Exp.	Temperature (°C)	Relative Humidity (%)	External Pressure (mbar)	Internal Pressure (mbar)	PM_{10} ($\mu g\ m^{-3}$)	CO_2 (ppm)
1	20	66	1018	1022	317	403
2	21	64	1018	1023	304	400
3	19	66	998,4	1003	241	397
4	21	63	1003	1007	30	395
5	22	61	1014	1018	27	402
6	22	63	1009	1013	32	439
7	22	60	1003	1007	19	458
8	22	61	1002	1002	55	446
9	22	60	1013	1012	65	435
10	22	61	1013	1012	71	440

Table 3.7 *E. coli* experiments: CFU injected, initial bacteria concentration inside ChAMBRe and average number of colonies collected on the Petri dishes.

Exp.	Nebulizer	Bacteria Injected (CFU)	Cell m^{-3}	Mean CFU counts
1	SLAG	$(3.5 \pm 0.2) \times 10^8$	$(1.20 \pm 0.05) \times 10^6$	338 ± 18
2	SLAG	$(1.9 \pm 0.2) \times 10^8$	$(0.58 \pm 0.04) \times 10^6$	225 ± 15
3	SLAG	$(1.5 \pm 0.1) \times 10^8$	$(0.43 \pm 0.02) \times 10^6$	171 ± 13
4	SLAG	$(1.8 \pm 0.2) \times 10^8$	$(0.55 \pm 0.03) \times 10^6$	208 ± 14
5	COLLISON	$(1.0 \pm 0.1) \times 10^8$	$(0.14 \pm 0.04) \times 10^6$	103 ± 10
6	BLAM	$(6.3 \pm 0.6) \times 10^7$	$(0.40 \pm 0.10) \times 10^6$	119 ± 11
7	COLLISON	$(0.9 \pm 0.1) \times 10^8$	$(0.22 \pm 0.05) \times 10^6$	117 ± 11
8	BLAM	$(4.6 \pm 0.5) \times 10^7$	$(0.19 \pm 0.04) \times 10^6$	146 ± 12
9	COLLISON	$(0.9 \pm 0.1) \times 10^8$	$(0.35 \pm 0.01) \times 10^6$	112 ± 11
10	SLAG	$(6.3 \pm 0.8) \times 10^7$	$(0.15 \pm 0.02) \times 10^6$	36 ± 6

Table 3.8 *B. subtilis* experiments: CFU injected, initial bacteria concentration inside ChAMBRe and average number of colonies collected on the Petri dishes.

Exp.	Nebulizer	Bacteria Injected (CFU)	Cell m^{-3}	Mean CFU counts
1	COLLISON	$(1.7 \pm 0.1) \times 10^8$	$(2.2 \pm 0.2) \times 10^5$	110 ± 10
2	BLAM	$(1.0 \pm 0.1) \times 10^8$	$(2.1 \pm 0.2) \times 10^5$	100 ± 10
3	BLAM	$(5.5 \pm 0.9) \times 10^7$	$(0.4 \pm 0.2) \times 10^5$	18 ± 4
4	SLAG	$(9.6 \pm 0.1) \times 10^7$	$(1.8 \pm 0.2) \times 10^5$	92 ± 10
5	SLAG	$(1.1 \pm 0.1) \times 10^8$	$(0.8 \pm 0.1) \times 10^5$	49 ± 7
6	SLAG	$(1.5 \pm 0.2) \times 10^8$	$(1.2 \pm 0.1) \times 10^5$	52 ± 7
7	SLAG	$(1.1 \pm 0.1) \times 10^8$	$(0.44 \pm 0.02) \times 10^5$	19 ± 6
8	SLAG	$(6.8 \pm 0.2) \times 10^8$	$(0.7 \pm 0.1) \times 10^5$	36 ± 6
9	SLAG	$(1.4 \pm 0.2) \times 10^8$	$(2.4 \pm 0.2) \times 10^5$	120 ± 11
10	SLAG	$(1.0 \pm 0.2) \times 10^8$	$(1.3 \pm 0.2) \times 10^5$	64 ± 8

The uncertainties quoted in Tables 3.7-3.8 are just those deriving from the Poisson fluctuation, and they do not include any other systematic or statistical contribute.

The initial aerosol concentration of microorganisms in ChAMBRe after the injection, retrieved off-line by the WIBS data, turned out to be about 10^6 cell m^{-3} for the *E. coli* and 10^5 cell m^{-3} for the *B. subtilis*, pretty similar to the total average bacterial aerosol centration in near-surface air, over lands, which are estimated to be between 10^4 and 10^5 cell m^{-3} (Burrows et al., 2009a).

The baseline figure (i.e., ratio between collected viable bacteria and the initial concentration of the bacteria injected in ChAMBRe) for the two strains is shown in Figures 3.22 and 3.23. The baseline shows a very good correlation (i.e., R^2 0.99, Figure 3.23) with *B. subtilis* while with *E. coli*, the correlation is worse (i.e., R^2 0.78, Figure 3.23), with some experiments with BLAM and Collison which deviate from the average trend. A quite high PM_{10} concentration (approximately in the range between 200 and 400 μg m^{-3}, see Tables 3.5 and 3.6) was obtained in the chamber after the bacteria injection by BLAM and Collison, due to the nebulization of many salt particles originating from the saline solution in which the bacteria were suspended. With the SLAG the typical PM_{10} concentration was around 30 - 40 μg m^{-3}. As total PM increases, dead time and multiple-counting effects in the WIBS (see paragraph 3.3.1) become increasingly significant and could lead to subsequent underestimation of bacteria concentration, which could explain the deviation from the average trend measured in some of the BLAM and Collison experiments. An experiment with *E. coli* suspended in simple Milli-Q water (experiment 9 in Tables 3.5 and 3.7; indicated as COLLISON * in Figure 3.22) was performed to elucidate a possible interference of the salt particles in the WIBS counting of *E. coli* particles. The test provided a result well in agreement with the baseline. The high concentration of salt particles produced by BLAM and the Collison was suspected to affect the bacteria count by the WIBS. However, the possibility of replacing saline with Milli-Q water as a means of bacterial resuspension was rejected, since saline solutions are recommended for the bacteria suspensions preparation. Normal saline solution (0.9% NaCl) is isotonic to microbial cells and preserve cells osmotic. Therefore, it was decided to use the SLAG only, which anyway allows to obtain adequate concentrations of bacteria with both the bacteria strain. Considering the results of "*SLAG experiments*" only, summarized in Figures 3.24 and 3.25, the baseline reproducibility turned out to be 12% and 13%, respectively with *E. coli* and *B. subtilis*. This value corresponds to the standard deviation of the results of each bunch of experiments around the mean value of the collected to injected CFU ratio and measures the sensitivity of the whole procedure, which appears to be adequate to observe sizeable variations in bacteria viability when they are exposed to specific pollutants or conditions inside the chamber.

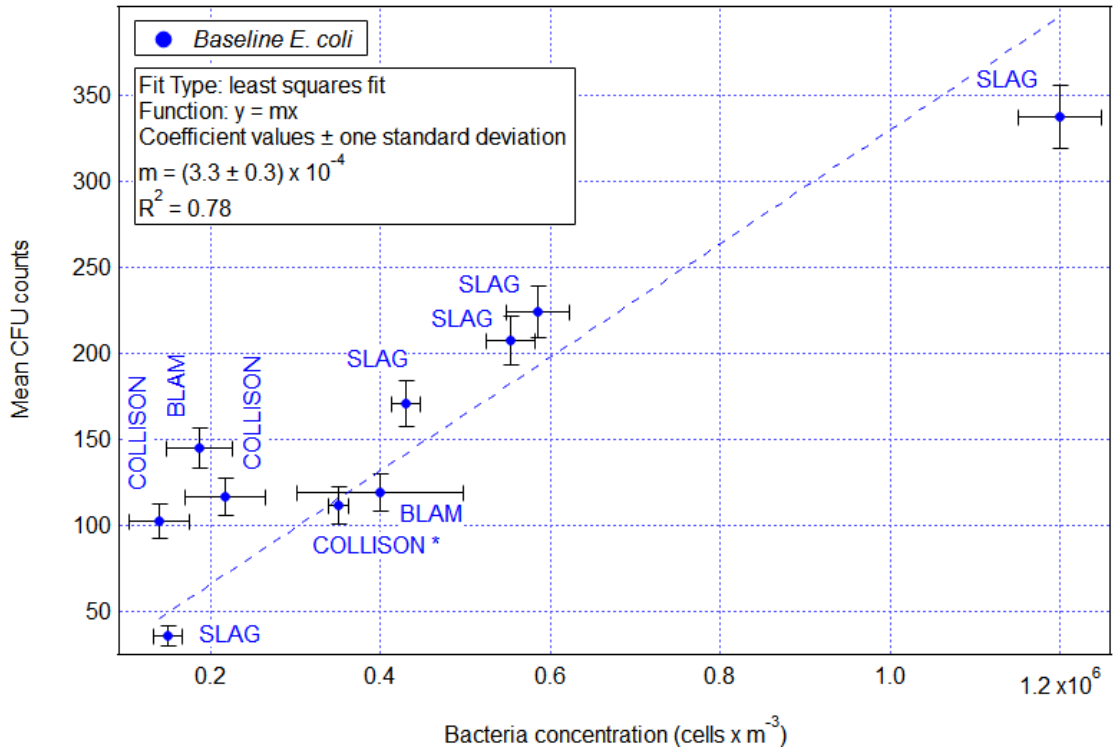

Figure 3.22 Baseline experiments with the *E. coli* strain: correlation curve between of the average count on the four Petri dishes exposed in each experiment with the bacteria concentration measured by the WIBS.

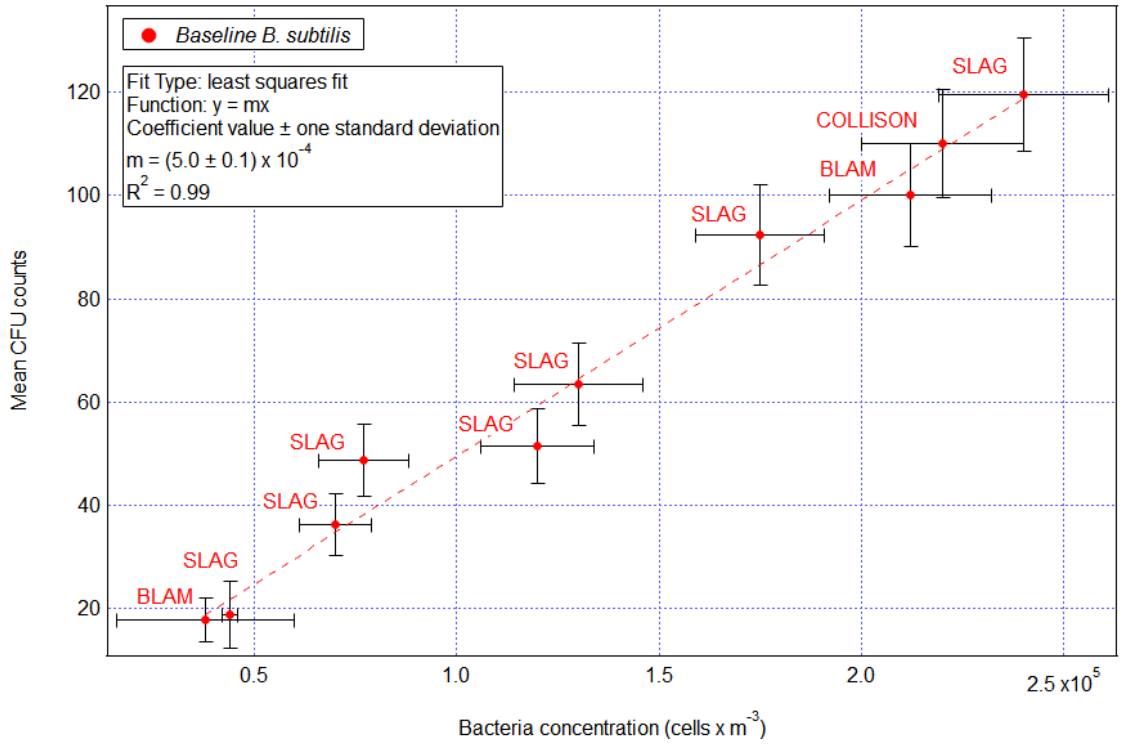

Figure 3.23 Baseline experiments with the *B. subtilis* strain: correlation curve between of the average count on the four Petri dishes exposed in each experiment with the bacteria concentration measured by the WIBS.

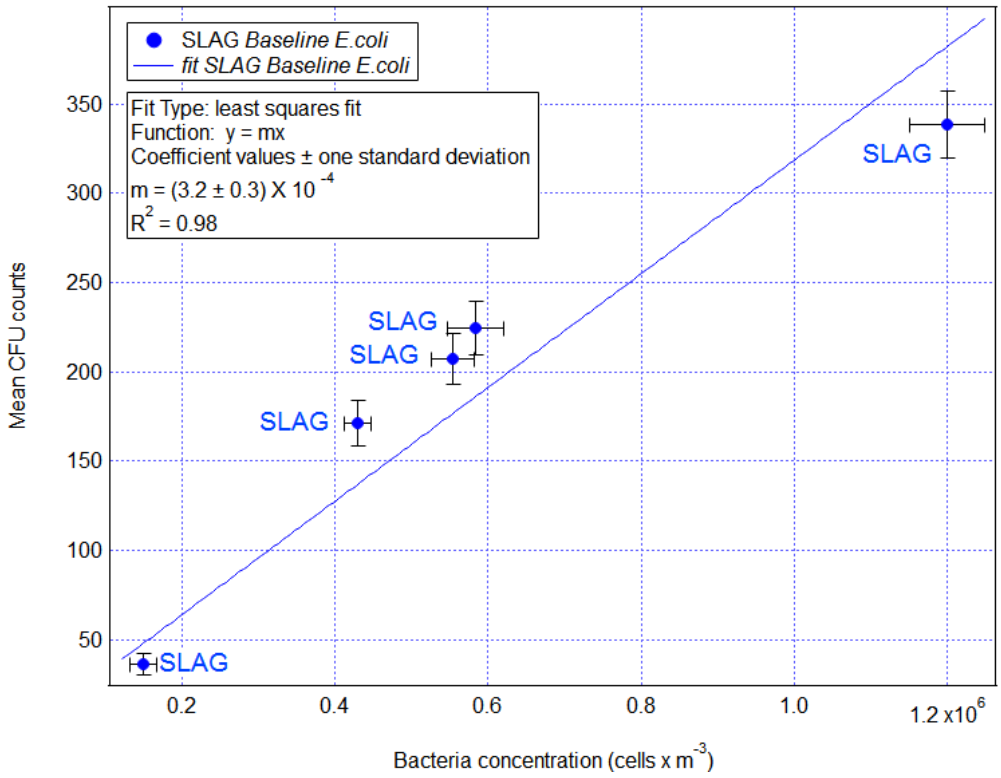

Figure 3.24 Baseline experiments with the *E. coli* strain considering the experiments performed with the SLAG nebulizer only.

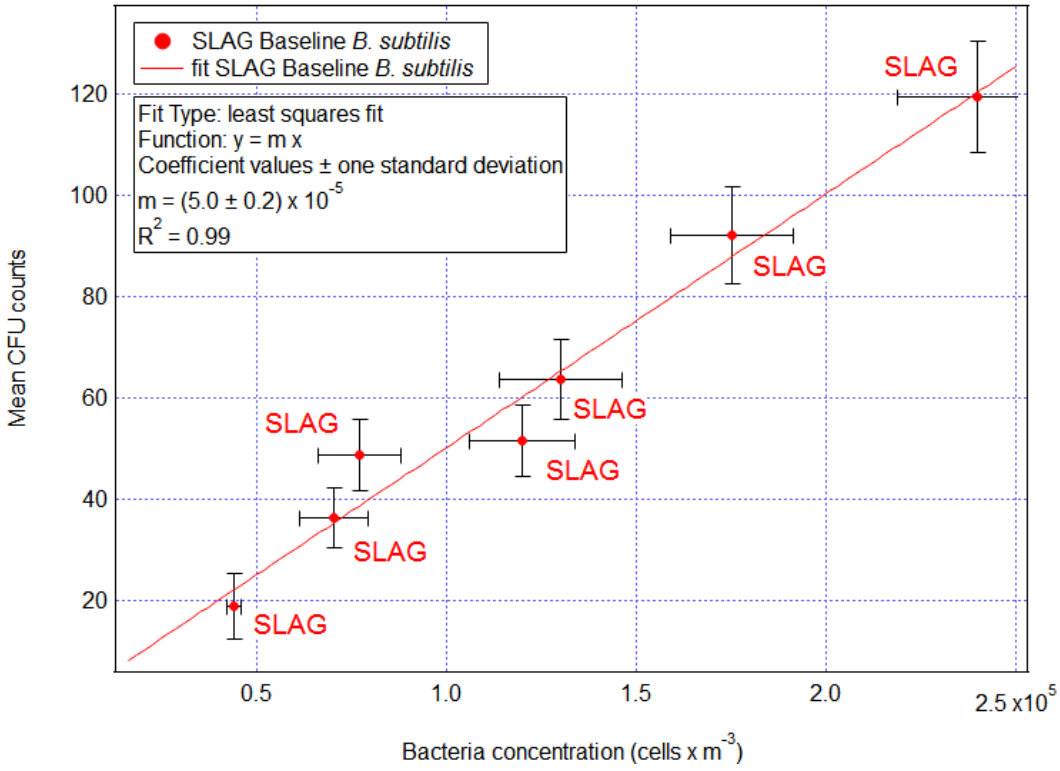

Figure 3.25 Baseline experiments with the *E. coli* strain considering the experiments performed with the SLAG nebulizer only.

3.4.2 Bacteria and pollutants

The baselines assessment was followed by a set of exploratory experiments with the two bacteria strains exposed to selected pollutants. The experiments focused on the bacterial response to the exposure to high concentrations of two of the most common pollutants emitted by anthropogenic sources: nitrogen oxides and soot particles (Monks et al., 2009; Pöschl and Shiraiwa, 2015; Seinfeld and Pandis, 1998; Sonwani and Saxena, 2016).

Nitrogen oxides (NO_x) usually denotes the total concentration of nitric oxide (NO) and nitrogen dioxide (NO_2), since the conversion between these two species is rapid in the atmosphere. NO_x enters in the atmosphere as a result of anthropogenic activity (mostly fossil fuel combustion from vehicles) and natural processes (lightning and soil processes). Nitrogen oxides are formed in essentially all combustion processes, mostly as nitric oxide with smaller amounts of nitrogen dioxide. NO is subsequently oxidized to NO_2 in the atmosphere. These gases contribute to the formation of smog through photochemical reactions and are acid rain precursor (Glarborg et al., 2018; Hallquist et al., 2009; Harrison, 2005).

Soot particles are carbonaceous particles formed during incomplete combustion of organic hydrocarbons. These particles are intrinsically light absorbing and their presence in the atmosphere induces positive radiative forcing. Soot particles can have substantial adverse effects on human health (Finlayson-Pitts and Pitts, 2000; Michelsen, 2017; Seinfeld and Pandis, 1998; Shiraiwa et al., 2012). Previous studies suggest that atmospheric pollutants like NO_x and soot particles can influence the viability of airborne bacteria, e.g., by preventing bacteria from degradation processes (e.g., during UV irradiation) or inducing structural changes in their survival strategies (Brotto et al., 2015, Hussey et al., 2017, Noda et al., 2019 and 2021).

3.4.2.1 Soot experiments

All the experiments were carried out by keeping the pressure inside the chamber 1 mbar below the atmospheric pressure. Soot particles were generated with the miniature inverted soot generator (MISG; Chapter 2, paragraph 2.4.2). Fueled with propane and with an injection time of about one minute, the soot generator produced between 400 and 600 μg m^{-3} of black carbon (mean diameter =180 nm, typical concentration = 10^5 particle cm^{-3}) inside ChAMBRe (Vernocchi et al., 2021). Soot particles were injected into the chamber 10 minutes after the bacteria injection. Just before the soot injection, WIBS was disconnected to ChAMBRe to protect the instrument from soot contamination, which is known to cause fluorescence interference (Savage et al., 2017). The size distribution of soot particles was measured by the SMPS (Chapter 2, paragraph 2.3.2) and the optical properties and black carbon mass concentration were measured by the 870 nm-PAX (Chapter 2, paragraph 2.3.3). At the

end of the soot injection, the CO_2 concentration in the chamber was typically between 500 - 550 ppm while NO and NO_2 concentration values were 170 - 200 ppb and 10 - 80 ppb, respectively.

The chamber condition in each experiment are reported in Table 3.9. The PM_{10} concentration immediately at the end of the bacteria injection is indicated in Table 3.10, as well as the concentration of black carbon (BC), CO_2 and NO_x reached in ChAMBRe before the soot injection. The number of injected CFU, the bacteria concentration inside the chamber and the average number of colonies counted on the Petri dishes after the exposure in ChAMBRe are reported in Table 3.11.

Results are given in Figures 3.26 and 3.27 for *E coli* and *B. subtilis* respectively. In the figures, the baseline with its uncertainty interval (12% and 13%, respectively for *E. coli* and *B. subtilis),* is also shown for reference.

The Gram-negative *E. coli* appears to be almost unaffected by the presence of the soot particles (Figure 3.26). Two point are comparable to the sensitivity interval around the baseline value, while in one point the ratio between the collected CFU and the airborne bacteria concentration increases by a factor 1.5.

With *B. subtilis*, the picture is more complex: the ratio between the number of collected colonies and the airborne bacteria concentration shows a significant reduction with respect to the baseline in four experiments, suggesting a soot-induced reduction of the bacteria viability. However, two experiments result close to the baseline (Figure 3.27).

Table 3.9 ChAMBRe conditions in the experiments with soot.

Exp.	Temperature (°C)	Relative Humidity (%)	External Pressure (mbar)	Internal Pressure (mbar)
		E. coli		
SOOT E1	23	58	1017	1017
SOOT E2	22	61	1009	1008
SOOT E3	22	60	1007	1006
		B. subtilis		
SOOT B1	23	60	1011	1010
SOOT B2	22	60	1014	1013
SOOT B3	22	62	1018	1017
SOOT B4	22	60	1015	1014
SOOT B5	22	60	1013	1013
SOOT B6	22	59	1014	1013

Table 3.10 PM_{10}, BC, CO_2 and NO_x concentration values in the experiments with soot.

Exp.	PM_{10} ($\mu g\ m^{-3}$)	CO_2 (ppm)	BC ($\mu g\ m^{-3}$)	NO (ppb)	NO_2 (ppb)
		E. coli			
SOOT E1	85	515	395	170	15
SOOT E2	56	500	530	215	12
SOOT E3	50	555	560	190	16
		B. subtilis			
SOOT B1	56	550	580	200	40
SOOT B2	60	502	560	215	80
SOOT B3	50	500	660	180	50
SOOT B4	55	530	610	230	27
SOOT B5	60	530	560	170	20
SOOT B6	80	530	420	170	10

Table 3.11 CFU injected, bacteria concentration inside ChAMBRe and average number of colonies counted on each Petri dish in the experiments with soot.

E×p.	Bacteria Injected (CFU)	Cell m^{-3}	Mean CFU counts
		E. coli	
SOOT E1	$(1.9 \pm 0.3) \times 10^8$	$(5.6 \pm 0.4) \times 10^5$	220 ± 15
SOOT E2	$(5.4 \pm 0.2) \times 10^7$	$(2.5 \pm 0.3) \times 10^5$	120 ± 10
SOOT E3	$(1,1 \pm 0.1) \times 10^8$	$(4.6 \pm 0.3) \times 10^5$	190 ± 14
		B. subtilis	
SOOT B1	$(1.2 \pm 0.1) \times 10^8$	$(1.8 \pm 0.3) \times 10^5$	80 ± 10
SOOT B2	$(1.7 \pm 0.1) \times 10^8$	$(3.9 \pm 0.4) \times 10^5$	75 ± 9
SOOT B3	$(1.3 \pm 0.1) \times 10^8$	$(1.7 \pm 0.3) \times 10^5$	40 ± 6
SOOT B4	$(1.5 \pm 0.1) \times 10^8$	$(2.6 \pm 0.2) \times 10^5$	180 ± 13
SOOT B5	$(1.2 \pm 0.1) \times 10^8$	$(2.8 \pm 0.2) \times 10^5$	85 ± 9
SOOT B6	$(6.9 \pm 0.8) \times 10^7$	$(1.5 \pm 0.4) \times 10^5$	20 ± 4

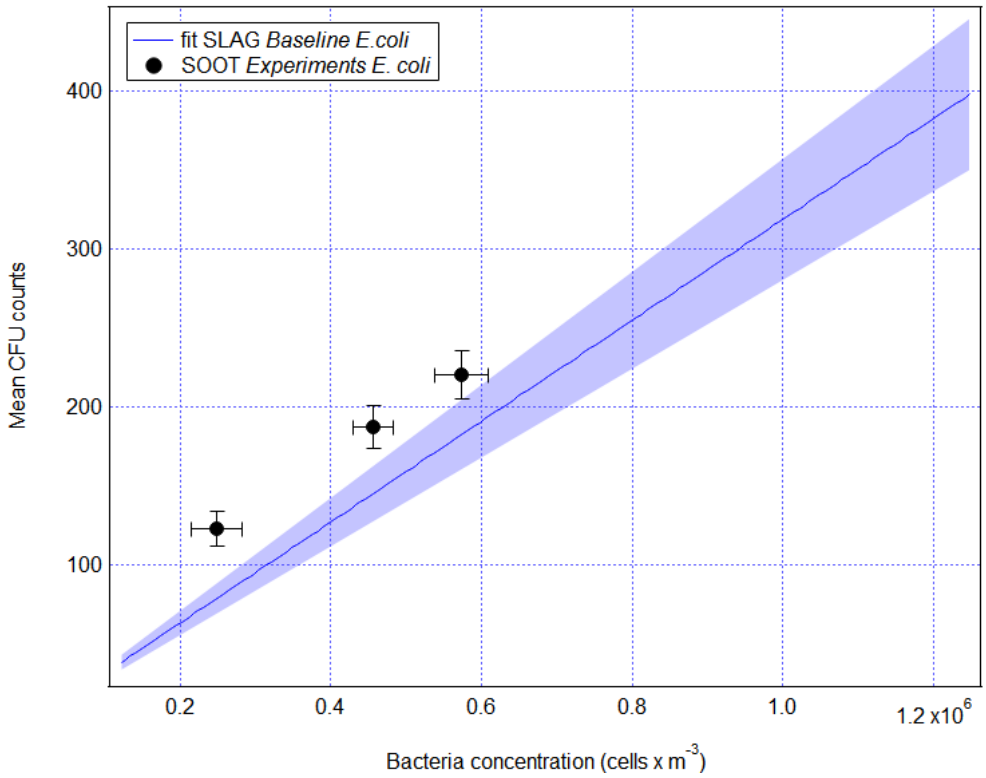

Figure 3.26 *E. coli* experiments with soot*:* mean CFU counted on the Petri dishes vs the initial bacteria concentration in ChAMBRe. The baseline and its uncertainty band are also shown.

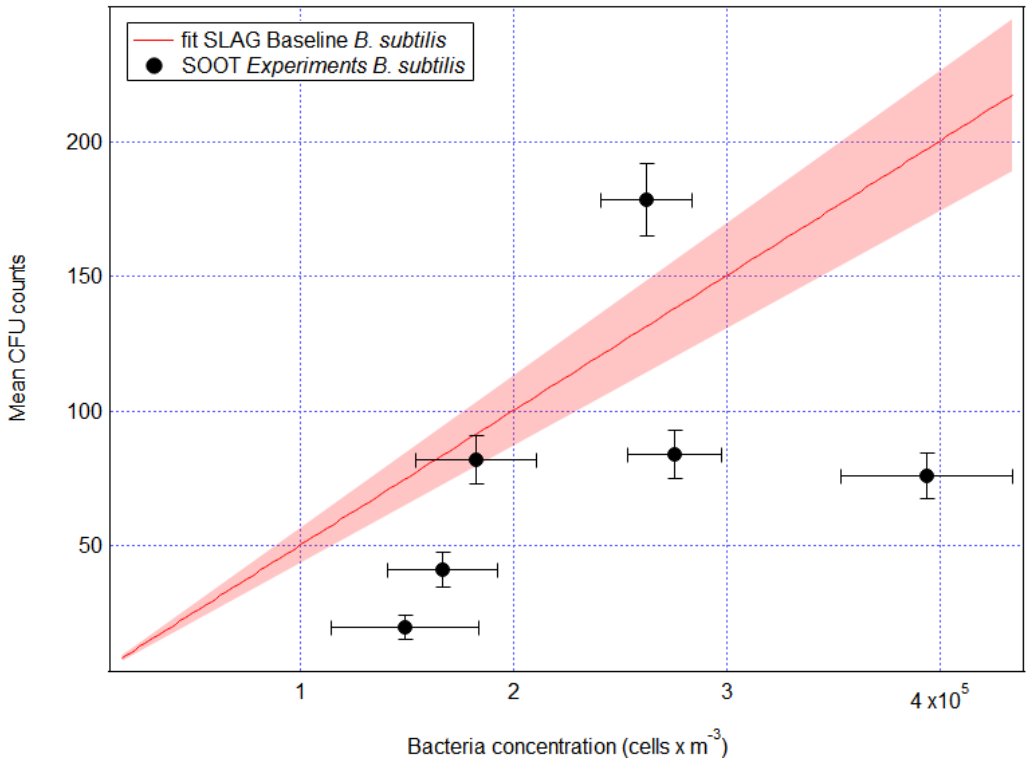

Figure 3.27 *B. subtilis* experiments with soot*:* mean CFU counted on the Petri dishes vs the initial bacteria concentration in ChAMBRe. The baseline and its uncertainty band are also shown.

3.4.2.2 NO_x experiments

The production of soot particles also generates concentrations of NO_x gases (NO concentration in the range of 170 - 200 ppb and NO_2 in the range of 10 - 80 ppb), respectively, which could predominantly have a toxic effect on bacteria. The possible effect due to the NO_x levels recorded during the soot experiments were therefore investigated separately, without the presence of soot particles.

Three different experiments were performed whit the *E. coli* and two with the *B. subtilis*, as reported in Tables 3.12 and 3.13. NO concentration was kept constant at 200 ppb, thanks to a feedback control system. The NO_2 concentration value was those deriving from the small concentration of this gas present in the cylinder of NO and it was kept indirectly constant by the feedback system acting on the NO concentration as well. CO_2 concentration was constantly monitored, and the value was those deriving from the ambient air through the air inlet system of the chamber. The value of CO_2 concentration reported in Table 3.12 is the averaged concentration along experiment.

Table 3.12 ChAMBRe conditions in the NO_x experiments. The PM_{10} level immediately after the bacteria injection and the concentration of CO_2 and NO_x are also reported.

Exp.	T (°C)	R. H. (%)	Ext. P. (mbar)	Int. P. (mbar)	PM_{10} (µg m^{-3})	CO_2 (ppm)	NO (ppb)	NO_2 (ppb)
				E. coli				
NO_X E1	22	58	1010	1009	45	425	200	10
NO_X E2	21	60	1014	1013	50	425	200	20
NO_X E3	21	60	1012	1011	45	430	200	20
				B. subtilis				
NO_X B1	22	63	1017	1016	60	440	200	80
NO_X B2	22	60	1017	1016	70	450	230	25

Table 3.13 CFU injected, bacteria concentration inside ChAMBRe and average number of colonies counted on each Petri dish in the NO_x experiments.

Exp.	Bacteria Injected (CFU)	Cell m^{-3}	Mean CFU counts
		E. coli	
NO× E1	$(9.4 \pm 0.7) \times 10^7$	$(4.6 \pm 0.4) \times 10^5$	190 ± 14
NO× E2	$(9.8 \pm 0.6) \times 10^7$	$(4.4 \pm 0.3) \times 10^5$	125 ± 11
NO× E3	$(9.9 \pm 0.6) \times 10^7$	$(4.0 \pm 0.3) \times 10^5$	115 ± 11
		B. subtilis	
NO× B1	$(1.5 \pm 0.1) \times 10^8$	$(2.4 \pm 0.2) \times 10^5$	60 ± 8
NO× B2	$(1.8 \pm 0.1) \times 10^8$	$(3.6 \pm 0.3) \times 10^5$	90 ± 10

Results are also shown in Figures 3.28 and 3.29.

E. coli does not show sizable variation in the vitality after the exposure at the gaseous pollutants (Figure 3.28), while the two experiments with the *B. subtilis* show a viability reduction: the ratio between the collected CFU and the airborne bacteria concentration decrease by a factor 2 in both the experiments. Even if the overall picture is not completely clear, with *B. subtilis* results suggest the presence of a toxic effect of the NO_x gases (nitric oxide in particular), and a reduction of bacterial viability. Such effects are close to the effects measured in the "soot experiments" (Figure 3.27) suggesting the possibility that the primarily toxic effects is due to the gaseous species formed during the combustion process and not to the soot particles themselves.

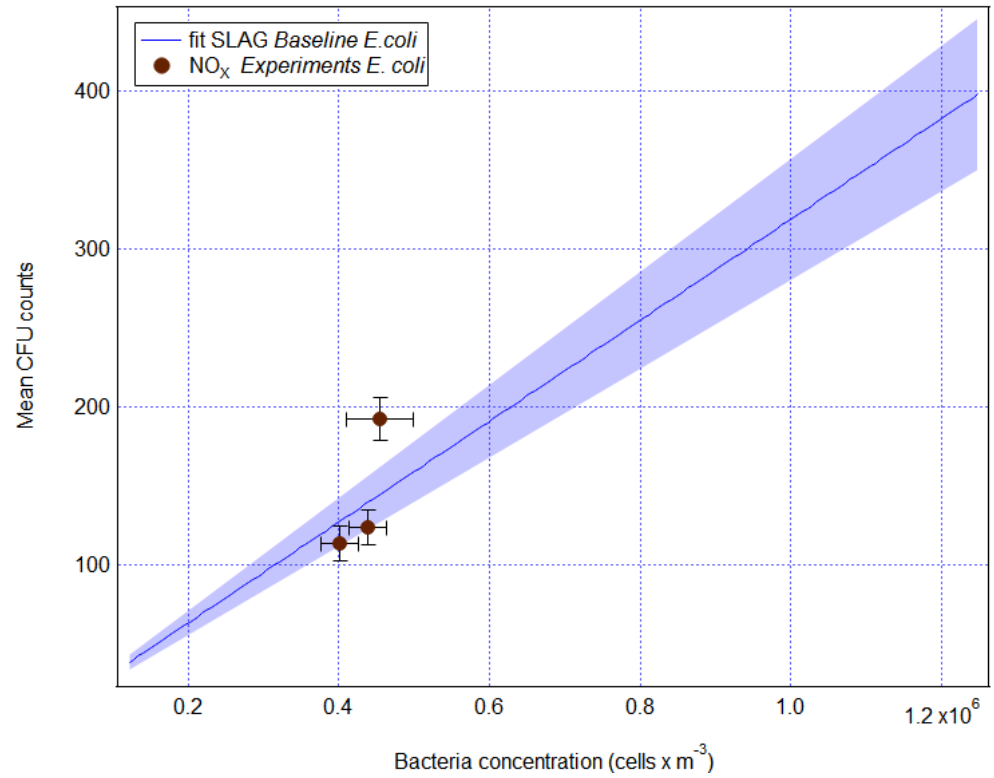

Figure 3. 28 *E. coli* experiments with NO_x*:* mean CFU counted on the Petri dishes vs the initial bacteria concentration in ChAMBRe. The baseline and its uncertainty band are also shown.

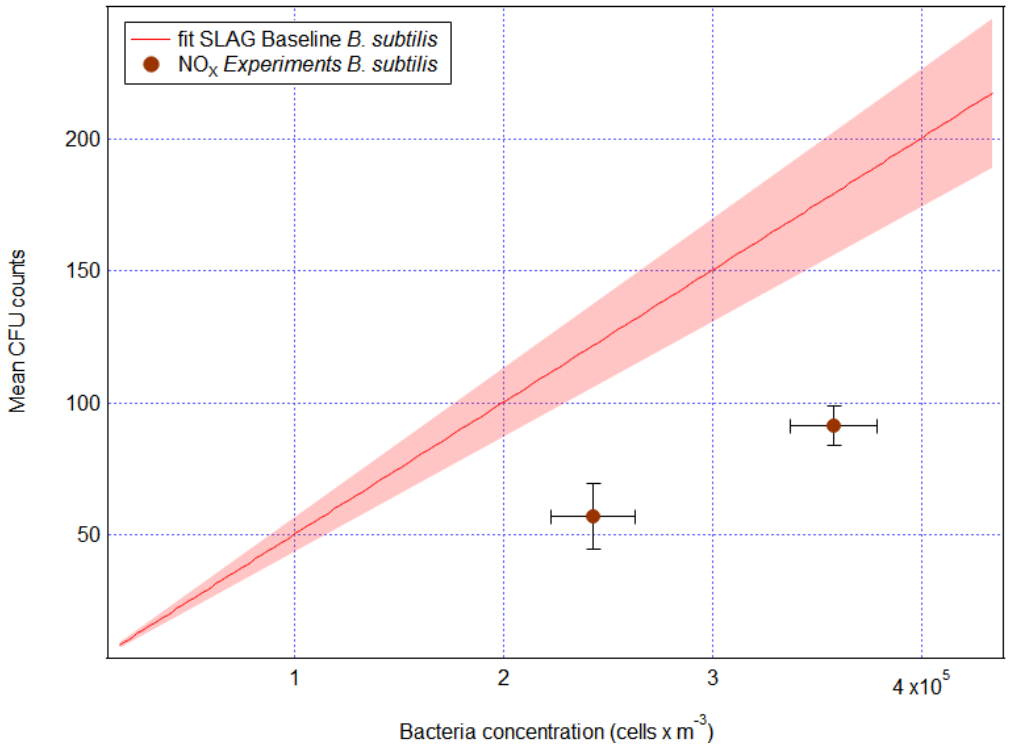

Figure 3. 29 *B. subtilis* experiments with NO_x*:* mean CFU counted on the Petri dishes vs the initial bacteria concentration in ChAMBRe. The baseline and its uncertainty band are also shown.

A second set of experiments with NO_x was also performed, to investigate the effect of a different ratio between the two nitrogen oxides. Following a pilot experiment performed on *B. subtilis* at the French simulation chamber CESAM (Brotto et al., 2015), the average concentration of NO was kept in the range of 100 pbb and the NO_2 concentration was kept between 600 and 650 ppb, through the feedback control system. Experimental conditions are reported in Tables 3.14 and 3.15. Results are shown in Figure 3.30 and 3.31. In two *E. coli* experiments, the bacteria viability seems to increase, while the third experiment results close to the baseline (Figure 3.30). In the case of *B. subtilis*, both the experiments give results in line with the baseline reference. *B. subtilis* seems to be unaffected by the NO_x concentration investigated in the second set of experiments, suggesting that this strain appears to be more sensitive to high concentration of NO respect to NO_2.

Table 3.14 ChAMBRe conditions during the second set of NO_x experiments. The PM_{10} level immediately after the bacteria injection and the concentration of CO_2 and NO_x are also reported.

Exp.	T (°C)	R. H. (%)	Ext. P. (mbar)	Int. P. (mbar)	PM_{10} (μg m^{-3})	CO_2 (ppm)	NO (ppb)	NO_2 (ppb)
				E. coli				
NO_X E4	23	65	1008	1012	55	455	110	615
NO_X E5	24	60	1011	1010	47	410	100	645
NO_X E6	22	60	1011	1007	30	410	150	640
				B. subtilis				
NO_X B3	22	65	1014	1013	68	430	125	610
NO_X B4	23	60	1008	1008	55	410	140	610

Table 3.15 CFU injected, bacteria concentration inside ChAMBRe and average number of colonies counted on each Petri dish in the second set of NO_x experiments.

Exp.	Bacteria Injected (CFU)	Cell m^{-3}	Mean CFU counts
		E. coli	
$NO_×$ E4	$(1.0 \pm 0.1) \times 10^8$	$(3.7 \pm 0.8) \times 10^5$	90 ± 10
$NO_×$ E5	$(5.4 \pm 0.7) \times 10^7$	$(2.2 \pm 0.2) \times 10^5$	120 ± 11
$NO_×$ E6	$(1.0 \pm 0.1) \times 10^8$	$(2.4 \pm 0.2) \times 10^5$	145 ± 12
		B. subtilis	
$NO_×$ B3	$(1.3 \pm 0.1) \times 10^8$	$(1.7 \pm 0.2) \times 10^5$	80 ± 9
$NO_×$ B4	$(1.6 \pm 0.1) \times 10^8$	$(2.3 \pm 0.2) \times 10^5$	105 ± 10

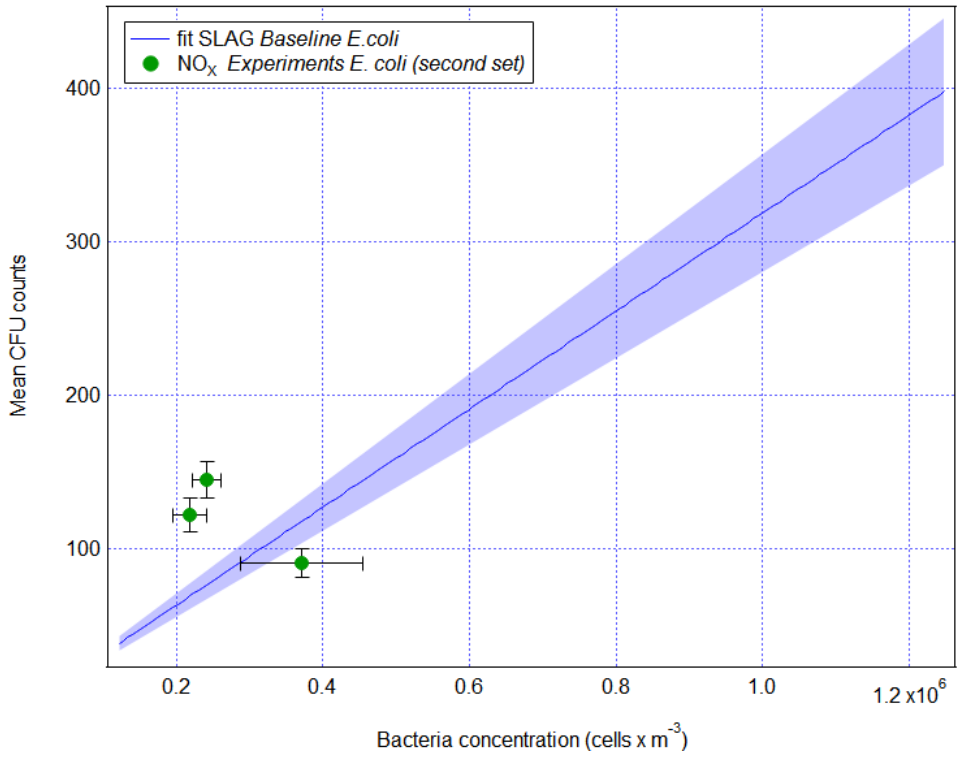

Figure 3.30 Second set of *E. coli* experiments with NO_x*:* mean CFU counted on the Petri dishes vs the initial bacteria concentration in ChAMBRe. The baseline and its uncertainty band are also shown.

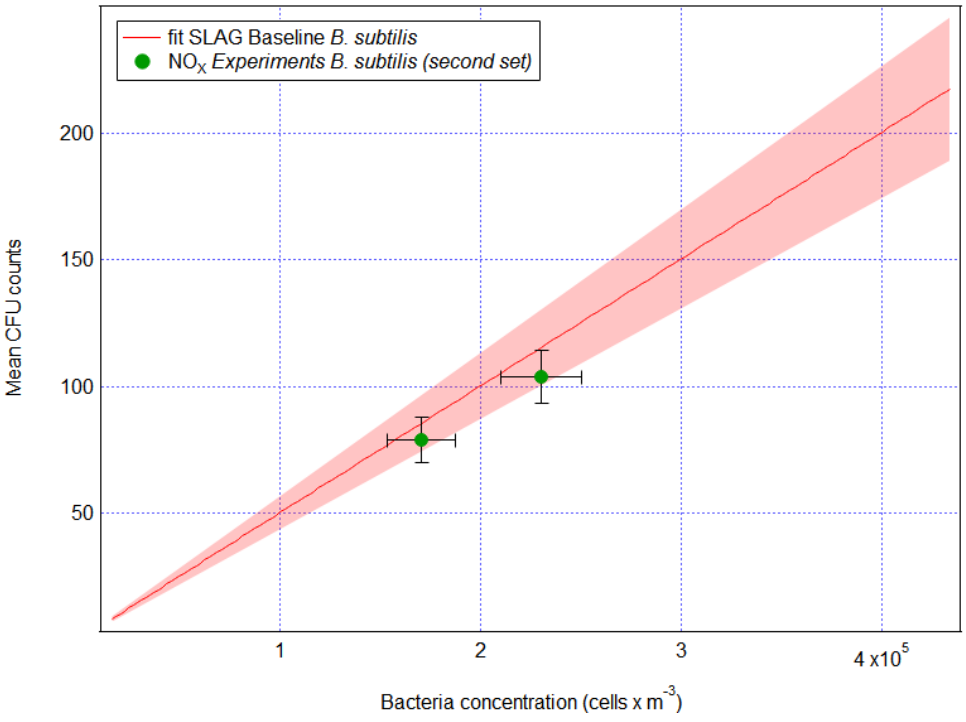

Figure 3.31 Second set of *B. Subtilis* experiments with NO_x*:* mean CFU counted on the Petri dishes vs the initial bacteria concentration in ChAMBRe. The baseline and its uncertainty band are also shown.

The overall picture is summarized in Figures 3.32 and 3.33. With the Gram-negative *E. coli*, in most of the experiments no sizable effects were measured on the viability when bacteria were exposed to pollutants. However, three experiments show a deviation above the baseline: one soot experiment (*SOOT E5*) and two of the NOx experiment (*NO_x E5, E6*) show an increase in the bacteria viability (the ratio between collected CFU and bacteria concentration increase by a factor 1.5 and 2 respectively for *SOOT E5* and *NO_x E5, E6*).

The Gram-positive *B. subtilis* shows an overall decrease of the bacterial viability at the presence of soot particles and nitric oxide. The results suggest that the toxic effect measured in these cases is probably due to the presence of nitric oxide in concentrations above a critical threshold. When the NO concentration is kept under 150 ppb, (*NO_x B3* and *B4* experiments), bacteria are not affected by the NOx concentration tested.

The difference in the bacteria envelope could explain a different response to the pollutants. In Gram-negative strains the outer membrane helps to protect the organisms from the environment by excluding toxic molecules, such as in this case the NO molecule, which is a small, neutral molecule that easily penetrates cell membranes (Hughes, 2008). Gram-positive bacteria do not have the outer membrane and could thus be more exposed to the environmental conditions.

The mechanism of bacteria-pollutants interaction and the possible critical concentration of NO need to be further investigated by systematic studies. In this sense, the present methodological work, paved the way to future prolonged researches.

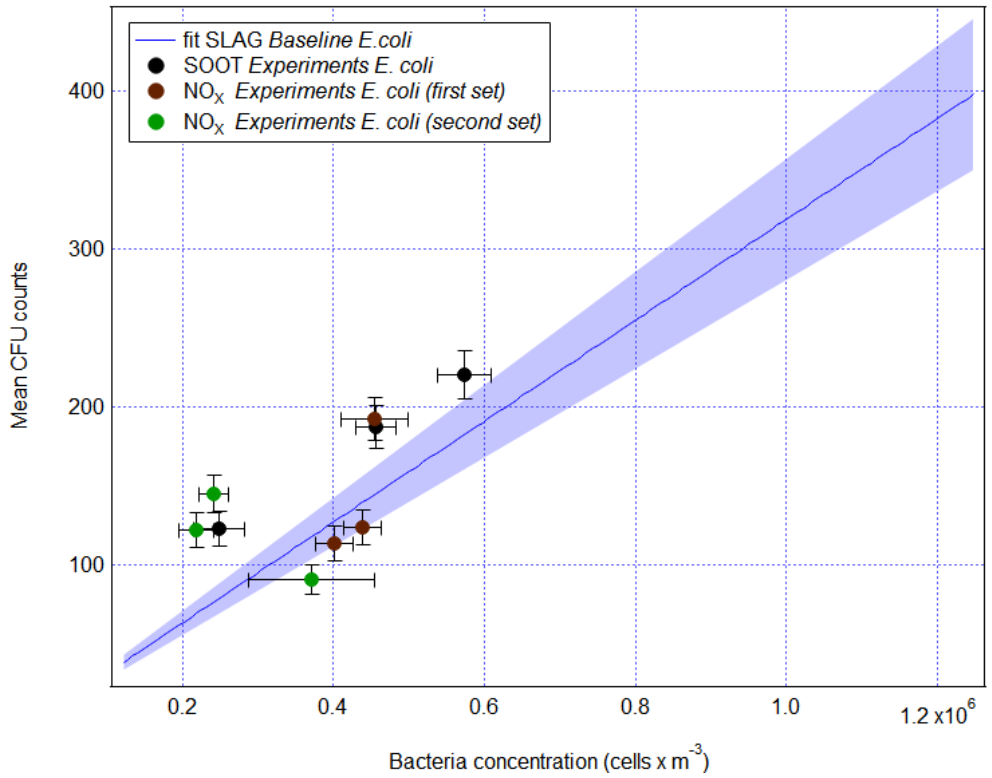

Figure 3.32 Summary of the *E. coli* experiments.

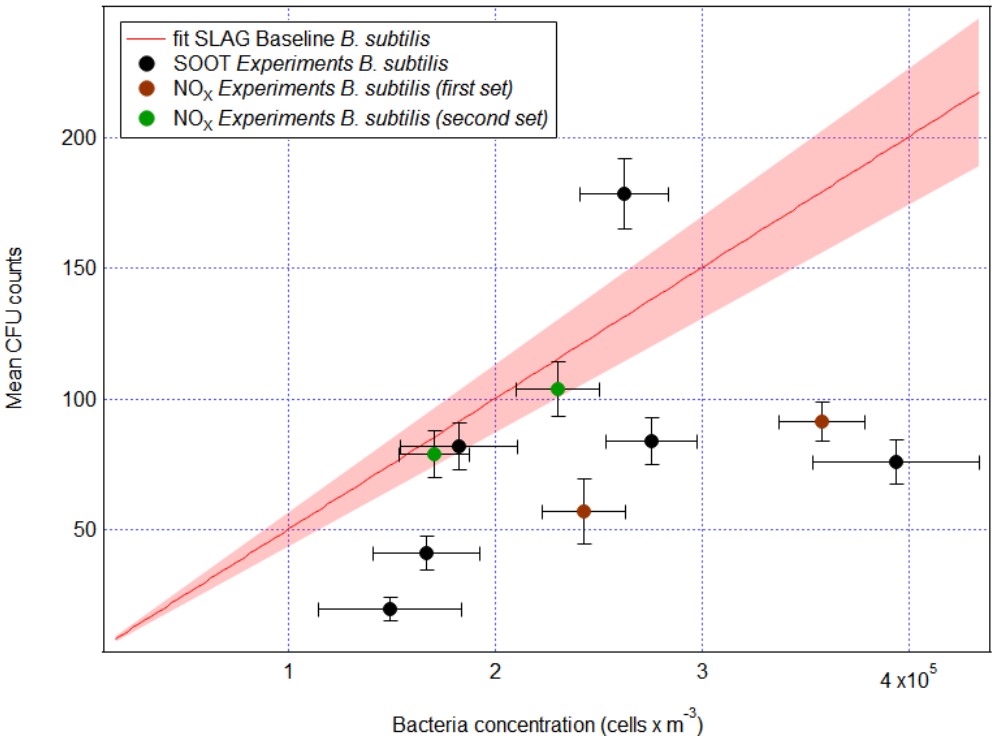

Figure 3. 33 Summary of the *B. subtilis* experiments**.**

4. Summary and Perspective

The aim of my PhD project was to make possible quantitative studies of the bio-aerosols behavior in different atmospheric conditions by an atmospheric simulation chamber, with a specific focus on bacteria.

An experimental protocol for chamber studies on bio-aerosols was developed and thoroughly tested with Gram-positive and Gram-negative bacterial strains. Bacteria were cultivated until the mid-exponential phase and resuspended in saline solution (NaCl 0.9%) before the injection in ChAMBRe. The injections were performed with the SLAG nebulizer, which had demonstrated the best characteristics to perform chamber experiments. Inside the chamber, bacteria were collected by gravitational settling on four Petri dishes filled with a solid culture media. At the end of the exposure time (i.e., 5 hours, according to the bacteria lifetime inside ChAMBRe), Petri dishes were extracted and incubated overnight at 37 °C, to determine the bacteria culturable fraction by CFUs visual counting. The survival rate of the airborne bacteria was therefore evaluated in a set of "*baseline experiments*", i.e., exposing bacteria to clean air, without contaminants or pollutants, and subsequently in a set of exploratory experiments with the two bacteria strains exposed to two of the most common anthropogenic pollutants, NO_x and soot particles.

With a "clean" atmosphere, the ratio between injected and viable bacteria after a 5 hour exposure inside ChAMBRe turned out to be reproducible at 12% and 13% level with *E. coli* and *B. subtilis* respectively. The sensitivity of the whole procedure to changes in the bacteria viability appears to be adequate to design experiments with an atmospheric simulation chamber.

As an initial step, the effect of soot particles and different concentrations of NO_x on the two bacteria strains was explored. In the "soot experiments" bacteria were exposed to high concentration of soot particles (BC concentration between 400 and 600 μg m^{-3}) and NO_x gases, originating during the combustion process (NO in the range of 170 - 200 ppb and NO_2 in the range of 10 - 80 ppb). The effects of NO_x were subsequently investigated separately, in two series of experiments, in which different concentration of NO_x were tested. In the first set, bacteria were exposed at the same NO_x concentration obtained at the end of the soot particles production (NO in the range of 170 - 200 ppb and NO_2 in the range of 10 - 80 ppb). In the second set of experiments, a different ratio between the two nitrogen oxides were investigated: the NO was about 100 pbb and the NO_2 about 600 ppb.

The Gram-negative *E. coli*, in most of the experiments appeared to be unaffected by the pollutants. However, an increase of the bacteria viability was registered in three experiments (one soot experiment and two of the second set of NOx experiments), suggesting the possibility of some protecting mechanisms or helping in the recovery of vital functions.

The Gram-positive *B. subtilis* showed an overall decrease of the bacterial viability at the presence of soot particles and at the NO_x concentration quoted in the first set of NO_x experiments, where the concentration of NO was the highest. Results suggest that the toxic effect measured with the *B. subtilis* at the presence of soot particles may be due to the joint presence of nitric oxide.

Definitely, the two strains showed different response to the pollutants probably as consequence of their different cell envelope and, reasonably, the Gram-negative *E. coli* appears to be a more resistant strain than the *B. subtilis*. However, such preliminary picture is not clear enough and the effects of soot particles and related gases on bacteria viability still need to be assessed through more systematic studies. Moreover, in this investigation, soot particles are freshly generated while the atmospheric soot suspended in the air is subjected to aging processes. The aged soot with an oxidized form could become more reactive and lead a different toxicity to airborne bacteria. Future studies could also focus on the possibilities to age soot particles inside the chamber and test the bacteria viability with different type of oxidized product of soot.

After a long and complex preparatory work, the first tests consider a few pollutants only but show that the protocol developed at ChAMBRe makes possible systematic studies of the effects of atmospheric composition (i.e., pollution levels) on bacteria viability and likely on other bio-aerosol species. The data reduction procedure developed for the WIBS-NEO can be further improved, in terms of counting efficiency, dead time correction, resolving power, this possibly leading to upgrades or even a new generation of bioaerosol monitors.

The present methodological work open to future systematic researches on the effect of pollutions levels on the biological fraction of the atmospheric aerosol.

APPENDIX A

A.1 Determination of BLAM size distribution at the CESAM facility

At the beginning of my PhD I spent a training week at the CESAM simulation chamber, at Centre National de la Recherche Scientifique - Laboratoire Interuniversitaire des Systèmes Atmosphériques (CNRS-LISA),Créteil, France. The purpose was to learn how to program and carry out experiments, manage and correctly use a complex structure such as an atmospheric simulation chamber. As a part of the training I performed the characterization of the size distribution of the aerosol produced by the BLAM nebulizer, according to different parameters (i.e. feed rate, pressure, air flow) and set up (expansion plates). This training week contributed to a deeper knowledge of the nebulizer although the technical information obtained did not play a central role in the thesis work.

As reported in the user manual, various expansion cone diameters combined with various cavity depth (see Table 2.3, Chapter 2) could provide a fine control on the output of the device and particle size distribution of the aerosol. The real size range of aerosols produced by the BLAM was not clearly known since there is no detailed characterization of this object in the literature nor in the technical documentation of the manufacturer.

The size distribution of the aerosol produced by the BLAM atomizer was determined using different saline solutions (NaCl and $(NH_4)_2SO_4$) at different concentration to produce poly-disperse particles. Tests were carried out through the CESAM chamber, equipped with an SMPS and, subsequently, by measuring the aerosol produced by the BLAM directly at the output by inserting two driers in series between the nebulizer and the SMPS. Three different BLAM plates were tested: the “1:20”, the “4:40” and the “10:40” with the two different saline solutions, at different concentration, and different parameters (airflow, injection feed rate). Eight experiments were performed by injecting the salt particle inside CESAM and the relative conditions tested are reported in Table A.1. In particular, in the last experiments (T-8), to avoid possible losses of larger particles along the stainless steel pipe used to connect the BLAM to the chamber, the aforementioned tube was removed and the nebulizer was directly connected to the chamber using one of the flanges in the lower dome, through a small Teflon connection.

Table A.1 Experimental conditions of the test performed in CESAM. (Dry conditions refers to a RH% ~ 0%).

TEST	Salt	Concentration	Liquid feed rate (mL min^{-1})	Airflow (L min^{-1})	Expansion plate	RH%
T-1	$(NH_4)_2SO_4$	0.01 M	0.4	2	1:20	Dry
T-2	NaCl	0.01 M	0.4	2	1:20	Dry
T-3	NaCl	9 g L^{-1}	0.4	2	1:20	Dry
T-4	NaCl	9 g L^{-1}	0.4	3	1:20	Dry
T-5	NaCl	9 g L^{-1}	1	2	1:20	Dry
T-6	NaCl	9 g L^{-1}	0.4	2	1:20	60%
T-7	NaCl	9 g L^{-1}	0.4	2	4:40	Dry
T-8	NaCl	9 g L^{-1}	0.4	2	1:20	Dry

As reported in the Figure A.1, SMPS data show approximately the same distribution for all the injection conditions: particle distribution has a peak around 50-60 nm. All the NaCl solutions have the same distribution, with a peak at 50 nm, and the $(NH_4)_2SO_4$ solution (T-1) seems to have a peak slightly shifted to 60 nm. One test (T-6) was performed with Relative Humidity around 60%, which seems to have a distribution shifted to smaller particles (peak at 40 nm).

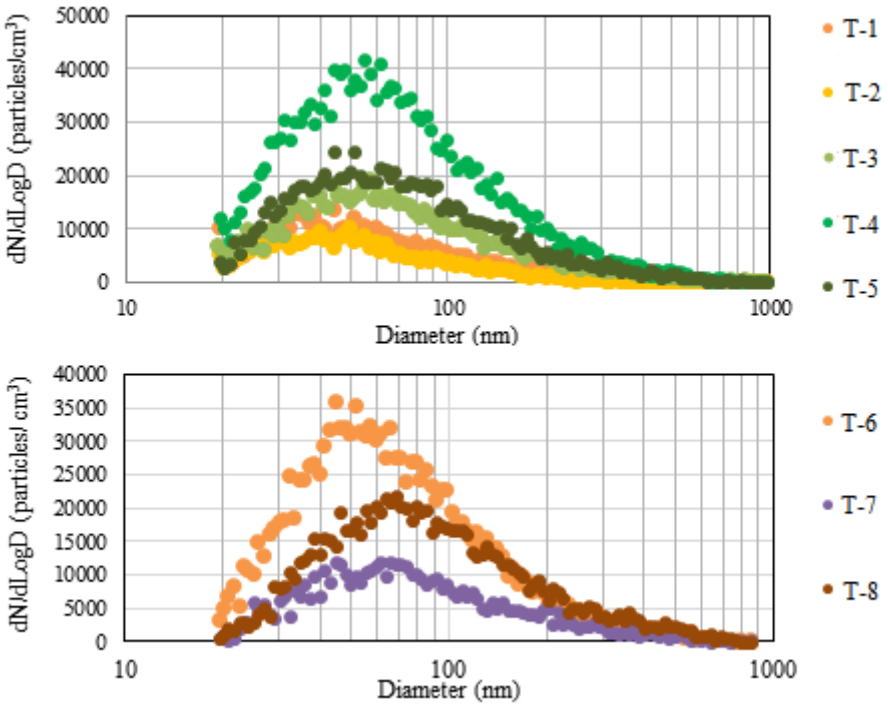

Figure A.1 SMPS data during chamber measurements.

Six tests were performed by measuring directly the BLAM output with two driers in series connected before the SMPS. The list of the experiments is reported in Table A.2, with the parameters used in each test. Relative humidity at the output of the BLAM was about 60%; while at the end of the driers is about 4%.

Table A.2 Experimental conditions of the test performed with the two driers.

TEST	Salt	Concentration	Liquid feed rate (mL min^{-1})	Airflow (L min^{-1})	Expansion plate
T-9	NaCl	9 g L^{-1}	0.4	2	1:20
T-10	NaCl	9 g L^{-1}	0.1	2	1:20
T-11	NaCl	0.09 g L^{-1}	1	2	10:40
T-12	NaCl	0.09 g L^{-1}	0.1	2	1:20
T-13	NaCl	0.09 g L^{-1}	0.1	3	1:20
T-14	NaCl	0.9 g L^{-1}	0.1	2	1:20

With this configuration some differences in the BLAM aerosol size distribution were observed only by changing the concentration of the injected solution, while, with the same solution and varying the other parameters (liquid feeding speed, plate diameter and airflow), the size distribution of the produced aerosol does not change. This behavior is clearly shown in the Figure A.2. With the most concentrated solution (T-9 and T-10), the size distribution of the aerosol produced seems to be slightly shifted to 80 nm, respect to the chamber experiments, but it remains almost unchanged in the two tests. With the less concentrated solutions (T-11, T-12 and T-13), the size distribution shows again a peak at 50 nm. In the last graph, which reports the comparison between T-10, T-12 and T-14, it is clearly observed that the maximum of the distribution slightly shift to bigger particles with the increase of the solution concentration. The peak moved from about 50 nm with the 0.09 g L^{-1} solution to about 60 nm with the 0.9 g L^{-1} solution and finally to about 80 nm with the 9 g L^{-1}. However, taking into account the large number of particles, it is possible that larger particles are the result of coagulation and growth phenomena in general.

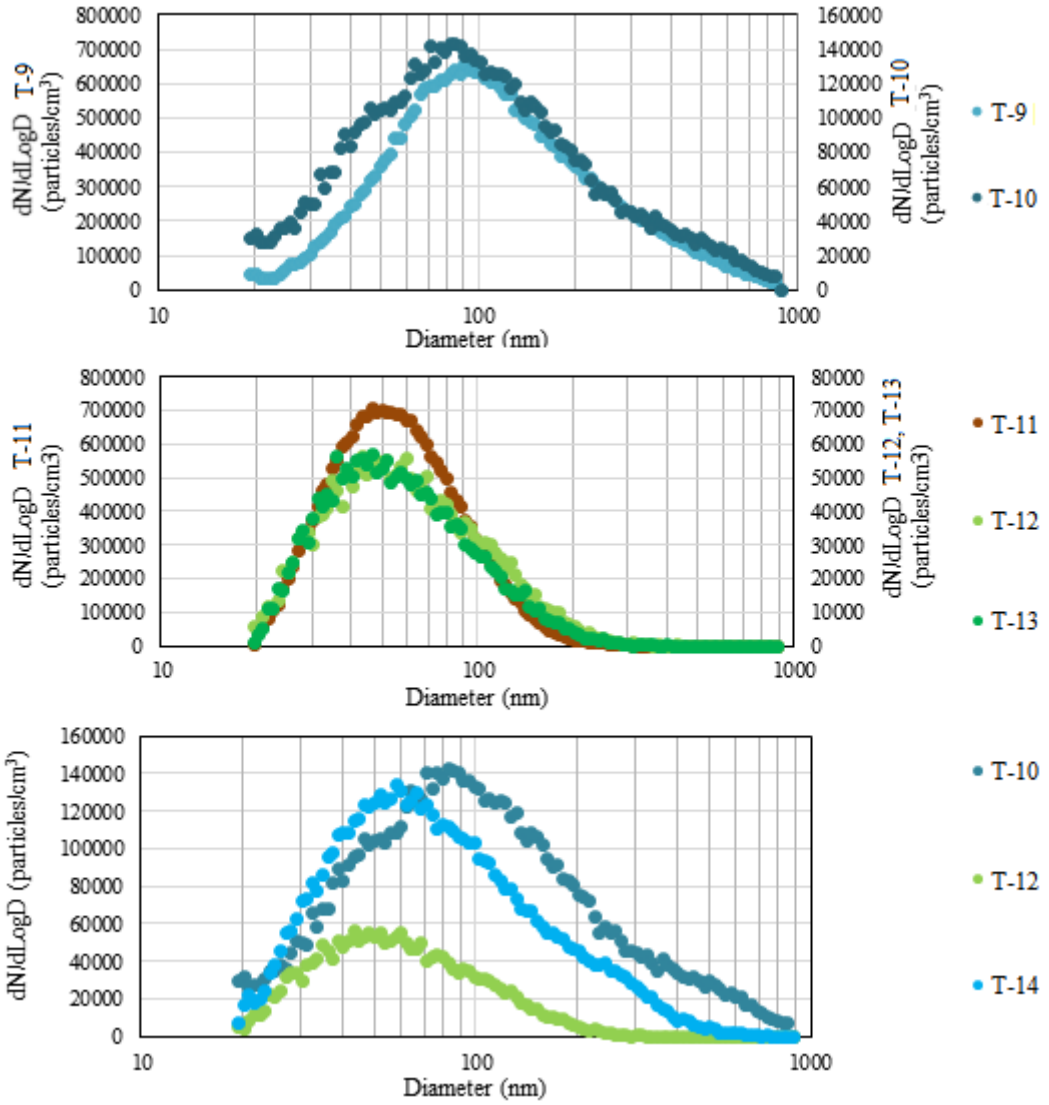

Figure A.2 SMPS data from the experiments carried out using the driers.

From the tests carried out at the CESAM simulation chamber it is clear that the size distribution of the aerosol produced by the BLAM system are almost independent to the operative parameters (i.e. feed rate and air flow) and set up (expansion plates) that can be set. Taking into account very small variations, the size distribution has a peak in the range of 50-70 nm, depending also to the relative humidity conditions of the environment.

APPENDIX B

B.1 Reproducibility tests of the CFUs counting procedure

Determination of bacterial cell number is among the most fundamental procedures in microbiology. The widely used gold standard method is Colonies Forming Units (CFU) counting on plates (Miller, 1972). The CFU method has two noteworthy advantages, namely the capacity for counts of any number of bacteria using dilutions; second, only viable bacteria are counted with this method as the CFU method excludes dead bacteria and debris. The most important disadvantage of the CFU method is that clumps of bacteria cells can be miscounted as single colonies; the potential for counting clumps as single units is in fact reason the results are reported as CFU/mL rather than bacteria/mL. Results are usually obtained after 1–2 days, because the bacteria have to grow and form a colony that is clearly visible.

Actually, several techniques are used to obtain CFUs counting. The serial dilutions and two different spread methods were investigated in order to obtain the best experimental condition in terms of reproducibility of CFUs counting.

The optimization procedure involved two different set-up solution to perform the dilution (microtubes vs well plates, Figure B.1) and the comparison of two plating techniques: the traditional L-rod spread method and the spot plating method (Figure B.2).

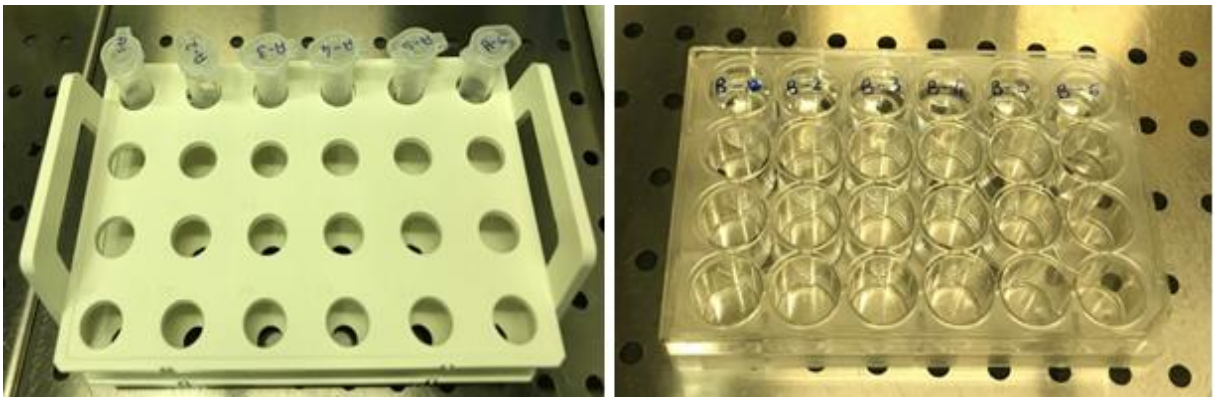

Figure B.1 Pictures of the microtubes (left side) and well plate (right side) used for the serial dilutions.

The L-rod procedure involves taking 100 μL of the corresponding dilution and placing them in the center of the assigned Petri dish, then with a sterile L-shaped rod the liquid is expanded with circular movements until it dries completely. The spot plating procedure is performed by taking 100 μL and

placing them in the center of the petri dish and gently shaking the plate to spread the liquid over the surface of the Petri dish, being careful not to reach the plastic edge.

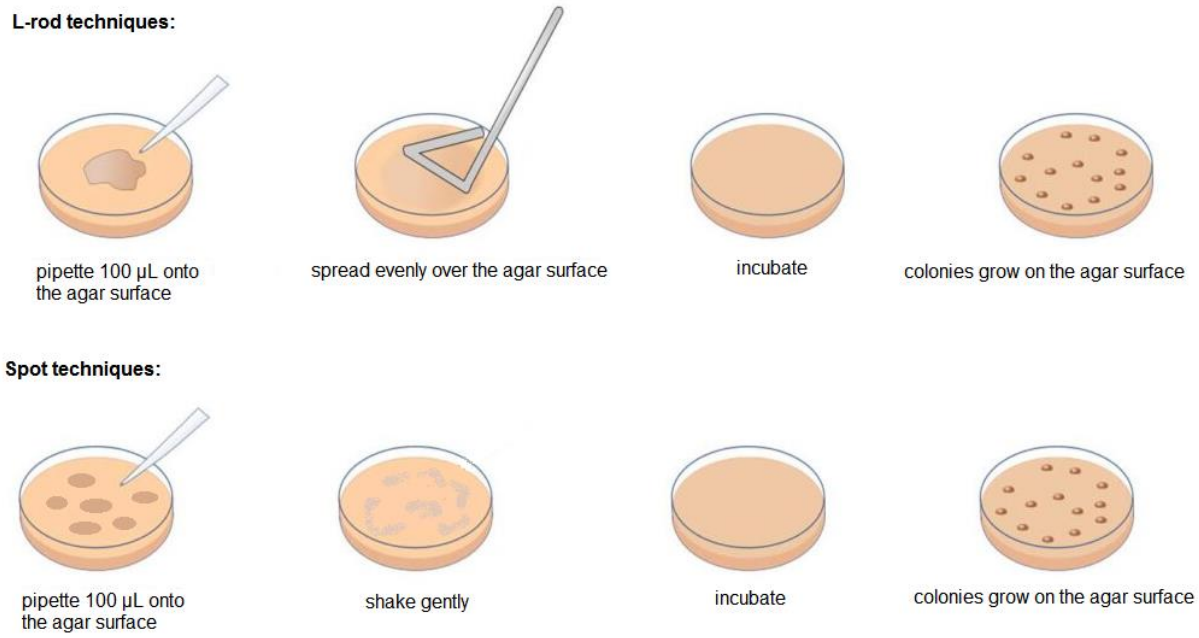

Figure B.2 Spread plate methods investigated.

Tests were performed with two bacteria strains: *Escherichia coli* and *Bacillus subtilis*. Bacteria were refreshed before each test by spreading some cells, using a sterile loop, on a Petri dish containing agar culture media (15 g of tryptic soy broth, TSB, and 9.5 g of agar for 500 mL of MIlliQ, sterilized in an autoclave at 121 ° C for 20 min) and then incubated at 37 ° C overnight. The next day, two or three colonies from the Petri dish were dissolved in 40-50 mL of a sterilized liquid culture medium (TSB). Growth curve was followed by checking periodically the OD_{600nm} of the suspension with a UV-Vis spectrophotometer (OD measurement every hour / half hour) until reaching OD_{600nm} of about 0.5. Once the value of OD_{600nm} was in the range of 0.4 - 0.5, 20 mL of the bacterial suspension were centrifuged for 10 min at 4000 rpm. The surnatante was discarded and the bacteria pellet was resuspended in sterile saline solution (NaCl 0.9 %) to prepare a bacterial solution with same concentration of the starting one (same final volume, 20 ml). The OD was measured again with the saline, and the number of the serial dilution was chosen based on the indicative bacterial concentration corresponding to the OD reading. For gram-positive strains an OD equal to one corresponds to an indicative CFU concentration of 10^8 CFU mL^{-1}, for gram-negative strains corresponds to 5×10^8 CFU mL^{-1}.

If the original solution was around 10^8 CFU mL^{-1}, six serial dilutions were performed, where each step is a factor ten dilution. If the original solution was around 10^7 CFU mL^{-1}, five serial dilutions

were performed. A schematic of the tenfold serial dilutions is reported in Figure B.3. The serial dilutions were made using sterile micro-tubes or the well plates (Figure B.1)

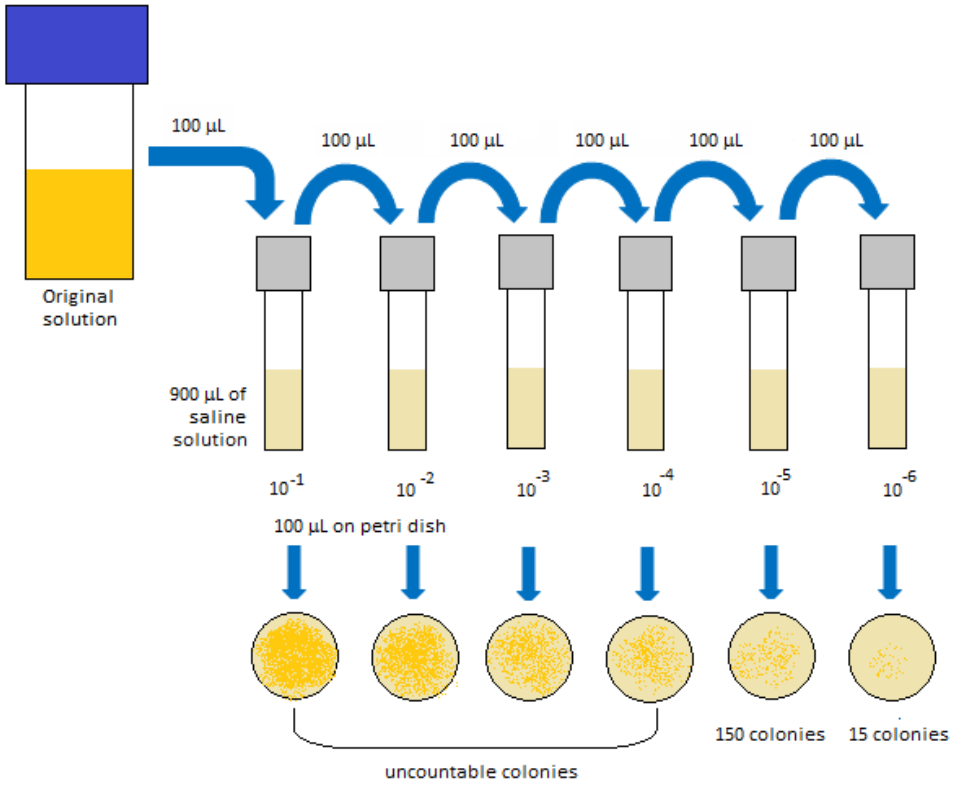

Figure B.3 Representation of serial dilutions.

E. coli TEST 1

Microtubes were firstly tested (Test 1.A): six microtubes of 2 mL with hermetic cap containing 900 µL of sterile saline solution were prepared and the tenfold serial dilutions performed (100 µL of the bacterial suspension were spread in each step). Each microtube was vortexed for few seconds during each step. 100 µL of the last two dilutions (called -5 and -6) were plated on an agar non-selective culture medium (trypticase soy agar, TSA) using the standard method of the L-rod plating and the spot method (total number of platted petri: 8, four replication for each dilution). Petri dishes were incubated at 37 °C overnight and the concentration of culturable cells, expressed as CFU mL^{-1}, was then determined by counting the colonies formed and multiplying by the appropriate dilution factor. Data, obtained from CFU counting on the agar plates, were averaged and used to estimate the uncertainty range of the bacterial concentration in the solution. Table B.1 shows the number of colonies obtained and the corresponding CFU concentrations.

Table B.1 CFU counting from *E. coli*, Test 1.A

OD600 = 0.6				**CFU mL^{-1} from the OD = 3.0 × 10^{8}**			
Test 1.A "spot plating"				**Test 1.A "L-rod plating"**			
		CFUs	**CFU mL^{-1}**			**CFUs**	**CFU mL^{-1}**
-5	A	194	1.9×10^{8}	-5	A	40	4.0×10^{7}
-5	B	234	2.3×10^{8}	-5	B	52	5.2×10^{7}
-5	C	317	3.2×10^{8}	-5	C	16	1.6×10^{7}
-5	D	268	2.7×10^{8}	-5	D	33	3.3×10^{7}
-6	A	18	1.8×10^{8}	-6	A	2	2.0×10^{7}
-6	B	29	2.9×10^{8}	-6	B	2	2.0×10^{7}
-6	C	28	2.9×10^{8}	-6	C	2	2.0×10^{7}
-6	D	23	2.3×10^{8}	-6	D	5	5.0×10^{7}

Subsequently, the dilutions were performed by using a six wells plate, each well filled with 1800 µL of sterile physiological solution. Serial dilution were performed by spreading 200 µL of the bacterial suspension (Test 1.B). 100 µL of the last two dilutions (-5 and -6) were plated using the standard method of the L-rod plating and the spot method (total number of platted petri: 8, four replication for each dilution). Petri dishes were incubated at 37 °C overnight. Table B.2 shows the number of colonies obtained and the corresponding CFU concentrations.

Table B.2 CFU counting from *E.coli* test 1.B

OD600 = 0.60				**CFU mL^{-1} from OD = 3.0 × 10^8**			
TEST 1.B "spot plating"				**TEST 1.B "L-rod plating"**			
		CFU	**CFU mL^{-1}**			**CFU**	**CFU mL^{-1}**
-5	A	283	2.8 × 10^8	-5	A	86	8.6 × 10^7
-5	B	256	2.6 × 10^8	-5	B	31	3.1 × 10^7
-5	C	294	2.9 × 10^8	-5	C	38	3.8 × 10^7
-5	D	280	2.8 × 10^8	-5	D	43	4.3 × 10^7
-6	A	34	3.4 × 10^8	-6	A	5	5.0 × 10^7
-6	B	29	2.9 × 10^8	-6	B	3	3.0 × 10^7
-6	C	30	3.0 × 10^8	-6	C	3	3.0 × 10^7
-6	D	26	2.6 × 10^8	-6	D	14	1.4 × 10^7

L-rod spread method always shows a strong underestimation of the CFUs number; in addition, results are not very reproducible. Spot spread method provides results in accordance with the theoretical CFUs counting deriving from the OD reading. The dilutions carried out in the wells and platted by spotting give results closer to the theoretical value as well.

E. coli TEST 2

In this test, possible differences between the traditional well plates dilution support and the microtubes were investigated, by platting only by spot technique (Test 2.A and 2.B). The dilution procedures were the same used in *E. coli* Test 1. 100 µL of the last two dilutions (-5 and -6) were plated in triplicate using the spot method. Petri dishes were incubated at 37 ° C overnight before the CFUs counting. Results are given in Table B.3.

Table B.3 CFU counting from *E.coli* Test 2

OD600 = 0.56				**CFU mL^{-1} from OD = 2.8 × 10^{8}**			
Test 2.A Dilutions in well plates				**Test 2.B Dilutions in microtubes**			
		CFU	**CFU mL^{-1}**			**CFU**	**CFU mL^{-1}**
-5	A	256	2.6 × 10^{8}	-5	A	257	2.6 × 10^{8}
-5	B	277	2.8 × 10^{8}	-5	B	285	2.9 × 10^{8}
-5	C	258	2.6 × 10^{8}	-5	C	265	2.7 × 10^{8}
-6	A	30	3.0 × 10^{8}	-6	A	32	3.2 × 10^{8}
-6	B	27	2.7 × 10^{8}	-6	B	29	2.9 × 10^{8}
-6	C	38	3.8 × 10^{8}	-6	C	30	3.0 × 10^{8}

Reproducible results with both microtubes and wells were obtained, in agreement with each other and with the theoretical CFU mL^{-1} data. For an easily employment and to avoid waste of material, it was therefore decided to use microtubes as the best support for making dilutions.

E. coli TEST 3

In this test, intermediate dilutions were introduced, in order to improve the statistic error associated with the number of colonies per Petri (Test 3). A schematic is represented in Figure B.4.

The serial dilutions were made using sterile microtubes containing 900 μL of sterile saline solution (with the exception of the intermediate dilutions, called -5.5, that containing 800 μL of saline) and 100 μL (200 μL in the case of -5.5 dilution) of the solution was diluted in series.

Finally, 100 μL of the last three dilutions were spread in triplicated, by using the spot procedure, on the agar plate. Petri dishes were incubated overnight at 37° C before the CFU counting. Results are shown in Table B.4.

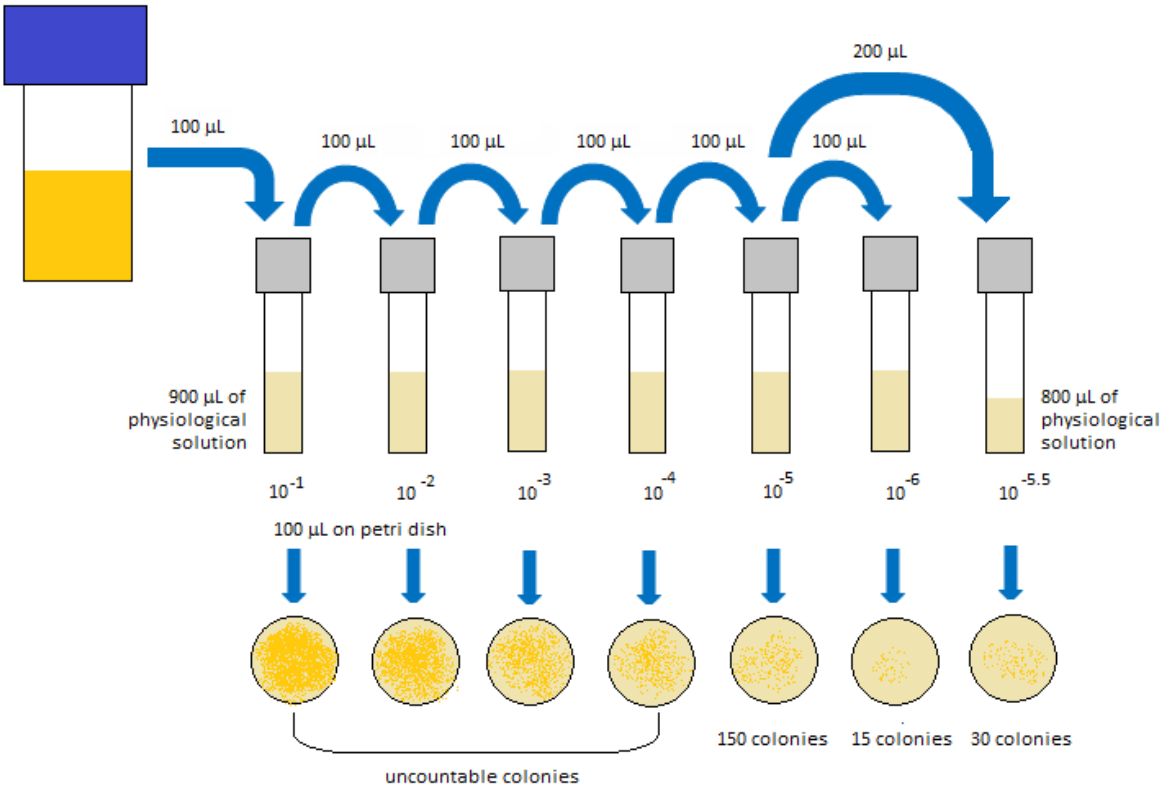

Figure B.4 Representation of serial dilutions with the addition of the intermediate dilution.

Table B.4 CFU counting from *E.coli* Test 3

OD600 = 0.58		**CFU mL^{-1} from OD = 2.9 × 10^{8}**	
		CFU	**CFU mL^{-1}**
-5	A	192	1.9 × 10^{8}
-5	B	213	2.1 × 10^{8}
-5	C	202	2.0 × 10^{8}
-5,5	A	52	2.6 × 10^{8}
-5,5	B	46	2.3 × 10^{8}
-5,5	C	46	2.3 × 10^{8}
-6	A	27	2.7 × 10^{8}
-6	B	25	2.5 × 10^{8}
-6	C	26	2.6 × 10^{8}

Results obtained with the intermediates dilutions are reasonable and in agreement with the traditional dilutions used (-5 and -6) with the advantage to give more statistics in comparison with the last dilution. It was therefore decided to use, with *E. coli*, the -5 and -5.5 dilutions as best dilution steps.

B. subtilis TEST 1

The same tests performed with the Gram-negative *E. coli* were also performed with the Gram-positive *B. subtilis*. A shorter experimental approach was used. The wells plate method was firstly tested, coupled with the spot plating technique (Test 1.A). Each well was filled with 1800 µL of sterile physiological solution and serial dilution were performed by spreading 200 µL of the bacterial suspension. With this strains, five tenfold dilution were performed. 100 µL of the last two dilutions (called -4 and -5) were plated in triplicate using the spot method. Table B.5 shows the number of colonies obtained and the corresponding CFU concentrations.

Table B.5 CFU counting from *B. subtilis* Test 1.A

OD600 = 0.43		**CFU mL^{-1} from OD = 4.3 × 10^7**	
		CFU	**CFU mL^{-1}**
-4	A	214	2.1×10^7
-4	B	205	2.1×10^7
-4	C	268	2.7×10^7
-5	A	41	4.1×10^7
-5	B	31	3.1×10^7
-5	C	36	3.6×10^7

Subsequently, the dilutions were performed by using the microtubes (filled with 900 µL of sterile physiological solution) and plating, in triplicate, 100 µL of the -4 and -5 dilutions by using the standard method of the L-rod plating and the spot method (Test 1.B). Results are given in Table B.6.

Table B.6 CFU counting from B. subtilis Test 1.B

OD600 = 0.43				**CFU mL^{-1} from OD = 4.3 × 10^7**			
TEST B.1 "Spot procedure"				**TEST B.1 "L-rod procedure"**			
		CFU	**CFU mL^{-1}**			**CFU**	**CFU mL^{-1}**
-4	A	236	2.4×10^7	-4	A	113	1.1×10^7
-4	B	218	2.2×10^7	-4	B	145	1.5×10^7
-4	C	226	2.3×10^7	-4	C	121	1.2×10^7
-5	A	39	3.9×10^7	-5	A	37	3.7×10^7
-5	B	43	4.3×10^7	-5	B	6	0.6×10^7
-5	C	43	4.3×10^7	-5	C	10	1.0×10^7

Results with *B. subtilis* are in accordance with the results obtained with *E. coli*: L-rod spread method underestimate the CFUs number, and the spot method provides the best results, in accordance with the theoretical CFUs counting deriving from the OD reading.

The two method used to make the dilutions give comparable results. However, a problem related to the choice of dilutions emerges: in the case of *B. subtilis*, the lowest dilution (i.e. -4) shows an underestimation of the CFUs number, probably due to the large size of the colonies of this bacteria strain, which, in this specific condition, leads to an overlap of several colonies.

B. subtilis TEST 2

In this test, intermediate dilutions were introduced, in order to improve the statistic error associated with the number of colonies per Petri and find a good solution for replacing the dilution -4 (Test 2).

The serial dilutions were made using sterile micro-tubes containing 900 μL of sterile physiological solution (with the exception of the intermediate dilutions, called -4.5 and -5.5, that containing 800 μL of physiological solution) and 100 μL (200 μL in case of -4.5 and -5.5 dilutions) of the solutions is diluted in a series. In this case the bacteria growth curve was interrupted close to the stationary phase (OD_{600} ~ 1) but, for the purposes of this reproducibility test, this was irrelevant. 100 μL of the last three dilutions (-4.5, -5.5, -5) were spread in triplicated, by using the spot procedure, on agar plates. Results are given in Table B.7.

Table B.7 CFU counting from *B. subtilis* Test 2 (microtubes and spot platting procedure)

OD600 = 1.1		**CFU mL^{-1} from OD = 1.1 × 10^{8}**	
		CFU	**CFU mL^{-1}**
-4,5	A	194	9.7×10^{8}
-4,5	B	201	1.0×10^{8}
-4,5	C	184	9.2×10^{8}
-5	A	125	1.3×10^{8}
-5	B	120	1.2×10^{8}
-5	C	113	1.1×10^{8}
-5,5	A	32	1.6×10^{8}
-5,5	B	39	1.9×10^{8}
-5,5	C	41	2.0×10^{8}
-6	A	14	1.4×10^{8}
-6	B	20	2.0×10^{8}
-6	C	23	2.3×10^{8}

The lowest intermediate dilution (i.e. -4.5) shows a slight underestimation of the CFUs number. Therefore, the best conditions identified for *B. subtilis* were the dilutions -5.5 and -5 and the spot plating technique.

Supplemetary pictures

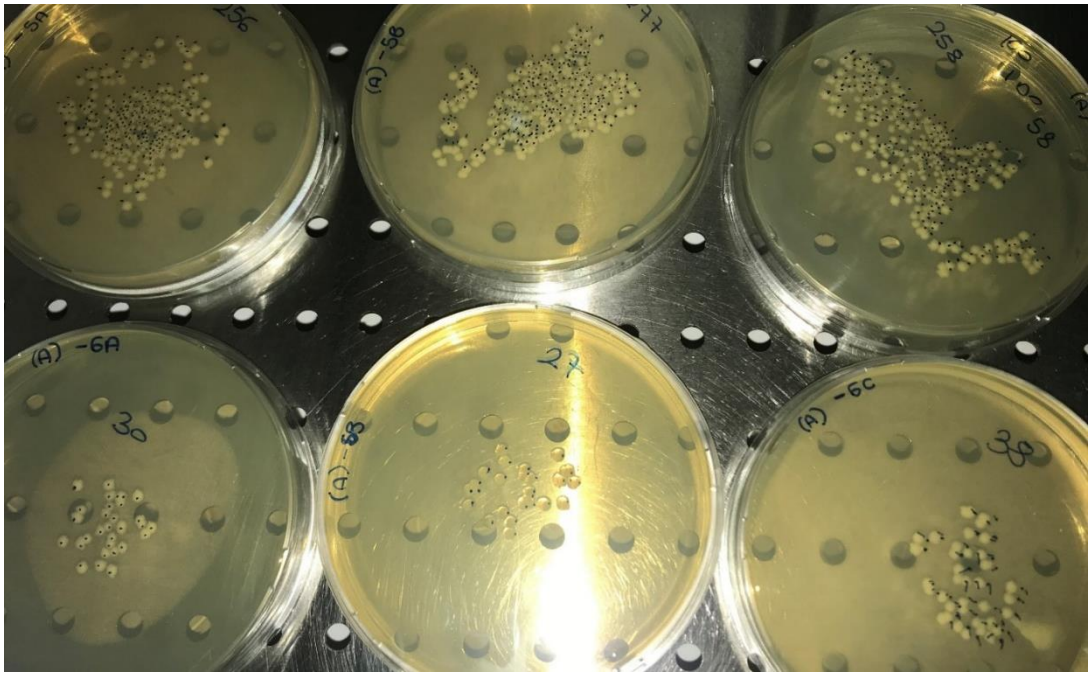

Figure B.5 Examples of CFUs of *E. coli* obtained by spot platting (Test 2). Colonies from the so-called -5 and -6 dilutions are shown.

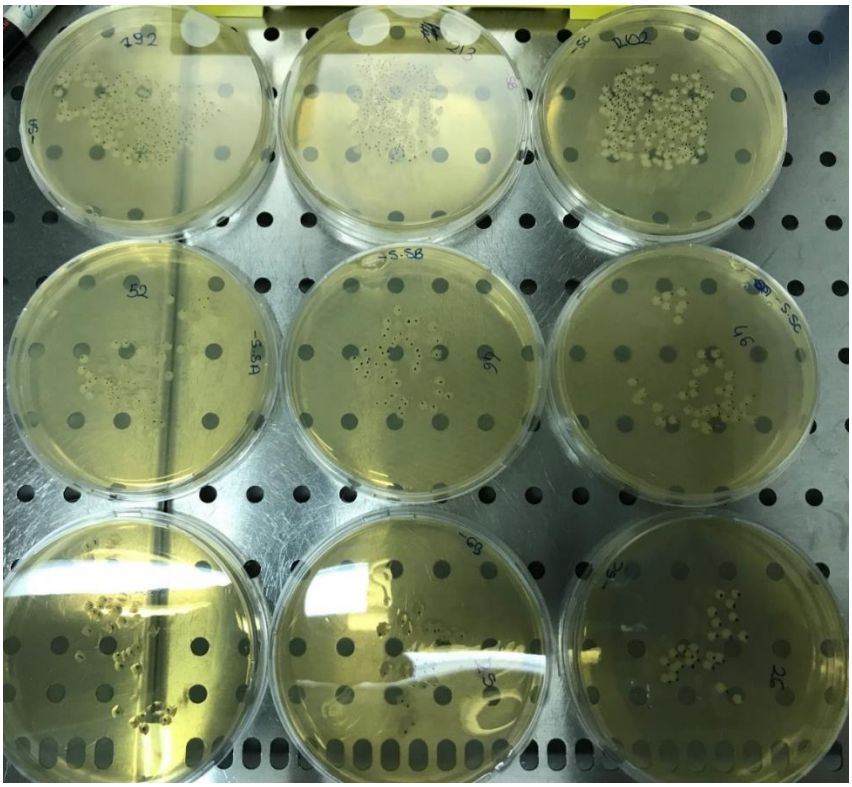

Figure B.3 Examples of CFUs of *E. coli* obtained by spot platting (Test 3). Colonies from the so-called -5, -5.5 and -6 dilutions are shown.

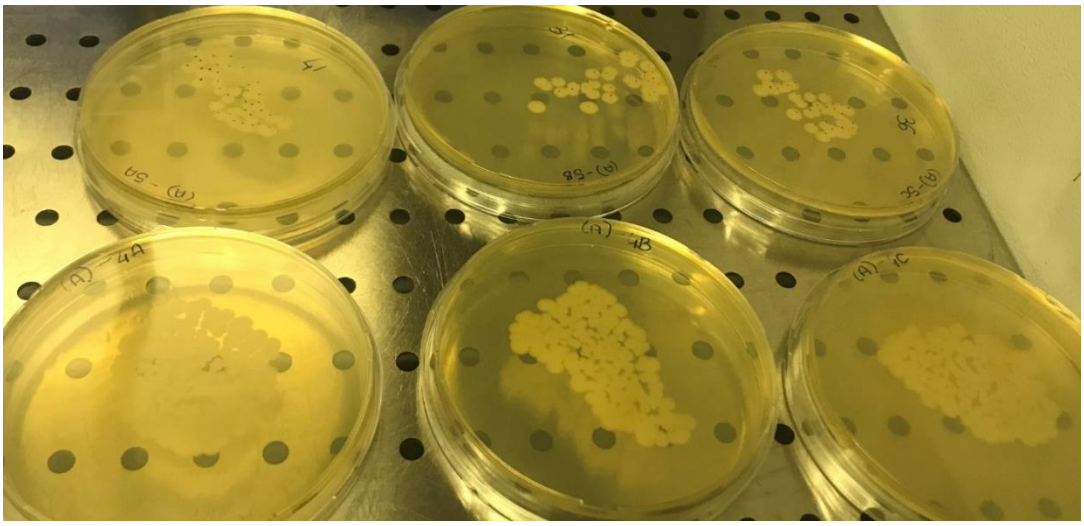

Figure B.4 Examples of CFUs of *B. subtilis* obtained by spot platting (Test 1). Colonies from the so-called -4 and -5 dilutions are shown.

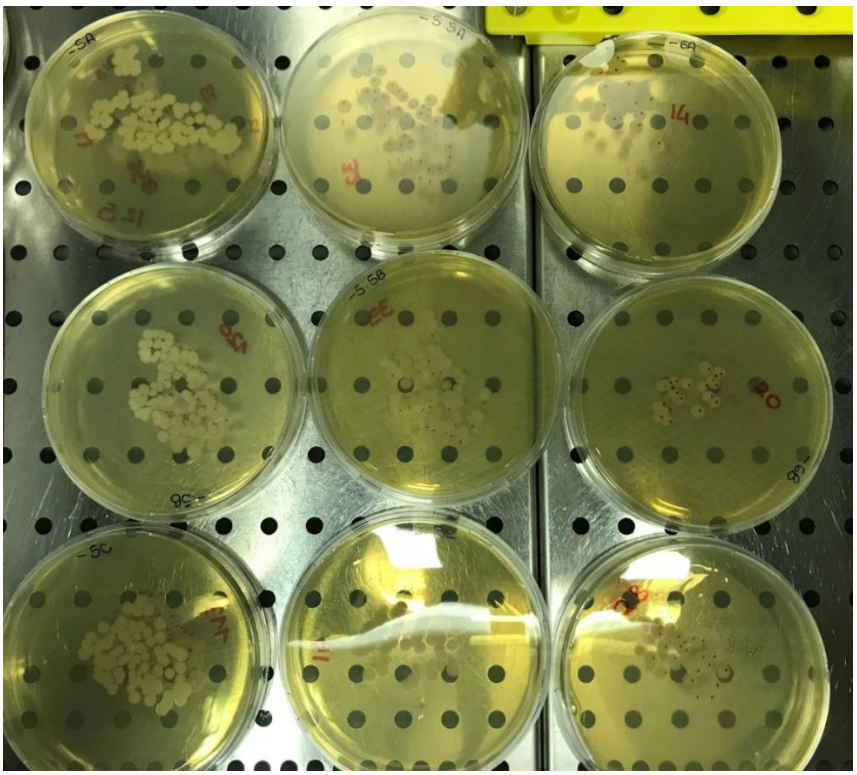

Figure B.5 Examples of CFUs of *B. subtilis* obtained by spot platting (Test 2). Colonies from the so-called -5, -5.5 and -6 dilutions are shown.

References

Alsved, M., Bourouiba, L., Duchaine, C., Löndahl, J., Marr, L.C., Parker, S.T., Prussin, A.J., Thomas, R.J., 2020. Natural sources and experimental generation of bioaerosols: Challenges and perspectives. Aerosol Sci. Technol. 54, 547–571. https://doi.org/10.1080/02786826.2019.1682509

Amato, P., Demeer, F., Melaouhi, A., Fontanella, S., Martin-Biesse, A.-S., Sancelme, M., Laj, P., Delort, A.-M., 2007. A fate for organic acids, formaldehyde and methanol in cloud water: their biotransformation by micro-organisms. Atmospheric Chem. Phys. 7, 4159–4169. https://doi.org/10.5194/acp-7-4159-2007

Amato, P., Joly, M., Schaupp, C., Attard, E., Möhler, O., Morris, C.E., Brunet, Y., Delort, A.-M., 2015. Survival and ice nucleation activity of bacteria as aerosols in a cloud simulation chamber. Atmospheric Chem. Phys. 15, 6455–6465. https://doi.org/10.5194/acp-15-6455-2015

Amato, P., Ménager, M., Sancelme, M., Laj, P., Mailhot, G., Delort, A.-M., 2005. Microbial population in cloud water at the Puy de Dôme: Implications for the chemistry of clouds. Atmos. Environ. 39, 4143–4153. https://doi.org/10.1016/j.atmosenv.2005.04.002

Amato, P., Parazols, M., Sancelme, M., Laj, P., Mailhot, G., Delort, A.-M., 2006. Microorganisms isolated from the water phase of tropospheric clouds at the Puy de Dôme: major groups and growth abilities at low temperatures. FEMS Microbiol. Ecol. 59, 242–254. https://doi.org/10.1111/j.1574-6941.2006.00199.x

Ariya, P.A., Amyot, M., 2004. New Directions: The role of bioaerosols in atmospheric chemistry and physics. Atmos. Environ. 38, 1231–1232. https://doi.org/10.1016/j.atmosenv.2003.12.006

Ariya, P.A., Nepotchatykh, O., Ignatova, O., Amyot, M., 2002. Microbiological degradation of atmospheric organic compounds. Geophys. Res. Lett. 29, 34-1-34–4. https://doi.org/10.1029/2002GL015637

Aydogdu, H., Asan, A., Tatman Otkun, M., 2010. Indoor and outdoor airborne bacteria in child day-care centers in Edirne City (Turkey), seasonal distribution and influence of meteorological factors. Environ. Monit. Assess. 164, 53–66. https://doi.org/10.1007/s10661-009-0874-0

Barnes, I., Becker, K.H., Mihalopoulos, N., 1994. An FTIR product study of the photooxidation of dimethyl disulfide. J. Atmospheric Chem. 18, 267–289. https://doi.org/10.1007/BF00696783

Bauer, H., Giebl, H., Hitzenberger, R., Kasper-Giebl, A., Reischl, G., Zibuschka, F., Puxbaum, H., 2003. Airborne bacteria as cloud condensation nuclei. J. Geophys. Res. Atmospheres 108. https://doi.org/10.1029/2003JD003545

Bauer, H., Kasper-Giebl, A., Löflund, M., Acar, H., Hitzenberger, R., Zibuschka, F., Puxbaum, H., 2002a. The contribution of bacteria and fungal spores to the organic carbon content of cloud water, precipitation and aerosols. Atmospheric Res., a 64, 109–119. https://doi.org/10.1016/S0169-8095(02)00084-4

Bauer, H., Kasper-Giebl, A., Zibuschka, F., Hitzenberger, R., Kraus, G.F., Puxbaum, H., 2002b. Determination of the Carbon Content of Airborne Fungal Spores. Anal. Chem., b 74, 91–95. https://doi.org/10.1021/ac010331+

Baumgardner, D., Strapp, W., Dye, J.E., 1985. Evaluation of the Forward Scattering Spectrometer Probe. Part II: Corrections for Coincidence and Dead-Time Losses. J. Atmospheric Ocean. Technol. 2, 626–632. https://doi.org/10.1175/1520-0426(1985)002<0626:EOTFSS>2.0.CO;2

Becker, K.H., 2006. Overview on the Development of Chambers for the Study of Atmospheric Chemical Processes, in: Barnes, I., Rudzinski, K.J. (Eds.), Environmental Simulation Chambers: Application to Atmospheric Chemical Processes, Nato Science Series: IV: Earth and Environmental Science. Springer Netherlands, Dordrecht, pp. 1–26. https://doi.org/10.1007/1-4020-4232-9_1

Benbough, J.E., 1967. Death Mechanisms in Airborne Escherichia coli. J. Gen. Microbiol. 47, 325–333. https://doi.org/10.1099/00221287-47-3-325

Benz, S., Megahed, K., Möhler, O., Saathoff, H., Wagner, R., Schurath, U., 2005. T-dependent rate measurements of homogeneous ice nucleation in cloud droplets using a large atmospheric simulation chamber. J. Photochem. Photobiol. Chem. 176, 208–217. https://doi.org/10.1016/j.jphotochem.2005.08.026

Bernstein, J.A., Alexis, N., Barnes, C., Bernstein, I.L., Nel, A., Peden, D., Diaz-Sanchez, D., Tarlo, S.M., Williams, P.B., Bernstein, J.A., 2004. Health effects of air pollution. J. Allergy Clin. Immunol. 114, 1116–1123. https://doi.org/10.1016/j.jaci.2004.08.030

Bischof, O.F., Weber, P., Bundke, U., Petzold, A., Kiendler-Scharr, A., 2020. Characterization of the Miniaturized Inverted Flame Burner as a Combustion Source to Generate a Nanoparticle Calibration Aerosol. Emiss. Control Sci. Technol. 6, 37–46. https://doi.org/10.1007/s40825-019-00147-w

Bond, T.C., Bergstrom, R.W., 2006. Light Absorption by Carbonaceous Particles: An Investigative Review. Aerosol Sci. Technol. 40, 27–67. https://doi.org/10.1080/02786820500421521

Boose, Y., Baloh, P., Plötze, M., Ofner, J., Grothe, H., Sierau, B., Lohmann, U., Kanji, Z.A., 2019. Heterogeneous ice nucleation on dust particles sourced from nine deserts worldwide – Part 2: Deposition nucleation and condensation freezing. Atmospheric Chem. Phys. 19, 1059–1076. https://doi.org/10.5194/acp-19-1059-2019

Boucher, O., Randall, D., Artaxo, P., Bretheton, C., Feingold, G., Forster, P., Kerminen, V.-M., Kondo, Y., Liao, H., Lohmann, U., Rasch, P., Satheesh, S.K., Sherwood, S., Stevens, B., Zhang, X.Y., 2013. Clouds and Aerosols. In: Climate Change 2013: The Physical Science Basis. Contribution of Working Group I to the Fifth Assessment Report of the Intergovernmental Panel on Climate Change, [Stocker, T.F., D. Qin, G.-K. Plattner, M. Tignor, S.K. Allen, J. Boschung, A. Nauels, Y. Xia, V. Bex and P.M. Midgley (eds.)]. Cambridge University Press. Cambridge, United Kingdom and New York, NY, USA.

Bowers, R.M., McLetchie, S., Knight, R., Fierer, N., 2011. Spatial variability in airborne bacterial communities across land-use types and their relationship to the bacterial communities of potential source environments. ISME J. 5, 601–612. https://doi.org/10.1038/ismej.2010.167

Breijyeh, Z., Jubeh, B., Karaman, R., 2020. Resistance of Gram-Negative Bacteria to Current Antibacterial Agents and Approaches to Resolve It. Molecules 25, 1340. https://doi.org/10.3390/molecules25061340

Brodie, E.L., DeSantis, T.Z., Parker, J.P.M., Zubietta, I.X., Piceno, Y.M., Andersen, G.L., 2007. Urban aerosols harbor diverse and dynamic bacterial populations. Proc. Natl. Acad. Sci. U. S. A. 104, 299–304. https://doi.org/10.1073/pnas.0608255104

Brotto, P., Repetto, B., Formenti, P., Pangui, E., Livet, A., Bousserrhine, N., Martini, I., Varnier, O., Doussin, J.F., Prati, P., 2015. Use of an atmospheric simulation chamber for bioaerosol investigation: a feasibility study. Aerobiologia 31, 445–455. https://doi.org/10.1007/s10453-015-9378-2

Burrows, S.M., Butler, T., Jöckel, P., Tost, H., Kerkweg, A., Pöschl, U., Lawrence, M.G., 2009a. Bacteria in the global atmosphere – Part 2: Modeling of emissions and transport between different ecosystems. Atmospheric Chem. Phys. 9, 9281–9297. https://doi.org/10.5194/acp-9-9281-2009

Burrows, S.M., Elbert, W., Lawrence, M.G., Pöschl, U., 2009b. Bacteria in the global atmosphere – Part 1: Review and synthesis of literature data for different ecosystems. Atmos Chem Phys 18.

Carter, W.P.L., Cocker, D.R., Fitz, D.R., Malkina, I.L., Bumiller, K., Sauer, C.G., Pisano, J.T., Bufalino, C., Song, C., 2005. A new environmental chamber for evaluation of gas-phase

chemical mechanisms and secondary aerosol formation. Atmos. Environ. 39, 7768–7788. https://doi.org/10.1016/j.atmosenv.2005.08.040

Cocker, D.R., Flagan, R.C., Seinfeld, J.H., 2001. State-of-the-Art Chamber Facility for Studying Atmospheric Aerosol Chemistry. Environ. Sci. Technol. 35, 2594–2601. https://doi.org/10.1021/es0019169

Conen, F., Morris, C.E., Leifeld, J., Yakutin, M.V., Alewell, C., 2011. Biological residues define the ice nucleation properties of soil dust. Atmospheric Chem. Phys. 11, 9643–9648. https://doi.org/10.5194/acp-11-9643-2011

Cox, C.S., 1966. The Survival of Escherichia coli sprayed into Air and into Nitrogen from Distilled Water and from Solutions of Protecting Agents, as a Function of Relative Humidity. J. Gen. Microbiol. 43, 383–399. https://doi.org/10.1099/00221287-43-3-383

Danelli, S.G., Brunoldi, M., Massabò, D., Parodi, F., Vernocchi, V., Prati, P., 2021. Comparative characterization of the performance of bio-aerosol nebulizers in connection with atmospheric simulation chambers. Atmospheric Meas. Tech. 14, 4461–4470. https://doi.org/10.5194/amt-14-4461-2021

Deguillaume, L., Leriche, M., Amato, P., Ariya, P.A., Delort, A.-M., Pöschl, U., Chaumerliac, N., Bauer, H., Flossmann, A.I., Morris, C.E., 2008. Microbiology and atmospheric processes: chemical interactions of primary biological aerosols. Biogeosciences 5, 1073–1084. https://doi.org/10.5194/bg-5-1073-2008

Després, V.R., Huffman, J.A., Burrows, S.M., Hoose, C., Safatov, AleksandrS., Buryak, G., Fröhlich-Nowoisky, J., Elbert, W., Andreae, M.O., Pöschl, U., Jaenicke, R., 2012. Primary biological aerosol particles in the atmosphere: a review. Tellus B Chem. Phys. Meteorol. 64, 15598. https://doi.org/10.3402/tellusb.v64i0.15598

Dodge, M., 2000. Chemical oxidant mechanisms for air quality modeling: critical review. Atmos. Environ. 34, 2103–2130. https://doi.org/10.1016/S1352-2310(99)00461-6

Doussin, J.F., Ritz, D., Durand-Jolibois, R., Monod, A., Carlier, P., 1997. Design of an environmental chamber for the study of atmospheric chemistry: New developments in the analytical device. Analusis 25, 236–242.

Dunklin, E.W., Puck, T.T., 1948. The lethal effect of relative humidity on airborne bacteria. J. Exp. Med. 87, 87–101. https://doi.org/10.1084/jem.87.2.87

Earl, A.M., Losick, R., Kolter, R., 2008. Ecology and genomics of Bacillus subtilis. Trends Microbiol. 16, 269–275. https://doi.org/10.1016/j.tim.2008.03.004

Federici, E., Petroselli, C., Montalbani, E., Casagrande, C., Ceci, E., Moroni, B., La Porta, G., Castellini, S., Selvaggi, R., Sebastiani, B., Crocchianti, S., Gandolfi, I., Franzetti, A.,

Cappelletti, D., 2018. Airborne bacteria and persistent organic pollutants associated with an intense Saharan dust event in the Central Mediterranean. Sci. Total Environ. 645, 401–410. https://doi.org/10.1016/j.scitotenv.2018.07.128

Feng, J.Q., Go, L.-S., Calubayan, J., Tomaska, R., 2021. Working Mechanism and Behavior of Collison Nebulizer. Aerosol Sci. Eng. 5, 285–291. https://doi.org/10.1007/s41810-021-00102-9

Finlayson-Pitts, B., Pitts, J., 2000. Chemistry of Upper and Lower Atmosphere. https://doi.org/10.1016/B978-012257060-5/50010-1

Finlayson-Pitts, B.J., Pitts, J.N., 1997. Tropospheric air pollution: ozone, airborne toxics, polycyclic aromatic hydrocarbons, and particles. Science 276, 1045–1052. https://doi.org/10.1126/science.276.5315.1045

Fröhlich-Nowoisky, J., Kampf, C.J., Weber, B., Huffman, J.A., Pöhlker, C., Andreae, M.O., Lang-Yona, N., Burrows, S.M., Gunthe, S.S., Elbert, W., Su, H., Hoor, P., Thines, E., Hoffmann, T., Després, V.R., Pöschl, U., 2016. Bioaerosols in the Earth system: Climate, health, and ecosystem interactions. Atmospheric Res. 182, 346–376. https://doi.org/10.1016/j.atmosres.2016.07.018

Fuzzi, S., Andreae, M.O., Huebert, B.J., Kulmala, M., Bond, T.C., Boy, M., Doherty, S.J., Guenther, A., Kanakidou, M., Kawamura, K., Kerminen, V.-M., Lohmann, U., Russell, L.M., Pöschl, U., 2006. Critical assessment of the current state of scientific knowledge, terminology, and research needs concerning the role of organic aerosols in the atmosphere, climate, and global change. Atmospheric Chem. Phys. 6, 2017–2038. https://doi.org/10.5194/acp-6-2017-2006

Gandolfi, I., Bertolini, V., Bestetti, G., Ambrosini, R., Innocente, E., Rampazzo, G., Papacchini, M., Franzetti, A., 2015. Spatio-temporal variability of airborne bacterial communities and their correlation with particulate matter chemical composition across two urban areas. Appl. Microbiol. Biotechnol. 99, 4867–4877. https://doi.org/10.1007/s00253-014-6348-5

Gauderman, W.J., Avol, E., Gilliland, F., Vora, H., Thomas, D., Berhane, K., McConnell, R., Kuenzli, N., Lurmann, F., Rappaport, E., Margolis, H., Bates, D., Peters, J., 2004. The Effect of Air Pollution on Lung Development from 10 to 18 Years of Age. N. Engl. J. Med. 11.

Georgakopoulos, D.G., Despres, V., Frohlich-Nowoisky, J., Psenner, R., Ariya, P.A., Posfai, M., Ahern, H.E., Moffett, B.F., Hill, T.C.J., 2009. Microbiology and atmospheric processes: biological, physical and chemical characterization of aerosol particles 17.

Glarborg, P., Miller, J.A., Ruscic, B., Klippenstein, S.J., 2018. Modeling nitrogen chemistry in combustion. Prog. Energy Combust. Sci. 67, 31–68. https://doi.org/10.1016/j.pecs.2018.01.002

Griffin, D., Westphal, D., Gray, M., 2006. Airborne microorganisms in the African desert dust corridor over the mid-Atlantic ridge, Ocean Drilling Program, Leg 209. Aerobiologia 22, 211–226. https://doi.org/10.1007/s10453-006-9033-z

Hall, B.G., Acar, H., Nandipati, A., Barlow, M., 2014. Growth Rates Made Easy. Mol. Biol. Evol. 31, 232–238. https://doi.org/10.1093/molbev/mst187

Hallquist, M., Wenger, J.C., Baltensperger, U., Rudich, Y., Simpson, D., Claeys, M., Dommen, J., Donahue, N.M., George, C., Goldstein, A.H., Hamilton, J.F., Herrmann, H., Hoffmann, T., Iinuma, Y., Jang, M., Jenkin, M.E., Jimenez, J.L., Kiendler-Scharr, A., Maenhaut, W., McFiggans, G., Mentel, T.F., Monod, A., Prevot, A.S.H., Seinfeld, J.H., Surratt, J.D., Szmigielski, R., Wildt, J., 2009. The formation, properties and impact of secondary organic aerosol: current and emerging issues. Atmos Chem Phys 82.

Harrison, R.M., 2005. AIR ANALYSIS | Outdoor Air, in: Encyclopedia of Analytical Science. Elsevier, pp. 43–48. https://doi.org/10.1016/B0-12-369397-7/00008-X

He, M., Ichinose, T., Yoshida, S., Yamamoto, S., Inoue, K., Takano, H., Yanagisawa, R., Nishikawa, M., Mori, I., Sun, G., Shibamoto, T., 2012. Asian sand dust enhances murine lung inflammation caused by Klebsiella pneumoniae. Toxicol. Appl. Pharmacol. 258. https://doi.org/10.1016/J.TAAP.2011.11.003

Hernandez, M., Perring, A.E., McCabe, K., Kok, G., Granger, G., Baumgardner, D., 2016. Chamber catalogues of optical and fluorescent signatures distinguishbioaerosol classes. Atmospheric Meas. Tech. 9, 3283–3292. https://doi.org/10.5194/amt-9-3283-2016

Hinds, W.C., 1999. Aerosol Technology: Properties, Behavior, and Measurement of Airborne Particles. John Wiley & Sons.

Houghton, J.E.T., Ding, Y., Griggs, D., Noguer, M., van der Linden, P., Dai, X., Maskell, M., Johnson, C., 2001. Climate Change 2001: The Scientific Basis, Contribution of Working Group I to the Third Assessment Report of the Intergovernmental Panel on Climate Change (IPCC).

Huffman, J.A., Prenni, A.J., DeMott, P.J., Pöhlker, C., Mason, R.H., Robinson, N.H., Fröhlich-Nowoisky, J., Tobo, Y., Després, V.R., Garcia, E., Gochis, D.J., Harris, E., Müller-Germann, I., Ruzene, C., Schmer, B., Sinha, B., Day, D.A., Andreae, M.O., Jimenez, J.L., Gallagher, M., Kreidenweis, S.M., Bertram, A.K., Pöschl, U., 2013. High concentrations of biological aerosol particles and ice nuclei during and after rain. Atmospheric Chem. Phys. 13, 6151–6164. https://doi.org/10.5194/acp-13-6151-2013

Huffman, J.A., Sinha, B., Garland, R.M., Snee-Pollmann, A., Gunthe, S.S., Artaxo, P., Martin, S.T., Andreae, M.O., Pöschl, U., 2012. Size distributions and temporal variations of biological

aerosol particles in the Amazon rainforest characterized by microscopy and real-time UV-APS fluorescence techniques during AMAZE-08. Atmospheric Chem. Phys. 12, 11997–12019. https://doi.org/10.5194/acp-12-11997-2012

Hughes, M.N., 2008. Chapter One - Chemistry of Nitric Oxide and Related Species, in: Poole, R.K. (Ed.), Methods in Enzymology, Globins and Other Nitric Oxide-Reactive Proteins, Part A. Academic Press, pp. 3–19. https://doi.org/10.1016/S0076-6879(08)36001-7

Hussey, Shane.J.K., Purves, J., Allcock, N., Fernandes, V.E., Monks, P.S., Ketley, J.M., Andrew, P.W., Morrissey, J.A., 2017. Air pollution alters *Staphylococcus aureus* and *Streptococcus pneumoniae* biofilms, antibiotic tolerance and colonisation: Air pollution affects biofilms and colonisation. Environ. Microbiol. 19, 1868–1880. https://doi.org/10.1111/1462-2920.13686

IPCC, 2021: Climate Change 2021: The Physical Science Basis. Contribution of Working Group I to the Sixth Assessment Report of the Intergovernmental Panel on Climate Change, 2021. [Masson-Delmotte, V., P. Zhai, A. Pirani, S.L. Connors, C. Péan, S. Berger, N. Caud, Y. Chen, L. Goldfarb, M.I. Gomis, M. Huang, K. Leitzell, E. Lonnoy, J.B.R. Matthews, T.K. Maycock, T. Waterfield, O. Yelekçi, R. Yu, and B. Zhou (eds.)]., Cambridge University Press. In Press.

Jang, J., Hur, H.-G., Sadowsky, M.J., Byappanahalli, M.N., Yan, T., Ishii, S., 2017. Environmental Escherichia coli: ecology and public health implications-a review. J. Appl. Microbiol. 123, 570–581. https://doi.org/10.1111/jam.13468

Johansson, S.A.E., Campbell, J.L., Malmqvist, K.G., 1995. Particle-Induced X-Ray Emission Spectrometry (PIXE). John Wiley & Sons., New York.

Lai, K.A.C., Nazaroff, W.W., 2000. Modeling indoor particle deposition from turbulent flow onto smooth surfaces. J. Aerosol Sci. 31, 463–476. https://doi.org/10.1016/S0021-8502(99)00536-4

Lang-Yona, N., Shuster-Meiseles, T., Mazar, Y., Yarden, O., Rudich, Y., 2016. Impact of urban air pollution on the allergenicity of Aspergillus fumigatus conidia: Outdoor exposure study supported by laboratory experiments. Sci. Total Environ. 541, 365–371. https://doi.org/10.1016/j.scitotenv.2015.09.058

Lee, B.U., Kim, S.H., Kim, S.S., 2002. Hygroscopic growth of E. coli and B. subtilis bioaerosols. Aerosol Sci. 3.

Lee, B.U., Kim, S.S., 2003. Sampling E. coli and B. subtilis bacteria bioaerosols by a new type of impactor with a cooled impaction plate. J. Aerosol Sci. 34, 1097–1100. https://doi.org/10.1016/S0021-8502(03)00076-4

Lee, Y.H., Lee, B.U., 2006. Inactivation of Airborne E. coli and B. subtilis Bioaerosols Utilizing Thermal Energy. J. Microbiol. Biotechnol. 16, 1684–1689.

Li, N., Sioutas, C., Cho, A., Schmitz, D., Misra, C., Sempf, J., Wang, M., Oberley, T., Froines, J., Nel, A., 2003. Ultrafine particulate pollutants induce oxidative stress and mitochondrial damage. Environ. Health Perspect. 111, 455–460. https://doi.org/10.1289/ehp.6000

Lieberherr, G., Auderset, K., Calpini, B., Clot, B., Crouzy, B., Gysel-Beer, M., Konzelmann, T., Manzano, J., Mihajlovic, A., Moallemi, A., O'Connor, D., Sikoparija, B., Sauvageat, E., Tummon, F., Vasilatou, K., 2021. Assessment of real-time bioaerosol particle counters using reference chamber experiments. Atmospheric Meas. Tech. 14, 7693–7706. https://doi.org/10.5194/amt-14-7693-2021

Lighthart, B., 2006. The ecology of bacteria in the alfresco atmosphere. FEMS Microbiol. Ecol. 23, 263–274. https://doi.org/10.1111/j.1574-6941.1997.tb00408.x

Lindsley, W.G., Green, B.J., Blachere, F.M., Martin, S.B., Jensen, P.A., Schafer, M.P., 1984. Sampling and characterization of bioaerosols, in: NIOSH Manual of Analytical Methods. U.S. Department of Health and Human Services, Public Health Service, National Institute for Occupational Safety and Health, Division of Physical Sciences and Engineering, Cincinnati, Ohio, p. 948.

Lohmann, U., Feichter, J., 2005. Global indirect aerosol effects: a review. Atmos Chem Phys 23.

Mainelis, G., Berry, D., Reoun An, H., Yao, M., DeVoe, K., Fennell, D.E., Jaeger, R., 2005. Design and performance of a single-pass bubbling bioaerosol generator. Atmos. Environ. 39, 3521–3533. https://doi.org/10.1016/j.atmosenv.2005.02.043

Marple, V.A., Willeke, K., 1976. Impactor design. Atmospheric Environ. 1967 10, 891–896. https://doi.org/10.1016/0004-6981(76)90144-X

Martiny, J.B.H., Bohannan, B.J.M., Brown, J.H., Colwell, R.K., Fuhrman, J.A., Green, J.L., Horner-Devine, M.C., Kane, M., Krumins, J.A., Kuske, C.R., Morin, P.J., Naeem, S., Ovreås, L., Reysenbach, A.-L., Smith, V.H., Staley, J.T., 2006. Microbial biogeography: putting microorganisms on the map. Nat. Rev. Microbiol. 4, 102–112. https://doi.org/10.1038/nrmicro1341

Massabó, D., Danelli, S.G., Brotto, P., Comite, A., Costa, C., Cesare, A., Doussin, J., Ferraro, F., Formenti, P., Gatta, E., Negretti, L., Oliva, M., Parodi, F., Vezzulli, L., Prati, P., 2018. ChAMBRe: a new atmospheric simulation chamber for aerosol modelling and bio-aerosol research. Atmos Meas Tech 17.

May, K.R., 1973. The collison nebulizer: Description, performance and application. J. Aerosol Sci. 4, 235–243. https://doi.org/10.1016/0021-8502(73)90006-2

Michelsen, H.A., 2017. Probing soot formation, chemical and physical evolution, and oxidation: A review of in situ diagnostic techniques and needs. Proc. Combust. Inst. 36, 717–735. https://doi.org/10.1016/j.proci.2016.08.027

Miller, J., 1972. Determination of viable cell counts: bacterial growth curves. Exp. Mol. Genet. 31, 36.

Moallemi, A., Kazemimanesh, M., Corbin, J.C., Thomson, K., Smallwood, G., Olfert, J.S., Lobo, P., 2019. Characterization of black carbon particles generated by a propane-fueled miniature inverted soot generator. J. Aerosol Sci. 135, 46–57. https://doi.org/10.1016/j.jaerosci.2019.05.004

Möhler, O., DeMott, P.J., Vali, G., Levin, Z., 2007. Microbiology and atmospheric processes: the role of biological particles in cloud physics. Biogeosciences 4, 1059–1071. https://doi.org/10.5194/bg-4-1059-2007

Monks, P.S., Granier, C., Fuzzi, S., Stohl, A., Williams, M.L., Akimoto, H., Amann, M., Baklanov, A., Baltensperger, U., Bey, I., Blake, N., Blake, R.S., Carslaw, K., Cooper, O.R., Dentener, F., Fowler, D., Fragkou, E., Frost, G.J., Generoso, S., Ginoux, P., Grewe, V., Guenther, A., Hansson, H.C., Henne, S., Hjorth, J., Hofzumahaus, A., Huntrieser, H., Isaksen, I.S.A., Jenkin, M.E., Kaiser, J., Kanakidou, M., Klimont, Z., Kulmala, M., Laj, P., Lawrence, M.G., Lee, J.D., Liousse, C., Maione, M., McFiggans, G., Metzger, A., Mieville, A., Moussiopoulos, N., Orlando, J.J., O'Dowd, C.D., Palmer, P.I., Parrish, D.D., Petzold, A., Platt, U., Pöschl, U., Prévôt, A.S.H., Reeves, C.E., Reimann, S., Rudich, Y., Sellegri, K., Steinbrecher, R., Simpson, D., ten Brink, H., Theloke, J., van der Werf, G.R., Vautard, R., Vestreng, V., Vlachokostas, Ch., von Glasow, R., 2009. Atmospheric composition change – global and regional air quality. Atmos. Environ. 43, 5268–5350. https://doi.org/10.1016/j.atmosenv.2009.08.021

Moosmüller, H., Chakrabarty, R.K., Arnott, W.P., 2009. Aerosol light absorption and its measurement: A review. J. Quant. Spectrosc. Radiat. Transf. 110, 844–878. https://doi.org/10.1016/j.jqsrt.2009.02.035

Morris, C.E., Georgakopoulos, D.G., Sands, D.C., 2004. Ice nucleation active bacteria and their potential role in precipitation. J. Phys. IV Proc. 121, 87–103. https://doi.org/10.1051/jp4:2004121004

Morris, C.E., Leyronas, C., Nicot, P.C., 2014. Movement of Bioaerosols in the Atmosphere and the Consequences for Climate and Microbial Evolution, in: Colbeck, I., Lazaridis, M. (Eds.), Aerosol Science: Technology and Applications. John Wiley & Sons, Ltd, Chichester, UK, pp. 393–415. https://doi.org/10.1002/9781118682555.ch16

Myhre, G., Shindell, D., Bréon, F.-M., Collins, W., Fuglestvedt, J., Huang, J., Koch, D., Lamarque, J.-F., Lee, D., Mendoza, B., Nakajima, T., Robock, A., Stephens, G., Zhang, H., Aamaas, B., Boucher, O., Dalsøren, S.B., Daniel, J.S., Forster, P., Granier, C., Haigh, J., Hodnebrog, Ø., Kaplan, J.O., Marston, G., Nielsen, C.J., O'Neill, B.C., Peters, G.P., Pongratz, J., Ramaswamy, V., Roth, R., Rotstayn, L., Smith, S.J., Stevenson, D., Vernier, J.-P., Wild, O., Young, P., Jacob, D., Ravishankara, A.R., Shine, K., 2013. Anthropogenic and Natural Radiative Forcing. In: Climate Change 2013: The Physical Science Basis. Contribution of Working Group I to the Fifth Assessment Report of the Intergovernmental Panel on Climate Change (No. [Stocker, T.F., D. Qin, G.-K. Plattner, M. Tignor, S.K. Allen, J. Boschung, A. Nauels, Y. Xia, V. Bex and P.M. Midgley (eds.)]. Cambridge University Press). Cambridge, United Kingdom and New York, NY, USA.

Mytilinaios, I., Salih, M., Schofield, H.K., Lambert, R.J.W., 2012. Growth curve prediction from optical density data. Int. J. Food Microbiol. 154, 169–176. https://doi.org/10.1016/j.ijfoodmicro.2011.12.035

Nemmar, A., Hoet, P.H.M., Vanquickenborne, B., Dinsdale, D., Thomeer, M., Hoylaerts, M.F., Vanbilloen, H., Mortelmans, L., Nemery, B., 2002. Passage of Inhaled Particles Into the Blood Circulation in Humans. Circulation. 105, 411–414.

Noda, J., Tomizawa, S., Hoshino, B., Munkhjargal, E., Kawai, K., Kai, K., 2019. Atmospheric dust as a possible survival factor for bioaerosols. E3S Web Conf. 99, 04007. https://doi.org/10.1051/e3sconf/20199904007

Noda, J., Tomizawa, S., Takahashi, K., Morimoto, K., Mitarai, S., 2021. Air pollution and airborne infection with mycobacterial bioaerosols: a potential attribution of soot. Int. J. Environ. Sci. Technol. https://doi.org/10.1007/s13762-021-03203-7

Oberdörster, G., Oberdörster, E., Oberdörster, J., 2005. Nanotoxicology: An Emerging Discipline Evolving from Studies of Ultrafine Particles. Environ. Health Perspect. 113, 823–839. https://doi.org/10.1289/ehp.7339

O'Dowd, C.D., Facchini, M.C., Cavalli, F., Ceburnis, D., Mircea, M., Decesari, S., Fuzzi, S., Yoon, Y.J., Putaud, J.-P., 2004. Biogenically driven organic contribution to marine aerosol. Nature 431, 676–680. https://doi.org/10.1038/nature02959

Petroselli, C., Montalbani, E., La Porta, G., Crocchianti, S., Moroni, B., Casagrande, C., Ceci, E., Selvaggi, R., Sebastiani, B., Gandolfi, I., Franzetti, A., Federici, E., Cappelletti, D., 2021. Characterization of long-range transported bioaerosols in the Central Mediterranean. Sci. Total Environ. 763, 143010. https://doi.org/10.1016/j.scitotenv.2020.143010

Pöhlker, C., Huffman, J.A., Pöschl, U., 2012. Autofluorescence of atmospheric bioaerosols – fluorescent biomolecules and potential interferences. Atmospheric Meas. Tech. 5, 37–71. https://doi.org/10.5194/amt-5-37-2012

Pope, C.A., Burnett, R.T., Thurston, G.D., Thun, M.J., Calle, E.E., Krewski, D., Godleski, J.J., 2004. Cardiovascular Mortality and Long-Term Exposure to Particulate Air Pollution: Epidemiological Evidence of General Pathophysiological Pathways of Disease. Circulation 109, 71–77. https://doi.org/10.1161/01.CIR.0000108927.80044.7F

Pöschl, U., 2005. Atmospheric Aerosols: Composition, Transformation, Climate and Health Effects. Angew. Chem. Int. Ed. 44, 7520–7540. https://doi.org/10.1002/anie.200501122

Pöschl, U., Martin, S.T., Sinha, B., Chen, Q., Gunthe, S.S., Huffman, J.A., Borrmann, S., Farmer, D.K., Garland, R.M., Helas, G., Jimenez, J.L., King, S.M., Manzi, A., Mikhailov, E., Pauliquevis, T., Petters, M.D., Prenni, A.J., Roldin, P., Rose, D., Schneider, J., Su, H., Zorn, S.R., Artaxo, P., Andreae, M.O., 2010. Rainforest aerosols as biogenic nuclei of clouds and precipitation in the Amazon. Science 329, 1513–1516. https://doi.org/10.1126/science.1191056

Pöschl, U., Shiraiwa, M., 2015. Multiphase Chemistry at the Atmosphere–Biosphere Interface Influencing Climate and Public Health in the Anthropocene. Chem. Rev. 115, 4440–4475. https://doi.org/10.1021/cr500487s

Prospero, J., Blades, E., Mathison, G., Naidu, R., 2005. Prospero JM, Blades E, Mathison G, Naidu R.. Interhemispheric transport of viable fungi and bacteria from Africa to the Caribbean with soil dust. Aerobiologia 21: 1-19. Aerobiologia 21, 1–19. https://doi.org/10.1007/s10453-004-5872-7

Putaud, J.-P., Raes, F., Van Dingenen, R., Brüggemann, E., Facchini, M.-C., Decesari, S., Fuzzi, S., Gehrig, R., Hüglin, C., Laj, P., Lorbeer, G., Maenhaut, W., Mihalopoulos, N., Müller, K., Querol, X., Rodriguez, S., Schneider, J., Spindler, G., Brink, H. ten, Tørseth, K., Wiedensohler, A., 2004. A European aerosol phenomenology—2: chemical characteristics of particulate matter at kerbside, urban, rural and background sites in Europe. Atmos. Environ. 38, 2579–2595. https://doi.org/10.1016/j.atmosenv.2004.01.041

Raes, F., Dingenen, R.V., Vignati, E., Wilson, J., Putaud, J.-P., Seinfeld, J.H., Adams, P., 2000. Formation and cycling of aerosols in the global troposphere. Atmos. Environ. 26.

Reinmuth-Selzle, K., Kampf, C.J., Lucas, K., Lang-Yona, N., Fröhlich-Nowoisky, J., Shiraiwa, M., Lakey, P.S.J., Lai, S., Liu, F., Kunert, A.T., Ziegler, K., Shen, F., Sgarbanti, R., Weber, B., Bellinghausen, I., Saloga, J., Weller, M.G., Duschl, A., Schuppan, D., Pöschl, U., 2017. Air Pollution and Climate Change Effects on Allergies in the Anthropocene: Abundance,

Interaction, and Modification of Allergens and Adjuvants. Environ. Sci. Technol. 51, 4119–4141. https://doi.org/10.1021/acs.est.6b04908

Ren, Y., Grosselin, B., Daële, V., Mellouki, A., 2017. Investigation of the reaction of ozone with isoprene, methacrolein and methyl vinyl ketone using the HELIOS chamber. Faraday Discuss. 200, 289–311. https://doi.org/10.1039/C7FD00014F

Reponen, T., Willeke, K., Ulevicius, V., Grinshpun, S.A., Donnelly, J., 1997. Techniques for Dispersion of Microorganisms into Air. Aerosol Sci. Technol. 27, 405–421. https://doi.org/10.1080/02786829708965481

Samet, J., Wassel, R., Holmes, K.J., Abt, E., Bakshi, K., 2005. Research Priorities for Airborne Particulate Matter in the United States 6.

Santarpia, J.L., Pan, Y.-L., Hill, S.C., Baker, N., Cottrell, B., McKee, L., Ratnesar-Shumate, S., Pinnick, R.G., 2012. Changes in fluorescence spectra of bioaerosols exposed to ozone in a laboratory reaction chamber to simulate atmospheric aging. Opt. Express 20, 29867–29881. https://doi.org/10.1364/OE.20.029867

Savage, N.J., Krentz, C.E., Könemann, T., Han, T.T., Mainelis, G., Pöhlker, C., Huffman, J.A., 2017. Systematic characterization and fluorescence threshold strategies for the wideband integrated bioaerosol sensor (WIBS) using size-resolved biological and interfering particles. Atmospheric Meas. Tech. 10, 4279–4302. https://doi.org/10.5194/amt-10-4279-2017

Seinfeld, J.H., Pandis, S.N., 1998. Atmospheric Chemistry and Physics: From Air Pollution to Climate Change. John Wiley and Sons, Inc., New York.

Shaffer, B.T., Lighthart, B., 1997. Survey of Culturable Airborne Bacteria at Four Diverse Locations in Oregon: Urban, Rural, Forest, and Coastal. Microb. Ecol. 34, 167–177. https://doi.org/10.1007/s002489900046

Shiraiwa, M., Selzle, K., Pöschl, U., 2012. Hazardous components and health effects of atmospheric aerosol particles: reactive oxygen species, soot, polycyclic aromatic compounds and allergenic proteins. Free Radic. Res. 46, 927–939. https://doi.org/10.3109/10715762.2012.663084

Silhavy, T.J., Kahne, D., Walker, S., 2010. The Bacterial Cell Envelope. Cold Spring Harb. Perspect. Biol. 2, a000414. https://doi.org/10.1101/cshperspect.a000414

Simon, X., Duquenne, P., Koehler, V., Piernot, C., Coulais, C., Faure, M., 2011. Aerosolisation of Escherichia coli and associated endotoxin using an improved bubbling bioaerosol generator. J. Aerosol Sci. 42, 517–531. https://doi.org/10.1016/j.jaerosci.2011.05.002

Sonwani, S., Saxena, P., 2016. Identifying the Sources of Primary Air Pollutants and their Impact on Environmental Health: A Review 6, 21.

Stone, R.C., Johnson, D.L., 2002. A Note on the Effect of Nebulization Time and Pressure on the Culturability of Bacillus subtilis and Pseudomonas fluorescens. Aerosol Sci. Technol. 36, 536–539. https://doi.org/10.1080/02786820252883775

Sun, J., Ariya, P., 2006. Atmospheric organic and bio-aerosols as cloud condensation nuclei (CCN): A review. Atmos. Environ. 40, 795–820. https://doi.org/10.1016/j.atmosenv.2005.05.052

Suni, T., Guenther, A., Hansson, H.C., Kulmala, M., Andreae, M.O., Arneth, A., Artaxo, P., Blyth, E., Brus, M., Ganzeveld, L., Kabat, P., de. Noblet-Ducoudré, N., Reichstein, M., Reissell, A., Rosenfeld, D., Seneviratne, S., 2015. The significance of land-atmosphere interactions in the Earth system—iLEAPS achievements and perspectives. Anthropocene 12, 69–84. https://doi.org/10.1016/j.ancene.2015.12.001

Sutton, S., 2011. Measurement of Microbial Cells by Optical Density. J. Valid. Technol. 17, 46–49.

Terzieva, S., Donnelly, J., Ulevicius, V., Grinshpun, S.A., Willeke, K., Stelma, G.N., Brenner, K.P., 1996. Comparison of methods for detection and enumeration of airborne microorganisms collected by liquid impingement. Appl. Environ. Microbiol. 62, 2264–2272. https://doi.org/10.1128/aem.62.7.2264-2272.1996

Thomas, R.J., Webber, D., Hopkins, R., Frost, A., Laws, T., Jayasekera, P.N., Atkins, T., 2011. The Cell Membrane as a Major Site of Damage during Aerosolization of *Escherichia coli*. Appl. Environ. Microbiol. 77, 920–925. https://doi.org/10.1128/AEM.01116-10

Tobo, Y., Adachi, K., DeMott, P.J., Hill, T.C.J., Hamilton, D.S., Mahowald, N.M., Nagatsuka, N., Ohata, S., Uetake, J., Kondo, Y., Koike, M., 2019. Glacially sourced dust as a potentially significant source of ice nucleating particles. Nat. Geosci. 12, 253–258. https://doi.org/10.1038/s41561-019-0314-x

Tong, Y., Lighthart, B., 1999. Diurnal Distribution of Total and Culturable Atmospheric Bacteria at a Rural Site. Aerosol Sci. Technol. 30, 246–254. https://doi.org/10.1080/027868299304822

Tong, Y., Lighthart, B., 1998. Effect of simulated solar radiation on mixed outdoor atmospheric bacterial populations. FEMS Microbiol. Ecol. 26, 311–316. https://doi.org/10.1111/j.1574-6941.1998.tb00515.x

Vernocchi, V., Brunoldi, M., Danelli, S.G., Parodi, F., Prati, P., Massabò, D., 2021. Characterization of the MISG soot generator with an atmospheric simulation chamber. Atmospheric Meas. Tech. Discuss. 1–27. https://doi.org/10.5194/amt-2021-345

Wagner, R., Bunz, H., Linke, C., Möhler, O., Naumann, K.-H., Saathoff, H., Schnaiter, M., Schurath, U., 2006. Chamber Simulations of Cloud Chemistry: The AIDA Chamber, in: Barnes, I., Rudzinski, K.J. (Eds.), Environmental Simulation Chambers: Application to Atmospheric

Chemical Processes, Nato Science Series: IV: Earth and Environmental Science. Springer Netherlands, Dordrecht, pp. 67–82. https://doi.org/10.1007/1-4020-4232-9_5

Wang, C.-C., Fang, G.-C., Lee, L., 2007. Bioaerosols study in central Taiwan during summer season. Toxicol. Ind. Health 23, 133–139. https://doi.org/10.1177/0748233707078741

Wang, J., Doussin, J.F., Perrier, S., Perraudin, E., Katrib, Y., Pangui, E., Picquet-Varrault, B., 2011. Design of a new multi-phase experimental simulation chamber for atmospheric photosmog, aerosol and cloud chemistry research. Atmospheric Meas. Tech. 4, 2465–2494. https://doi.org/10.5194/amt-4-2465-2011

Whitby, K.T., Cantrell, B.K., 1976. Atmospheric Aerosols: Characteristics and Measurement. Presented at the International Conference on Environmental Sensing and Assessment (ICESA), Institute of Electrical and Electronic Engineers (IEEE), Las Vegas, NV.

Wilson, T.W., Ladino, L.A., Alpert, P.A., Breckels, M.N., Brooks, I.M., Browse, J., Burrows, S.M., Carslaw, K.S., Huffman, J.A., Judd, C., Kilthau, W.P., Mason, R.H., McFiggans, G., Miller, L.A., Nájera, J.J., Polishchuk, E., Rae, S., Schiller, C.L., Si, M., Temprado, J.V., Whale, T.F., Wong, J.P.S., Wurl, O., Yakobi-Hancock, J.D., Abbatt, J.P.D., Aller, J.Y., Bertram, A.K., Knopf, D.A., Murray, B.J., 2015. A marine biogenic source of atmospheric ice-nucleating particles. Nature 525, 234–238. https://doi.org/10.1038/nature14986

Xu, Z., Yao, M., 2011. Analysis of Culturable Bacterial and Fungal Aerosol Diversity Obtained Using Different Samplers and Culturing Methods. Aerosol Sci. Technol. 45, 1143–1153. https://doi.org/10.1080/02786826.2011.582195

Zádor, J., Turányi, T., Wirtz, K., Pilling, M.J., 2006. Measurement and investigation of chamber radical sources in the European Photoreactor (EUPHORE). J. Atmospheric Chem. 55, 147–166. https://doi.org/10.1007/s10874-006-9033-y

Zhao, F., Elkelish, A., Durner, J., Lindermayr, C., Winkler, J.B., Ruëff, F., Behrendt, H., Traidl-Hoffmann, C., Holzinger, A., Kofler, W., Braun, P., von Toerne, C., Hauck, S.M., Ernst, D., Frank, U., 2016. Common ragweed (Ambrosia artemisiifolia L.): allergenicity and molecular characterization of pollen after plant exposure to elevated NO2. Plant Cell Environ. 39, 147–164. https://doi.org/10.1111/pce.12601

Zhen, H., Han, T., Fennell, D.E., Mainelis, G., 2014. A systematic comparison of four bioaerosol generators: Affect on culturability and cell membrane integrity when aerosolizing Escherichia coli bacteria. J. Aerosol Sci. 70, 67–79. https://doi.org/10.1016/j.jaerosci.2014.01.002

Zheng, Y., Yao, M., 2017. Liquid impinger BioSampler's performance for size-resolved viable bioaerosol particles. J. Aerosol Sci. 106, 34–42. https://doi.org/10.1016/j.jaerosci.2017.01.003

Acknowledgements

This research has been supported by the European Union's Horizon 2020 research and innovation program through the EUROCHAMP-2020 Infrastructure Activity under grant agreement no. 730997 and it has received funding by MIUR through the PON project PIR_00015 “PER-ACTRIS-IT” whose recipient is INFN.

Candidate publications

Danelli, S.G., Brunoldi, M., Massabò, D., Parodi, F., Vernocchi, V., Prati, P., 2021. Comparative characterization of the performance of bio-aerosol nebulizers in connection with atmospheric simulation chambers. Atmospheric Meas. Tech. 14, 4461–4470. https://doi.org/10.5194/amt-14-4461-2021.

Massabó, D., Danelli, S.G., Brotto, P., Comite, A., Costa, C., Cesare, A., Doussin, J., Ferraro, F., Formenti, P., Gatta, E., Negretti, L., Oliva, M., Parodi, F., Vezzulli, L., Prati, P., 2018. ChAMBRe: a new atmospheric simulation chamber for aerosol modelling and bio-aerosol research. Atmos Meas Tech, 11, 5885–5900, https://doi.org/10.5194/amt-11-5885-2018.

Vernocchi, V., Brunoldi, M., Danelli, S.G., Parodi, F., Prati, P., Massabò, D., 2021. Characterization of the MISG soot generator with an atmospheric simulation chamber. Atmospheric Meas. Tech. Discuss. 1–27. https://doi.org/10.5194/amt-2021-345.

Moschos, V.; Gysel-Beer, M.; Modini, R. L.; Corbin, J. C.; Massabò, D.; Costa, C.; Danelli, S. G.; Vlachou, A.; Daellenbach, K. R.; Szidat, S.; Prati, P.; Prévôt, A. S. H.; Baltensperger, U. and El Haddad, I. 2021. Source-specific light absorption by carbonaceous components in the complex aerosol matrix from yearly filter-based measurements, Atmos. Chem. Phys., 21, 12809–12833, DOI: 10.5194/acp-21-12809-2021.